This is to certify that the
dissertation entitled

SUPRAMOLECULAR ASSEMBLY OF ORGANO-FUNCTIONAL
MESOSTRUCTURES: SYNTHESIS, CHARACTERIZATION, AND
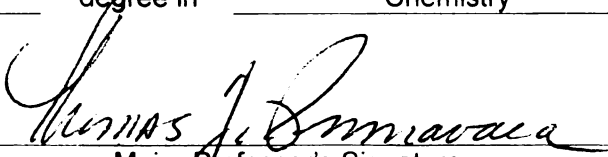APPLICATIONS IN ENVIRONMENTAL REMEDIATION

presented by

Emily Jane McKimmy

has been accepted towards fulfillment
of the requirements for the

Doctoral   degree in   Chemistry

_____
Major Professor's Signature

_____
Date

PLACE IN RETURN BOX to remove this checkout from your record.
TO AVOID FINES return on or before date due.
MAY BE RECALLED with earlier due date if requested.

DATE DUE	DATE DUE	DATE DUE

SUPRAMOLECULAR ASSEMBLY OF ORGANO-FUNCTIONAL

MESOSTRUCTURES: SYNTHESIS, CHARACTERIZATION, AND APPLICATIONS

IN ENVIRONMENTAL REMEDIATION

By

Emily Jane McKimmy

A DISSERTATION

Submitted to
Michigan State University
In partial fulfillment of the requirements
for the degree of

DOCTOR OF PHILOSOPHY

Department of Chemistry

2005

ABSTRACT

SUPRAMOLECULAR ASSEMBLY OF ORGANO-FUNCTIONAL MESOSTRUCTURES: SYNTHESIS, CHARACTERIZATION, AND APPLICATIONS IN ENVIRONMENTAL REMEDIATION

By

Emily Jane McKimmy

Mercury and arsenic are two heavy elements whose presence and persistence are of environmental concern due to their deleterious effects to human health. One promising technique for achieving the removal of low levels of mercury and arsenic from ground water is to trap them using complexing ligands (e.g. thiols and amines) that are covalently linked to porous structures. The overall goal of this work was to design organofunctional silica mesostructures for heavy element trapping. The organic moiety incorporation into the framework was accomplished by the direct assembly method and a hydrogen-bonding supramolecular assembly pathway between neutral alkylamine surfactant and nonionic silica source was utilized. The mesostructure thus prepared is denoted HMS.[1]

The advantage of functionalized mesoporous silicas for environmental remediation are their high surface areas, well-defined pore size, a framework structure that is stable under regeneration conditions, and the ability to covalently link organic groups to the framework to allow for selective adsorption of toxic heavy elements such as mercury and arsenic. A thiol-functionalized mesoporous silica with the anhydrous formula of $(SiO_2)_{1-x}(LSiO_{1.5})_x$, where L is a mercaptoalkyl group and x is the fraction of functionalized framework silicon centers, denoted MP-HMS[2] was examined for mercury

and arsenite (As(III)) remediation. MP-HMS has the highest mercury binding capacity of any reported mercaptan-functionalized mesostructure at 7.3 mmol Hg^{2+}/g. In addition to the exceptional binding capacity, microspherical MP-HMS with x=0.50 is capable of being packed into a column and to reduce mercury effluent concentration to the parts per trillion range, well below the EPA drinking water limit of 2 parts per billion. This work is also the first report of a functionalized mesostructure being used to trap arsenite. The binding capacity of MP-HMS for arsenite was 1.22 mmol $As(OH_3)$/g.

In addition to the synthesis and utilization of mono-functionalized mesoporous silicas, bi-functionalized HMS materials were prepared. Mercaptopropyl and aminopropyl organic moieties were incorporated into the HMS, and denoted MP+AP-HMS. The MP+AP-HMS was made with up to 25% of the silicon sites having thiol moieties, and 25% having amine moieties. This is the highest reported organic loading for a bi-functional mesostructure. The thiol groups were able to adsorb mercury and arsenite while the protonated amine groups had an affinity for arsenate (As(V)). Furthermore, the MP+AP-HMS appears to mimic the biologically important arsenate reductase mechanism. This is the system by which arsenate is reduced to arsenite in the body in order to rid itself of the pollutant.[3] Organically functionalized mesostructures are potentially valuable environmental remediation materials.

(1)   Tanev, P. T.; Pinnavaia, T. J. *Science* **1995**, *267*, 865-867.

(2)   Mori, Y.; Pinnavaia, T. J. *Chem.. Mater.* **2001**, *13*, 2173-2178.

(3)   Messens, J.; Martins, J. C.; Van Belle, K.; Brosens, E.; Desmyter, A.; De Gieter, M.; Wieruszeski, J.-M.; Willem, R.; Wyns, L.; Zegers, I. *P. Natl. Acad. Sci. USA.* **2002**, *99*, 8506-8511.

ACKNOWLEDGEMENTS

TABLE OF CONTENTS

LIST OF TABLES

LIST OF FIGURES

ABBREVIATIONS

AP	Aminopropyltrimethoxysilane
BET	Brunauer-Emmett-Teller
BJH	Barrett-Joyner-Halenda
BPMOs	Bifunctional periodic mesoporous organosilicates
BN	4-(triethoxysilyl)butyronitrile
BTEA	Bis(triethoxysilyl)acetylene
BTEB	1,4-Bis(triethoxysilyl)benzene
BTEBT	Bis(triethoxysilyl)bithiophene
BTEE	1,2-Bis(triethoxysilyl)ethane
BTEEY	1,2-Bis(triethoxysilyl)ethylene
BTEM	1,2-Bis(triethoxysilyl)methane
BTESE	1,2-Bis(triethoxysilyl)ethane
BTESM	Bis(triethoxysilyl)methane
BTET	2,5-Bis(triethoxysilyl)thiophene
BTME	1,2-Bis(trimethoxysilyl)ethane
BTMPA	Bis[3-(trimetholxysilyl)propyl]amine
BTMSE	1,2-Bis(trimethoxysilyl)ethane
Cl	Chloropropyl
CN	Propionitrile
DA	Direct-assmbly
DMe	Dimethyl
DNP	dinitrophenylaminopropyl
en	Ethylenediamine
EP	3-(2,3-Epoxypropoxy)propyl
Et	Ethyl
EtOH	Ethanol
H-bonding	Hydrogen bonding
HK	Horvath and Kawazoe

HMS	Wormhole mesostructured silica synthesized with amine surfactant using hydrogen bonding interactions
I^-	Anionic inorganic precursor
I^+	Cationic inorganic precursor
I^0	Neutral inorganic precursor
ICP	3-isocyanatopropyl
IUPAC	International Union of Pure and Applied Chemistry
M^+	Metal cation
MAS	Magic angle spinning
MCF	Mesostructured cellular foam
MCM-41	Mobil composition of matter 41
Me	Methyltriethoxysilane
mmol	Millimoles
MP	Mercaptopropy
MPTMS	3-mercaptopropyltrimethoxysilane
MP-MSU-F	Mercaptopropyl functionalized MSU-F mesostructured silicas
MP-MSU-X′	Mercaptopropyl functionalized MSU-X′ mesostructured silicas
MSU-F	Mesostructured cellular foam synthesized with P123 surfactant, trimethylbenzene and water soluble silicate at near neutral assembly conditions
MSU-H	Hexagonal mesostructured silica synthesized using PEO based surfactants and water soluble silicates at near neutral assembly conditions
MSU-SA	Mesostructured silica synthesized with amine surfactant and water soluble silicates
MSU-X	Wormhole mesostructured silica synthesized with PEO based surfactants and TEOS under neutral (N^0I^0) assembly conditions
MSU-X′	Wormhole mesostructured silicas synthesized with PEObased surfactants and water soluble silicates under neutral (N^0I^0) assembly conditions
NN	1-(2-aminoethyl)-3-aminopropyl

NNN	Propyldiethylenetriamine
N^0	Non-ionic amphiphilic PEO based surfactant
N^0I^0	Neutral assembly pathway utilizing H-bonding between PEO based surfactant and inorganic precursor
nm	Nanometer (10^{-9} m)
NMR	Nuclear magnetic resonance
Octyl	Octyl
OFMS	Organo-functionalized molecular sieves
P/P_0	Relative pressure P = pressure P_0 = saturation pressure
PEO	Polyethylene oxide
Ph	Phenyltrimethoxysilane
PMOs	Periodic Mesoporous Organosilicates
ppm	Parts per million
PXRD	Powder X-ray diffraction
Q^2	Incompletely condensed silica sites $Si(OSi)_2(OH)_2$
Q^3	Incompletely condensed silica sites $Si(OSi)_3(OH)$
Q^4	Completely condensed silica sites $Si(OSi)_4$
S^-	Anionic amphiphilic surfactant
S^+	Cationic amphiphilic surfactant
S^+I^-	Pathway 1 electrostatic assembly between cationic surfactant and anionic silica precursor
$S^+X^-I^+$	Electrostatic assembly between cationic surfactant and cationic silica precursors halogen ions as mediating counter ions
S^0	Neutral amphiphilic amine surfactant
S^0I^0	Neutral assembly pathway between neutral amine surfactant and TEOS
SBA	Mesostructured silica assembled under high acid, low pH conditions with TEOS as the inorganic precursor
SBA-15	Large pore hexagonal mesostructured silica assembled under high acid low pH conditions with TEOS as the inorganic precursor and triblock copolymer PEO based surfactant

SA_{BET} Specific surface area in m^2/g obtained from the linear part of the adsorption isotherm using the Brunauer Emmett Teller equation

SO_3H Sulfonic acid moiety from the oxidation of MP groups

T^2 Functionalized Q^2 site $RSi(OSi)_3OH$

T^3 Functionalized Q^3 site $RSi(OSi)_3$

TEOS   Tetraethylorthosilicate

TMB   Trimethylbenzene

TMCS   Trimethylchlorosilane

UDP   Ureidopropyl

Vy   Vinyltriethoxysilane

X^- Halogen or anionic counter ion

Chapter 1

Introduction

1.1 Research Objectives

The International Union of Pure and Applied Chemistry, IUPAC, has classified porous materials as microporous if the pore diameter is less than 2.0 nm, mesoporous for pore diameters between 2-50 nm, and macroporous for pore diameters greater than 50 nm. Porous materials are of interest to chemists due to their expansive applicability. Applications of porous materials include that of ion-exchangers, heterogeneous catalysts, gas adsorbents, and environmental remediation agents. The accessibility of the void space, i.e. pore size, of porous materials dictates the processes for which the porous derivative can be utilized, thus structures in the mesopore range are of great interest.

Mesoporous materials were first synthesized by Mobil Corporation in 1992 using an inorganic precursor and a surfactant as a porogen.[1] With their high surface areas (up to 1,400 m^2/g) and ability to easily tune the pore size (2-30 nm), mesoporous structures have been the focus of extensive research. To further expand the use of mesoporous silicas, organic functional groups have been incorporated into the framework of the structures. By the choice of organic moiety, mesoporous derivatives can be designed to selectively trap toxic pollutants such as mercury,[2] arsenic,[3] and lead,[4] as a support to immobilize enzymes,[5] or as chemical sensors.[6] There are two different pathways by which the organic functionality can be incorporated into the mesostructure, grafting or direct-assembly. Grafting is the incorporation of organic moieties into a silica network accomplished by surface anchoring through the hydroxyls of the incompletely condensed silica. The direct-assembly procedure for incorporation of organic groups in the silica

1

mesostructure framework entails the direct co-condensation of the organosilane with the inorganic precursor in the initial reaction mixture. Of the two different approaches, direct-assembly allows for a greater number of organic groups to be incorporated in to the mesostructure framework, more homogenous distribution of organic ligands, and fewer steps in the synthesis.

The interaction between the inorganic precursor and the surfactant template can be either an electrostatic or a hydrogen bonding assembly pathway. Electrostatic interactions between the surfactant and inorganic precursor yield mesostructures with long-range hexagonal morphology. Mesostructures prepared through hydrogen bonding interaction between the surfactant and inorganic precursor have short range order and a wormhole morphology. The wormhole morphology has been shown to allow for greater accessibility to ligands present in the pores.[7]

The overall goal of this work is to design organo-functional silica mesostructures for heavy element trapping. The organic moiety incorporation into the framework will be accomplished by the direct assembly method and a hydrogen bonding supramolecular assembly pathway between neutral alkylamine surfactant and nonionic silica source will be utilized. Specifically, this objective will be achieved by:

1. Preparation of functionalized mesoporous spheres for use in column adsorption applications. Spheres in both the nanoscale regime as well as the micron size range will be studied.

2. Development of a synthesis strategy to incorporate high loadings of two different organic moieties in a wormhole framework mesostructure to allow for selective adsorption of two different pollutants.

3. Examination of mercury remediation, regeneration, leaching of the trapped mercury, and coordination of the bound mercury including, but not limited to, columns packed with the spherical functionalized mesostructure.

4. Examination of the arsenite and arsenate adsorption capacity of functionalized wormhole mesostructures and large pore foam mesostructures.

1.2 Background of the Synthesis of Mesoporous Molecular Sieves

1.2.1 Electrostatic S^+I^- Assembly

In an attempt to expand the utility of microporous zeolites by enlarging the pore diameter to the meso range, Mobil Corporation researchers synthesized a new class of materials known as, Mobil Composition of Matter[1] and denoted MCM-41 (hexagonal), MCM-48 (cubic) and MCM-50 (lamellar). The MCM silicas are in the mesoporous range and are products of an electrostatic, hydrothermal reaction of aluminosilicate gel in the presence of quaternary ammonium surfactant under basic conditions. Electrostatic assembly utilizes charge matching of a cationic surfactant (S^+) and an anionic inorganic precursor (I^-) to produce long range ordered mesoporous materials with uniform pore size distribution. Surfactants are molecules which have a hydrophobic alkyl chain "tail" and a hydrophilic quaternary ammonium cation "head" $[C_nH_{2n+1}(CH_3)_3N]^+$. Individual surfactant molecules aggregate to form a micelle and in turn self assemble into close packed hexagonal arrays. These hexagonal arrays are the template around which the inorganic precursor assembles to yield a long-range ordered hexagonal mesoporous

3

silica. The mechanism for the assembly of long-range-ordered hexagonal MCM-41 was explained as the electrostatic charge matching assembly (S^+I^-) between the cationic surfactant (S^+) and anionic inorganic precursor (I^-). Brunauer-Emmett-Teller (BET) surface areas are estimated to be 1000 m^2/g for MCM-41.[8] The pore diameter can be tailored by use of swelling agents such as mesitylene or by varying the alkyl chain length, to range in size from 3.0 to ~10.0 nm.[9]

1.2.2 A Second Electrostatic Assembly Pathway, $S^+X^-I^+$

Stucky and co-workers assembled mesoporous materials via an electrostatic assembly between the cationic surfactant and cationic silica source mediated by a counter anion ($S^+X^-I^+$), denoted SBA materials.[10,11] The synthesis uses non-ionic triblock copolymer polyethylene oxide (PEO)-polypropylene oxide-polyethylene oxide (EO_x-PO_y-EO_x) based surfactants and an inorganic precursor like tetraethylorthosilicate (TEOS) at pH conditions near the isoelectric point of silica (pH~2). At these low pH values the silica source hydrolyzes into silicic acid and the PEO surfactants have the hydronium ion associated with them leading to the formation of a variety of mesophases via the electrostatic pathway (N^0H^+)(X^-I^+) depending on the choice of surfactant used.[12]

The high acid, low pH synthesis in the presence of high molecular weight tri-block co-polymer surfactants of the Pluronic series results in the formation of hexagonal mesoporous material designated as SBA-15.[10] The pore diameter of SBA-15 can be tailored to range from 5.0 to 30.0 nm, and the material has a surface area above 800 m^2/g. Additionally, SBA-15 has a regular structure and much thicker silica walls

than MCM-41, which impart a greater hydrothermal stability to the material.[10] The

hexagonal mesopores of SBA-15 are interconnected by micropores.

1.2.3. Neutral S^0I^0 Assembly Pathway

Tanev and Pinnavaia synthesized mesostructured silica termed HMS.[13] HMS is

assembled through non-electrostatic hydrogen-bonding interactions between neutral

primary alkylamine surfactant micelles (S^0) and an uncharged silica species (I^0) as the

inorganic precursor. As opposed to the long range order of hexagonal MCM-41 and

SBA-15, HMS has a large number of short disordered channels. Moreover, the pores are

regular in diameter yet they lack long-range packing order. The unique nature of the

HMS morphology has been termed wormhole as opposed to the long range ordered

hexagonal MCM-41. HMS has a surface area of about 1000 m^2/g and pore diameters in

the range of 3-5 nm.[14] Furthermore, the preparation conditions used in the S^0I^0 assembly

pathway are much milder than the electrostatic pathways. Also the alkyl amine surfactant

template can be easily recovered by solvent extraction and recycled instead of the

destructive calcination used to remove the quaternary ammonium template.

1.2.4 Non-Ionic N^0I^0 Assembly

Like HMS, MSU-X[15] mesostructures utilize a hydrogen-bonding interaction

between an uncharged silica species (I^0) and the surfactant (S^0), in contrast to an

electrostatic assembly pathway. The synthesis of MSU-X employs PEO surfactants as

the porogen.   Amphiphillic PEO-based surfactants have hydrophilic ethylene ether -

(CH_2CH_2O)- segments connected to hydrophobic R groups of varying lengths and

functionality depending on the type of surfactant examples of surfactants used.   The R

group could be an alkyl group as in the case of Brij and Tergitol surfactants or could be a phenyl group as in case of IGEPAL-RC and TRITON-X surfactants. Concomitantly, this material has a wormhole motif, a surface area of up to 1200 m^2/g, and a pore diameter of up to 5.8 nm.[15,16]

1.2.5 Microemulsion Assembly

In an ever-present quest for bigger and better, Stucky synthesized mesostructural cellar foams (MCF).[17] These foams have large cell dimensions in the range of 24-44 nm and pore volumes of 1.0- 2.4 cm^3/g, depending on the microemulsion template and reaction conditions. MCFs were synthesized under strongly acidic conditions by formation of an aqueous microemulsion. Using 1,3,5-trimethylbenzene (TMB) as a pore-expander and a triblock copolymer (Pluronic P123, $EO_{20}PO_{70}EO_{20}$) in an acidic media a microemulsion was formed around which TEOS polymerized. This process yielded extremely large cage-like structures. These large pores are attractive for enzyme immobilization, protein separations, accommodation of bulky functional groups as well as for separation and reactions of other large molecules.[18-20]

1.3 Characterization Techniques

Mesoporous molecular sieves are typically characterized by a battery of techniques including Powder X-ray diffraction (XRD), nitrogen adsorption , Transmission Electron Microscopy (TEM), ^{29}Si and ^{13}C Magic Angle Spinning Nuclear Magnetic Resonance (^{29}Si or ^{13}C MAS-NMR), Scanning Electron Microscopy (SEM), Thermogravimetric Analysis (TGA), Infrared Spectroscopy (IR), and elemental analysis.

XRD patterns for mesoporous materials are dominated by low-angle peaks and based on the reflection pattern it can be determined if the structure is of hexagonal or wormhole morphology. Representative XRD patterns for HMS and MCM-41 are shown in Figure 1.1. The HMS mesostructure exhibits a single low-angle peak indicating no long range order. The XRD patterns for MCM-41 typically show at least 3 peaks (d_{100}, d_{110}, d_{200}) that can be indexed to the hexagonal unit cell with a unit cell parameter $a_0 = 2d_{100}/\sqrt{3}$ and indicate hexagonal long-range order.

Representative nitrogen adsorption/desorption isotherms for HMS and MCM-41 are shown in Figure 1.2. The isotherms show a sharp step characteristic of adsorption uptake due to capillary condensation of the nitrogen within the framework mesopores. The relative pressure at which the step occurs is determined by the pore size and shifts to higher relative pressures as the pore diameter increases. Both the HMS and MCM-41 mesoporous molecular sieves exhibit a well defined mesopore step in the P/P_0 region of 0.4 and have Type IV isotherms.[21] However, the HMS isotherm has an additional uptake of nitrogen in the P/P_0 region above 0.8 indicative of textural porosity. Textural porosity is considered to be the void space between particles. The MCM-41 mesostructures do not display this second uptake of nitrogen and do not have textural porosity. The nitrogen isotherms are used to determine surface area by the Brunauer-Emmett-Teller (BET) model as well as pore volume and pore size. Pore size distribution is calculated from the adsorption branch using either the Horvath Kawazoe (HK) or Barrett-Joyner-Halenda (BJH) model.[22]

A broad single XRD peak usually typifies a wormhole structure where as the multiple low-angle peaks are typically indicative of a hexagonal structure. To confirm

the morphology of mesostructures, TEM analysis is done. Figure 1.3 shows the TEM images for a wormhole and hexagonal morphologies of HMS and MCM-41, respectively. In the TEM image for HMS, the sponge-like structure which gives rise to the textural porosity is observed. The presence of the textural porosity is indicated in the nitrogen isotherm and confirmed in the TEM image.

^{29}Si MAS NMR is done to asses the degree of framework cross-linking and degree of organic functionalization. The latter of which will be discussed in detail in the next section of this chapter. ^{13}C MAS-NMR is done in conjunction with ^{29}Si MAS NMR for characterization of the incorporation of organic moieties in the mesostructures. SEM is used to examine the topology of the mesostructures; the compositions can be synthesized to be spherical or rod-like.[23] TGA is typically done to determine if the surfactant is completely removed and to probe the thermal stability as well as hydrophobic or hydrophilic character of the structures. The latter property is imparted by the organofunctionalization of the mesostructures. IR and elemental analysis are also primarily used for characterization of organically modified mesoporous silicas.
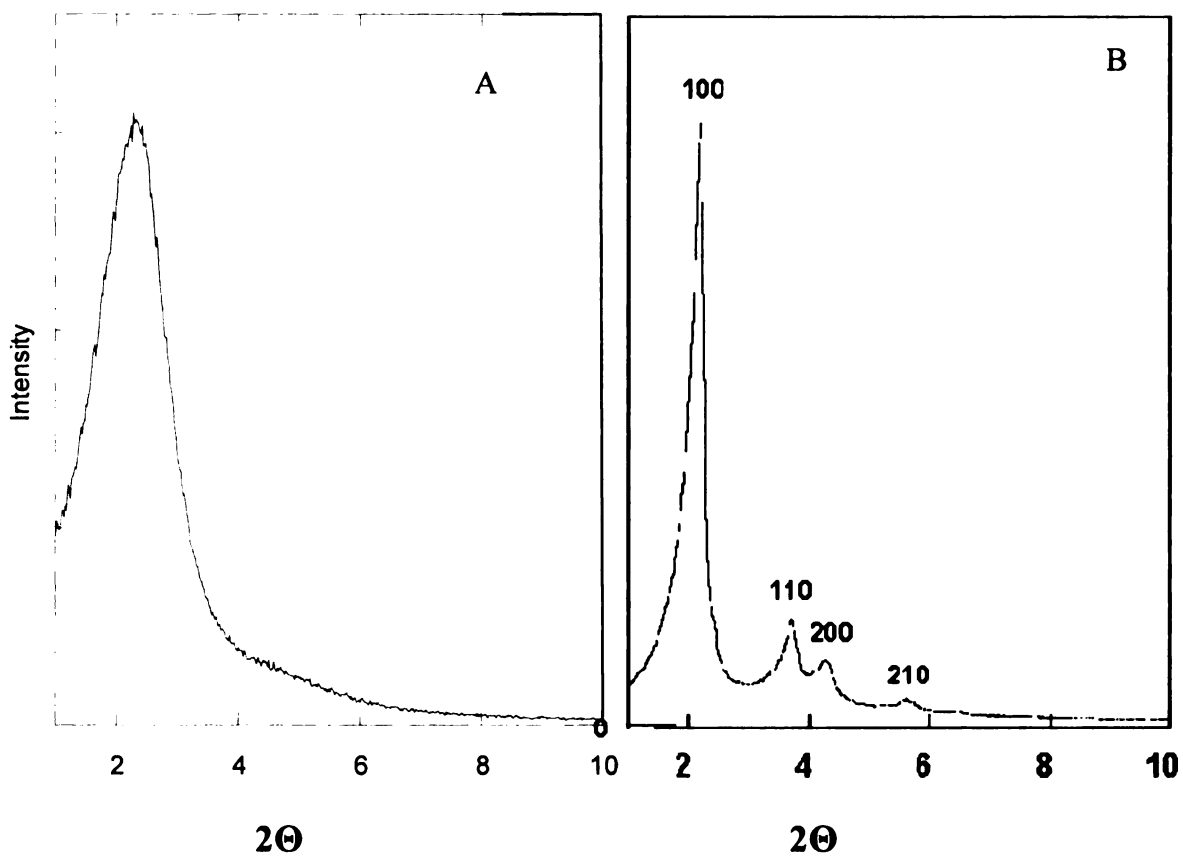
Figure 1.1. Representative XRD patterns for surfactant-free A. wormhole HMS mesostructure. B. hexagonal MCM-41 mesostructure.
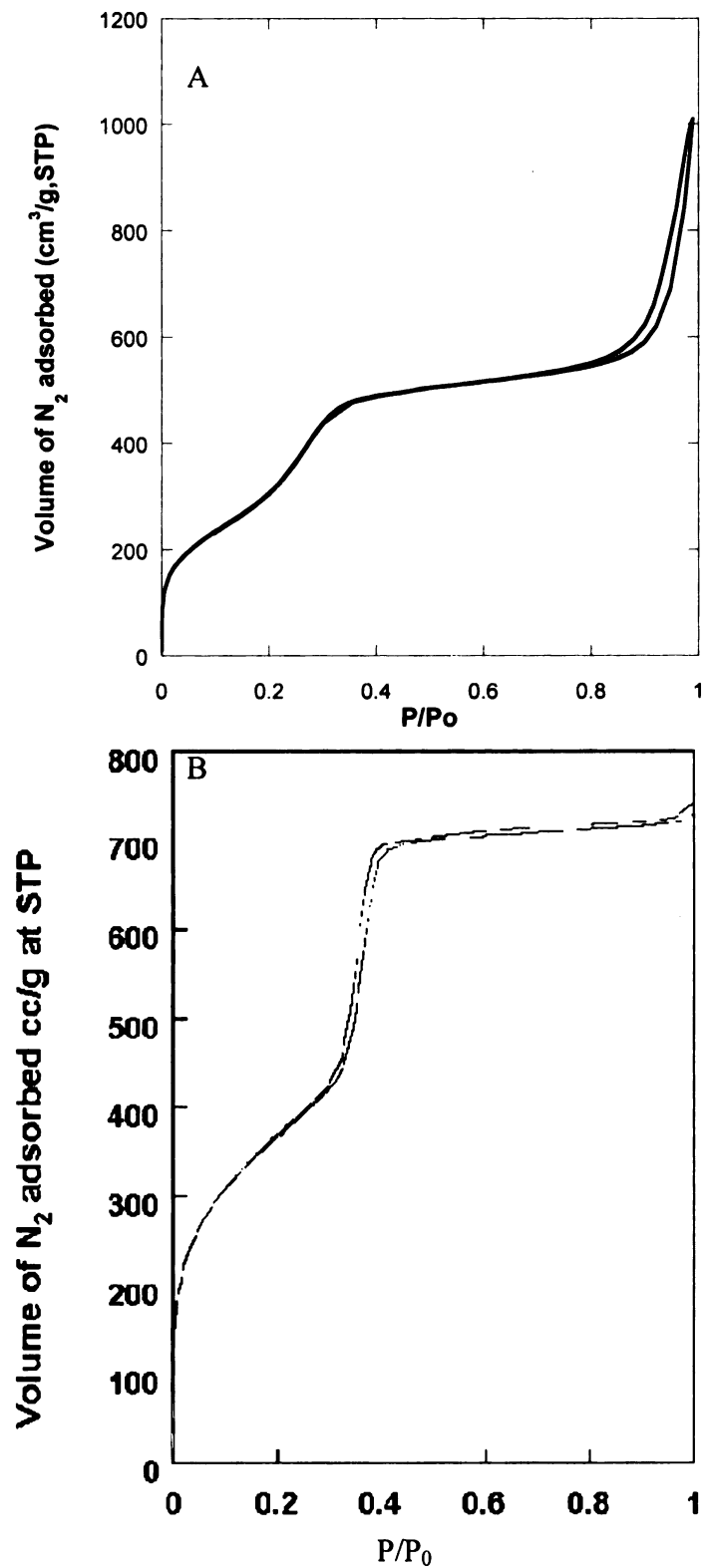
Figure 1.2. Representative Nitrogen Isotherms for surfactant-free A. wormhole HMS mesostructure. B. hexagonal MCM-41 mesostructure.
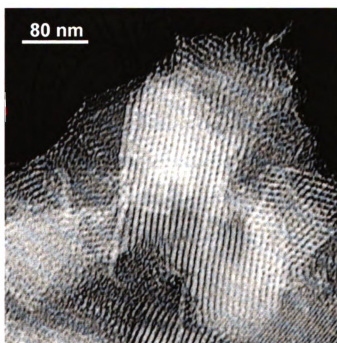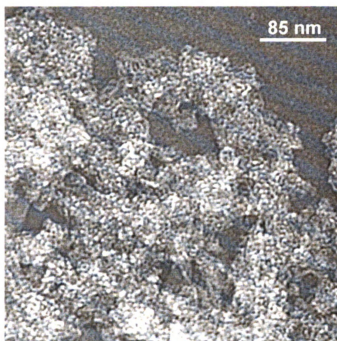
Figure 1.3. Representative TEM images for top wormhole HMS and bottom hexagonal MCM-41 mesostructure.

1.4 Organofunctionalization of Mesoporous Silicas

The advent of mesoporous materials opened new realms of possibility for catalysis of larger compounds that were too big for traditional zeolites. To expand utilization of mesoporous materials they have been functionalized with various organic moieties. Catalysis and environmental remediation are the two foremost fields where functionalized mesoporous materials have been employed. By addition of an appropriate organic group, mesoporous materials can be tuned for a specific reactivity, such as amine modification for arsenate adsorption[3,24] or thiol functionalization of structures for mercury adsorption.[2,4] A myriad of catalytic reactions such as: oxidation reactions,[25] acid catalysis,[26,27] base catalysis,[28,29] and chiral catalysis[30,31] have been accomplished over surface-modified mesoporous silicas. In addition, new fields such as enzyme immobilization,[5,20,32] drug delivery systems,[33-35] and chemical sensors[36] are also being examined as applications for functionalized mesoporous materials. In addition to advantages of mesoporous silicas due to their increased pore size, they also have greater catalytic activity and stability than modified silica gels.[37] There are two primary methods of functionalization: post-synthesis grafting and direct-assembly (co-condensation).

1.4.1 Incorporation of the Organic Functionality by Grafting

Grafting is the organic functionalization of silicas accomplished by surface anchoring of the organic moieties through the hydroxyls of the incompletely condensed silica as illustrated in Figure 1.4. Grafting was first employed by Beck et al.[8] Using

chlorotrimethylsilane as the organic moiety. Grafting has since been used to add organic functionality to MCM-41,[4] SBA-15,[38] and HMS.[2]

With pores in the 30 nm range, mesostructural cellular foams (MCFs) are attractive mesostructures for enzyme immobilization, protein separations, accommodation of bulky functional groups as well as for separation and reactions of other large molecules. In order to be used in these applications, MCFs have been functionalized by the two-step grafting method approach for protein separation and to immobilize enzymes like chloroperoxidase.[19,39]

Because there is no control over the location of the silanol groups, the grafting method of functionalization tends to yield islands of organic groups, limited loading of functionality, and cause pore blockage. Rehydration or degassing of the calcined material has been done in order to maximize the silanol content.[4] Yet this adds an extra step in the synthesis and complicates an already tedious procedure. Furthermore, the surface area and pore volume have been found to decrease upon organic modification by grafting. [40] Concomitantly, as more organic groups are grafted on, the more pronounced the decrease in surface area and pore volume. Also the accessibility of the grafted materials is typically less than that of the directly-assembled material. [3,7,41,42]
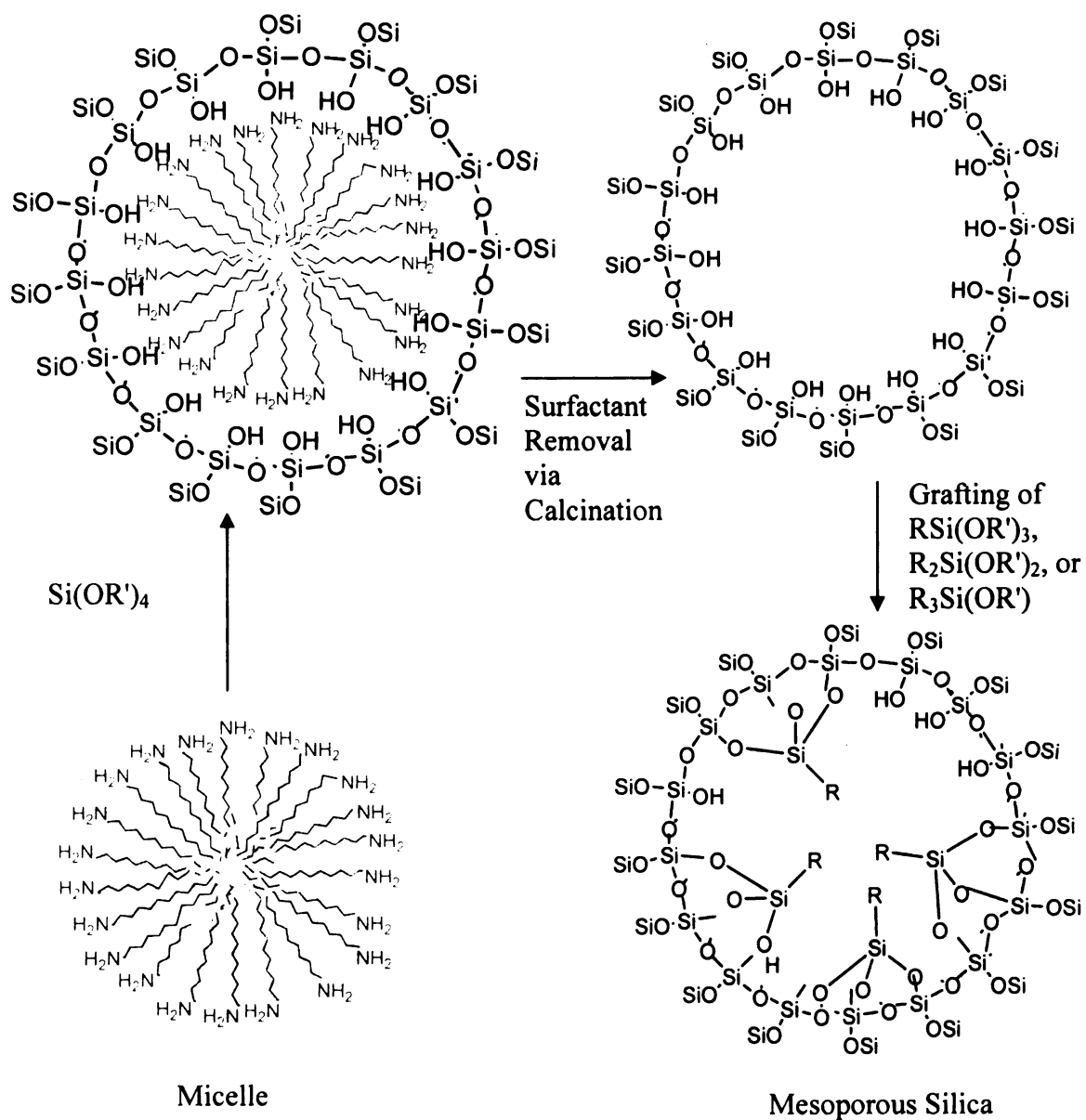
Figure 1.4. Schematic representation of the grafting method of incorporating organo-functional groups onto mesoporous silica.

1.4.2 Incorporation of the Organic Functionality by Direct-Assembly

Direct-assembly is co-condensation of an organosilane with the inorganic precursor in the initial reaction mixture as shown in Figure 1.5. The resulting products have the anhydrous formula $(SiO_2)_{1-x}(LSiO_{1.5})_x$, where L is the organic group of interest and x is the fraction of framework silicon centers that are functionalized. Thus the organic moiety is covalently linked within the structure through a non-hydrolyzable Si-C bond. This one-pot synthesis allows for a greater loading of the organic group, fewer steps in the overall synthesis, recovery of the surfactant, greater accessibility to the organic groups, and more homogenous distribution of the organic groups. Table 1.1 illustrates the multitude of directly-assembled functionalized mesoporous materials and some applications of these structures. Until recently, direct-assembly was limited to organosilanes and TEOS, since the two are miscible. However, this process has recently been extended to the use of sodium silicate as the inorganic silica source.[43,44] Mesoporous materials prepared with sodium silicate as the inorganic precursor are also included in Table 1.1.

By incorporating organic moieties in the mesostructure framework via the direct-assembly route, the organic groups are dangling like pendants and typically very accessible. Heteroatoms at the end of a propyl chain, e.g. mercaptopropyl, aminopropyl, or cyanopropyl are the most commonly incorporated groups. This is due to their myriad of applications in catalysis and environmental remediation and the length of the alkyl chain. One of the more complex moieties incorporated by direct-assembly is the calix[8]arene moiety.[45] The synthesis is shown in Figure 1.6. The calix[8]arene amide molecule was modified to form monomer 1 which in turn was co-polymerized with

15

tetramethoxysilane around the surfactant CTAB under basic conditions to form an

organo-functionalized mesostructure.[46]
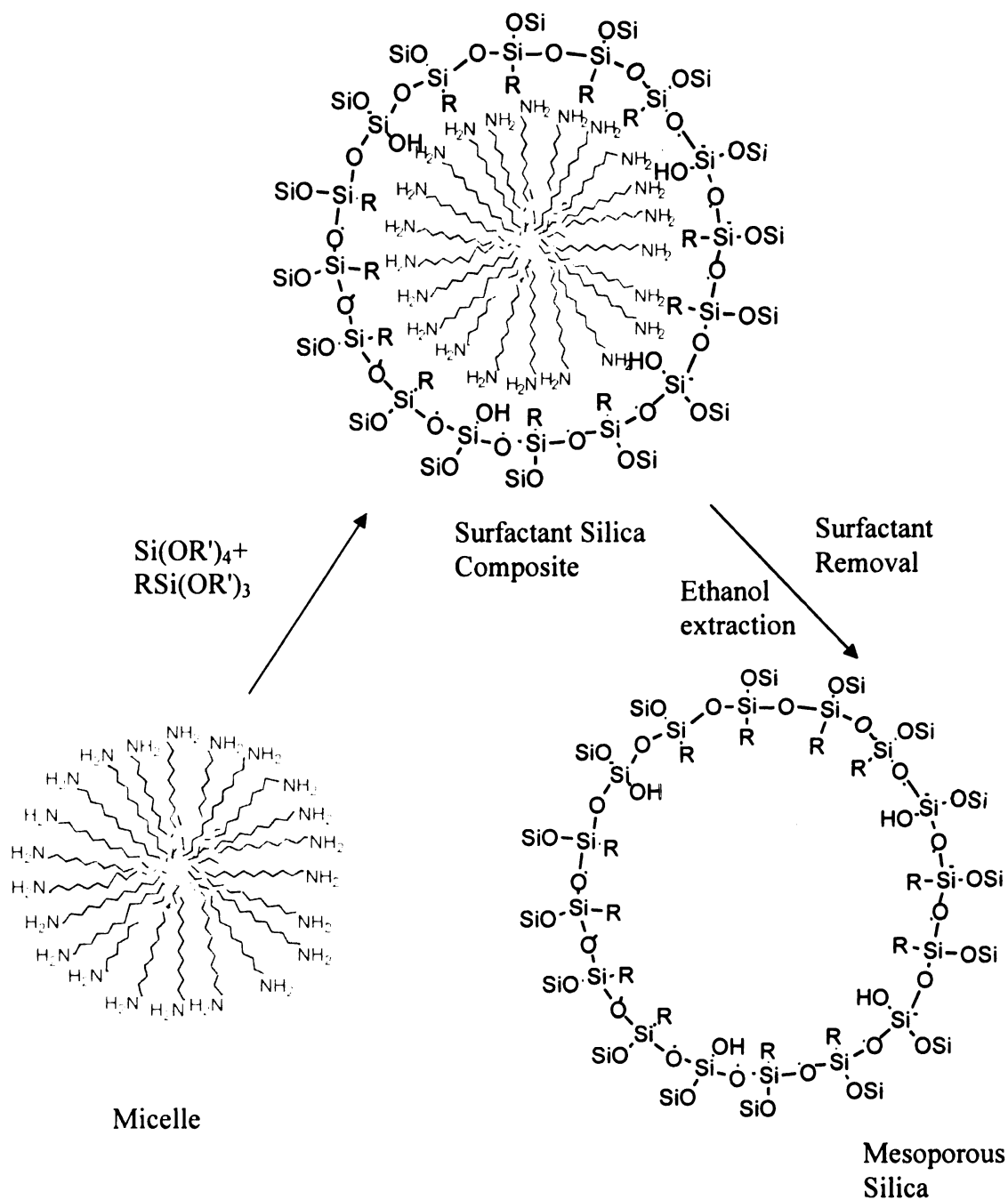
Figure 1.5 Schematic representation of direct-assembly process of organic incorporation into mesoporous silicas.

17

Table 1.1 Comparison of directly-assembled functionalized mesoporous silicas.

Mesostructure	Organofunctional group	Maximum organic loading incorporated mmol/g	Uses
MCM-41[47]	Vy	8.32	
MCM-41[41,48]	Vy	3.5 added	
MCM-41[49]	Ph, octyl	2.72, 1.5 added	
MCM-41[50]	MP, SO$_3$H	4.7	Solid acid catalyst and mercury adsorption
MCM-41[40]	MP	4.03	Mercury adsorption
MCM-41[42]	AP, NN, NNN	1.6, 1.70, 1.78	Iron and cobalt adsorption
MCM-41[51]	AP, NN, NNN, UDP, ICP, CN, Vy	1.7, 0.7, 1.0, 0.9, 1.5, 1.4, 1.7	
MCM-41[52]	MP,AP, EP,Vy	2.7 added	
MCM-41[53]	diMe (CH$_3$)$_2$SiO	5.35 added	
MCM-41[45]	Calix[8]arene	4 %	Humic acid removal
SBA-15[54]	MP, SO$_3$H	2.7 added	Examined acid capacities
SBA-15[55]	Et, NN	2.7 added	Cu^{2+} adsorption
SBA-15[56]	AP	1.18	
SBA-15[57]	AP, MP, Vy, Ph, BN	1.4, 2.14, 2.14, 3.8, 2.14 added	
HMS[58]	MP	5.6	
HMS[59]	MP,AP,NN,NNN	2.1,1.8,1.6,1.1	Cu^{2+},Ni^{2+},Co^{2+},Cd^{2+},CrO$_4^{2-}$ adsorption
HMS[60]	Octyl, MP, Ph, Bu, Pr, Et	0.86, 1.22,0.83, 0.90, 0.68, 0.30	
HMS[61,62]	AP, CN	1.5, 1.5 added	Knoevenagel condensation of ketones with ethyl cyanoacetate
HMS[63]	AP, MeNH, Cl, CN, Vy	3.0, 3.6, 3.9, 3.7, 3.6	
HMS[64]	AP, NN	5.0, 3.7	Scavenge electrophiles
HMS and MSU-X[65]	Cl	1.5, 1.24	React with cyclam to in turn trap metal salts
MSU-X[66-69]	MP	2.3	Mercury adsorption
MSU-X'[43]	AP, MP, CN, Ph,	2.69, 2.83, 5.06, 2.72	
MSU-X'[44]	Me, MP, Vy	1.5, 1.35, 1.35	

AP-aminopropyl, BN-butyronitrile, CN-cyanopropyl, EP-(epoxypropoxy)propyl, ICP- isocyanatopropyl, MP-mercaptopropyl, NN-ethylenediamine, NNN-diethylenetriamine, Octyl-C$_8$, Ph-phenyl, UDP-ureidopropyl, Vy-vinyl
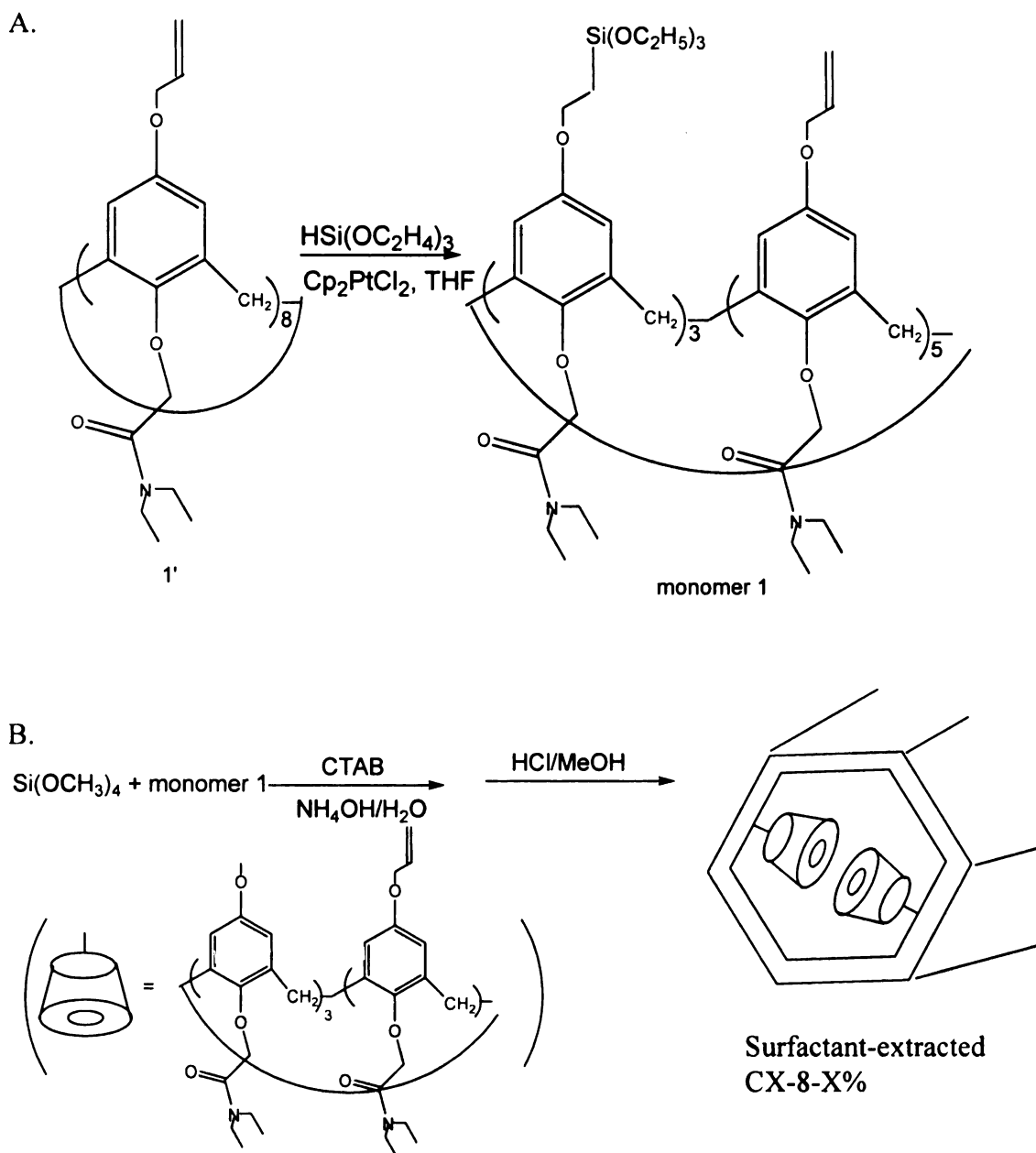
Figure 1.6. A. The synthetic route to CX-8-containing monomer **1**. B. The synthetic route to ordered mesoporous **CX-8-X%** silicas.[45]

19

A.

HSi(OC₂H₄)₃
Cp₂PtCl₂, THF

1'

monomer 1

B.

Si(OCH₃)₄ + monomer 1 —— CTAB / NH₄OH/H₂O —— HCl/MeOH ——→

Surfactant-extracted
CX-8-X%

Figure 1.6. A. The synthetic route to CX-8-containing monomer **1**. B. The synthetic route to ordered mesoporous **CX-8-X%** silicas.[45]

Stein examined the stability and reactivity of vinyl groups incorporated by direct assembly versus grafted on hexagonal MCM-41.[41] It was concluded that the vinyl groups incorporated by the grafting method were not uniformly distributed though the material, yet the grafted mesostructure was more hydrothermally stable. The grafting process also allows for the hexagonal long-range order of material to be retained. Directly assembled mesoporous silicas typically lose long-range order after 20% of the silanes are functionalized.

Mercier and Pinnavaia[60] compared various organo-functionalized HMS silicas prepared by direct assembly and grafting. It was determined that the silicas prepared by direct-assembly method of organo-functionalization retained higher surface areas (891 vs. 722 m^2/g) and pore volumes (0.60 vs. 0.56) than the grafted counter parts.[60] Moreover, the directly-assembled functionalized HMS displayed more uniformly distributed functional groups in the pore channels than the grafted silicas, based on the narrower pore size distributions from the Horvath-Kawazoe method of pore size distribution.

Overall, direct-assembly is the preferred method of organic incorporation, but amines seem to be a caveat to this generality. One of the difficulties with incorporation of amine in the mesostructure is their reactivity. Under acidic conditions, protonated terminal amine groups can interact with silanol groups to form zwitterions (-NH_3^+ --- SiO^-)[40] thus disrupting the interaction of the silane with the surfactant. Another problem is that the mesostructure might collapse due to the basic character of the amine which can contribute to the local hydrolysis of the organosilane reagent in the presence of water.[40] Tatsumi et al. examined the incorporation of mono-, di- and tri-amines via direct-assembly and grafting.[42] With the grafting procedure, more functionality could be

integrated into the mesostructure than with direct-assembly (up to 3.8 mmol/g versus 1.78 mmol/g respectively). Nonetheless, in cobalt and iron adsorption with an amine functionalized mesostructure the metal uptake was linear with respect to the amount of amines present for the direct-assembly method, i.e. the more amine ligands the greater the metal uptake. This was not the case for the amine grafted mesostructures. Cobalt adsorption was greatest for the monoamine and less for the di- and triamines. All of the grafted mesostructures adsorbed less cobalt than that of the directly-assembled materials. Iron uptake by the grafted mono-, di-, and triamine was independent of the amount of ligand present, but uptake was greater than for that of the direct-assembly method. The grafted triamine functionalized mesostructure had an uptake of iron less than that of the directly-assembled triamine as well as the grafted mono- and diamine mesostructure. All of which illustrates the inaccessibility and randomness of organic moiety distribution in the case of the grafting method.

1.4.4 Multifunctional Mesoporous Silicas

Going beyond the organo-functionalization of mesoporous materials with one functional group, the incorporation of two or more different organic groups has been accomplished. Incorporation of different organic groups within the same sample allows for those properties unique to each functional group to be imparted to the material. For example, one functional group might serve as a catalyst (covalent/active site), and the second will provide noncovalent interactions (change hydrophobicity/hydrophilicity). In addition to imparting different chemical properties to the material, bi-functionality can be used to control particle morphology.[51] As with mono-functional group incorporation, bi-functionality can be accomplished by either direct assembly incorporation of one moiety then grafting of the second organic group or direct-assembly of both organic groups.

Lin et al. has synthesized mercaptan functionalized MCM-41 by direct-assembly and then grafted propyl, phenyl, or pentafluorophenyl groups.[6] All other bi-functional mesoporous materials have been synthesized using the direct assembly approach for functionalization. Directly assembled multi-organically functionalized mesoporous materials have been prepared by both electrostatic and hydrogen bonding pathways. The resulting products have the anhydrous formula $(SiO_2)_{1-(x+y)}(LSiO_{1.5})_x(L'SiO_{1.5})_y$, where L and L' are the organic groups of interest and x and y are the fraction of framework silicon centers that are functionalized. Hexagonal MCM-41[70] was synthesized with triamine functionality and mercaptopropyl, or allyl, or ureidopropyl and used for competitive catalytic nitroaldol reactions. By the addition of the second organic moiety the polarity and hydrophobicity of the system was varied and in turn the selectivity for the product, alkoxybenzaldehyde. Hexagonal SBA-15[54] was synthesized with mercaptopropyl and

benzyl or mercaptopropyl and methyl groups. The mercaptopropyl moieties were oxidized with hydrogen peroxide to sulfonic acid groups, and the solid acid properties of the sulfonic acid functionalized structures assessed by monitoring the ^{31}P MAS NMR chemical shift of triethylphosphineoxide. With the addition of the second functional group, a single somewhat broader ^{31}P MAS NMR peak with a larger chemical shift was observed as compared to the mono-functionalized ^{31}P MAS NMR spectra. Wormhole HMS has been synthesized with bi-functional[62,71-73] and even tri-functional[74] moieties via direct assembly incorporation of the organic groups. Lee et al. incorporated aminopropyl and mercaptopropyl moieties and examined the mercury binding capacity.[71]

Mercaptopropyl (MP) groups are known to efficiently trap mercury, but the addition of MP groups causes the mesostructure to become more hydrophobic. Therefore, by the addition of hydrophilic aminopropyl groups they believed the dual functionalized HMS would be able to be more easily wetted and hence trap mercury more efficiently. The dual functional HMS did adsorb mercury, however, the mercury adsorption capacity was small as compared with other mercaptan only functionalized adsorbents, 0.76 mmol Hg^{2+}/ g[71] versus 2.3 mmol Hg^{2+}/ g.[67] One reason for the lower adsorption of mercury for the multifunctional mesostructure is the low loading of mercaptan 1.70 mmol SH/g for the multifunctional[71] versus 2.3 mmol SH/g for the monofunctional.[67] The total organic moiety incorporation of the multifunctional mesostructures to date has not been greater than 20 percent of the silicon centers being functionalized, as compared to up to 65 percent of the silicon centers being functionalized[47] for monofunctional mesoporous silicas. Present work is an effort to

achieve the synthesis of bi-functional HMS and incorporate high loadings (in excess of 20 mole percent) of the organosilanes.

1.5 Shape Modification of Mesoporous Materials

Shape control, specifically that of forming spheres for mesoporous materials, is of great importance. The ability to selectively manipulate the size and shape of mesoporous materials allows for expanded utilization in such areas as chromatography, optical materials, drug delivery, or catalytic supports. One method of forming silica spheres was developed by Stoeber. [75] The Stoeber synthesis is an ammonia-catalyzed reaction of tetraethylorthosilicate with water in low-molecular-weight alcohols which produces monodispersed spherical silica nanoparticles that range in size from 5-2000 nm. Under the dilute reaction conditions, nucleation is competitive with propagation of particle growth. The spherical shape is formed because it minimizes the interface between silica and solution. The Stoeber method has been adapted to make mesoporous spheres.[76-78]

Mesoporous spheres have also been synthesized by control of the condensation and hydrolysis of the silica source, typically tetraethylorthosilicate (TEOS). The isoelectronic point of silica is at pH=2.0, above this point, silica particles are charged. By controlling the pH and concentration of silica particles or forming an emulsion, spherical silica can be synthesized. Electrostatic[79] and hydrogen bonding[14,80] assembly pathways have been able to produce spherical mesoporous materials.

Although spherical mesoporous materials are of interest, add to this the ability to organically functionalize the spheres, and a very powerful media is born. Functionalized mesoporous materials will open new opportunities in the field of chromatography, catalysis, and drug delivery among others. The ability to specifically tune

chromatography columns for heavy metal adsorption, catalysis, or control hydrophobicity will allow for a myriad of new applications. Functionalized spherical mesoporous silicas have been prepared by both electrostatic[81-83] and hydrogen bonding[84] pathways with up to 40 percent of the silicon sites being functionalized. One objective of this work is to develop synthesis strategies for the formation of organo-functionalized mesoporous spheres.

1.6 Remediation of Recalcitrant Compounds with Functionalized Mesoporous Silicas

1.6.1 Mercury Trapping

Table 1.1 illustrates a few processes for which organo-functionalized mesoporous silicas have been used. One prominent and well-studied use of functionalized mesoporous derivatives is for removal of pollutants. Mercury is a ubiquitous toxic heavy metal, which has deleterious effects to human health. Mercury is released from the burning of fossil fuels, chlor-alkali plants, waste incinerators, and volcanic eruptions. The form of mercury usually released to the atmosphere is that of the elemental mercury vapor. The mercury vapor is then photochemically oxidized by ozone to inorganic Hg^{2+}, and the ionic mercury is washed into water bodies by precipitation.[85,86] Traditional approaches to the removal of mercury ions from solutions have included the use of activated carbon,[87] zeolites,[88] silica gel,[89] sulfide precipitates,[90] ion-exchange resins,[91,92] and clays[93,94] as trapping agents. Low loading capacities, poor selectivity, and in some cases relatively small metal ion binding constants, have impeded the adoption of these materials for remediation applications. As a "soft" Lewis acid, Hg^{2+} forms stable complexes preferentially with soft Lewis bases such as mercaptan ligands. Therefore, the

selectivity and binding constants of the mercuric ion to the adsorbent can be vastly improved by attaching chelating mercaptan ligands to a support matrix. Mercaptan functionalized clays[95-97] and mercaptan functionalized mesoporous silicas[67,71,98-103 104,105] have been shown to be highly selective, have good accessibility to the mercaptan ligands, and have a significantly higher binding capacity than the traditional mercury remediation agents. One research objective of this work is to examine mercury remediation with a functionalized mesoporous silica, denoted MP-HMS which has the anhydrous composition $(SiO_2)_{1-x}$ $(LSiO_{1.5})_x$ where L is the organic group, specifically mercaptopropyl, and x is the fraction of framework silicon centers that are functionalized.

In addition to mesoporous materials functionalized with mercaptans being used for mercury trapping, other functional groups incorporated into mesoporous silicas have been examined for removal of mercury from solution. A 1-allyl-3-propylthiourea (ATU) $(H_2C=CHCH_2NHC(=S)NHCH_2CH_2CH_2)$ modified mesoporous silica was synthesized and found to have a maximum binding capacity of 1.5 mmol Hg^{2+}/g adsorbent.[106] To prepare the 1-allyl-3-propylthiourea functionalized MCM-41, aminopropyl moieties were grafted onto the framework of hexagonal MCM-41 mesostructure. The aminopropyl functionalized MCM-41 was then reacted with allyl isothiocyanate to produce the final product ATU-MCM-41. Although the ATU functional groups did adsorb mercury, 1.5 mmol Hg^{2+}/g adsorbent is lower than the highest reported binding capacity of a mercaptan functionalized mesostructure of 3.8 mmol Hg^{2+}/g adsorbent.[104,105]

Furthermore, the process used to prepare the functional group is tedious, and the surface area of functionalized ATU MCM-41 is a third of the parent material, 320 vs. 900 m^2/g, respectively. Building upon this method Jaroniec also prepared 1-benzoyl-3-

propylthiourea, $C_6H_5C(=O)NHC(=S)NHCH_2CH_2CH_3$, functionalized MCM-41.[107]

Aminopropyl functionalized MCM-41 was prepared by grafting of aminopropyltrimethoxysilane onto MCM-41, followed by reaction of benzoyl isothiocyanate to yield 1-benzoyl-3-propylthiourea functionalized MCM-41. The mercury adsorption capacity of this silica was quite high, 5.0 mmol Hg^{2+}/g adsorbent, which is a 3 to 1 mercury: ligand ratio. The increased coordination was attributed to the formation of Hg-N bonds in addition to Hg-S bonds.[107]

1.6.2 Arsenic Trapping

Arsenic contaminated drinking water is a problem in many countries, including the United States. With the new 10 ppb US EPA MCL (maximum contaminant level), new technologies will be needed to remediate the drinking water. Arsenic in naturally occurring form is found in soil, air, and water. Of the two forms of inorganic arsenic found in ground water, namely, arsenite (As (III)) and arsenate (As (V)), arsenite is the predominant form found in ground water, whereas the arsenate is the major species associated with surface waters. A variety of health effects, e.g. skin and internal cancers, cardiovascular, and neurological effects have been attributed to arsenic exposure, primarily from drinking water.[108] Furthermore, arsenite is estimated to be 60-times more toxic than arsenate.[109] However, current remediation techniques[110,111] (e.g., coagulation, nanofiltration, or ion-exchange) are effective only in removing arsenate, but not arsenite. This is due in part to arsenite being a neutral species below pH 8.5 in aqueous solution. Thus, the common approach to the removal of arsenite from ground water anticipates oxidizing arsenite to arsenate.

Mesoporous materials have many benefits over traditional recalcitrant compound adsorbents. These include large surface areas, tailoring of pore sizes to be especially accessible, incorporation of organic ligands to provide selectivity towards a specific metal, and great access to the complexing ligands.

Current arsenic remediation efforts based on organo-functionalized mesoporous materials have focused on the trapping of arsenate.[24,112,113] One method of arsenate adsorption relies on the Lewis base properties of the anion and the formation of a complex with a Lewis acid metal centers (i.e., copper(II) or iron(III)) immobilized in the pores of the mesostructure.[112,113] Also, ion pairing of arsenate to tethered ammonium cations[24] has been used as a mechanism for trapping arsenate in mesostructures. However, neither binding mechanism is effective in trapping arsenite. This work will examine the synthesis of functionalized mesoporous silicas for of trapping arsenate, as well as arsenite, without oxidation of the latter to the former.

1.6.2 Radioactive Element Trapping

The US has vast amounts of mixed radioactive waste generated from nuclear arsenals built up during the Cold War era; these wastes include actinides. One ligand known to be suitable for chelation of the actinide cation is the carbamoylphospine oxide (CMPO) ligand(O=PC=ONH$_2$).[114] Aminopropyltrimethoxysilane was reacted with a trifluoroethyl ester in the reaction shown below, and the product was grafted onto MCM-41 to form CMPO functionalized MCM-41.[114]
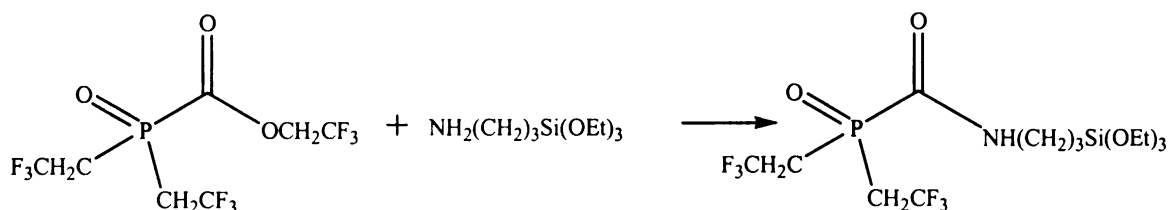
The CMPO MCM-41 has proven to be a highly efficient and selective Pu(IV) sequestrate.[115] The distribution coefficient (K_d) for the adsorption of Pu(IV) was 20,000. The K_d is a mass-weighted partition coefficient, defining the distribution of the target analyte between the solution and the solid at equilibrium. Thus with a K_d of 20,000, there was 200 times as much Pu(IV) adsorbed to the solid as was left in the filtrate.[115]

In addition to contamination with actinides, the production of nuclear materials also generated radionuclides including isotopes of cesium and technetium. Ferrocyanides have been shown to have a high affinity for the radiocesium.[116] The synthesis and use of copper ferrocyanide immobilized on MCM-41 for the sequestration of cesium has been reported.[117] The synthesis of cesium selective SAMMS (self-assembled monolayers on mesoporous supports) is depicted below.[117]
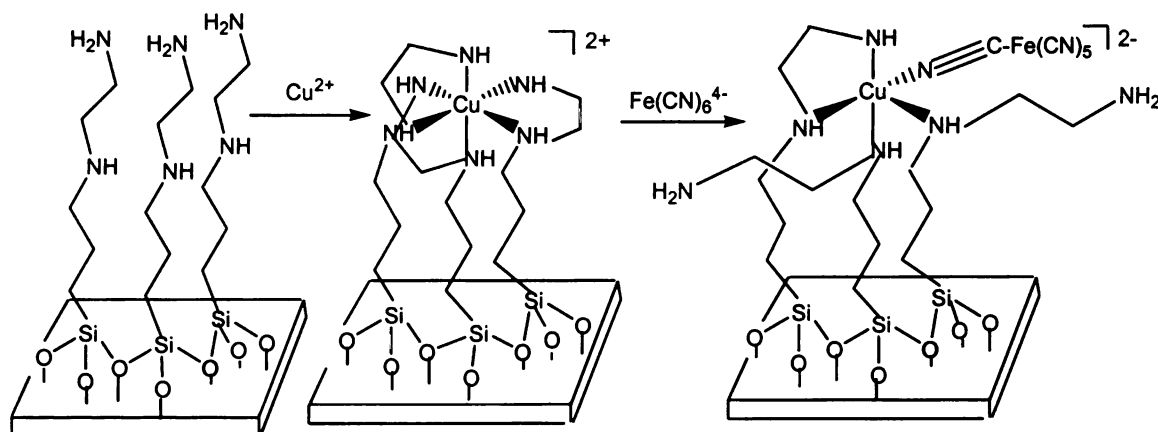
The parent mesostructure SAMMS is MCM-41 silica which is calcined to remove the surfactant. Ethylenediamine ligands were grafted onto the mesoporous support, and copper ions, from cuprous chloride were bonded to the amine ligands to form octahedral complexes on the surface of the mesoporous silica. Then, ferrocyanide was immobilized on the surface of the mesoporous silica by coordination with the copper. The final product denoted Cu-FC-EDA-SAMMS was used for cesium adsorption.[117] The cesium concentration was reduced from 2 ppm to less than 4 ppb within 1 min and to less than 1 ppb within 2 h.[117]

1.7 References

(1)   Beck, J. S., Vartuli, J.C., Roth, W.J., Leonowicz, M.E., Kresge, C.T., Schmitt,
        K.D., Chu, C.T-W., Olson, D.H., Sheppard, E.W., McCullen, B., Higgins, J.B.,
        Schlenker, J.L. *J. Am. Chem. Soc.* **1992**, *114*, 10834.

(2)   Mercier, L.; Pinnavaia, T. J. *Adv. Mater.* **1997**, *9*, 500-&.

(3)   Fryxell, G. E.; Liu, J.; Hauser, T. A.; Nie, Z. M.; Ferris, K. F.; Mattigod, S.;
        Gong, M. L.; Hallen, R. T. *Chem. Mater.* **1999**, *11*, 2148-2154.

(4)   Feng, X.; Fryxell, G. E.; Wang, L. Q.; Kim, A. Y.; Liu, J.; Kemner, K. M. *Science*
        1997, *276*, 923-926.

(5)   Takahashi, H.; Inagaki, S.; Kajino, T.; Usuki, A.; Li, B. In *Eur. Pat. Appl.*;
        (Kabushiki Kaisha Toyota Chuo Kenkyusho, Japan). Ep, 1999, p 18 pp.

(6)   Lin, V. S.; Lai, C. Y.; Huang, J.; Song, S. A.; Xu, S. *J. Am. Chem. Soc.*
        2001, *123*, 11510-11511.

(7)   Pauly, T. R.; Liu, Y.; Pinnavaia, T. J.; Billinge, S. J. L.; Rieker, T. P. *J. Am.
        Chem. Soc.* **1999**, *121*, 8835-8842.

(8)   Beck, J. S.; Vartuli, J. C.; Roth, W. J.; Leonowicz, M. E.; Kresge, C. T.; Schmitt,
        K. D.; Chu, C. T. W.; Olson, D. H.; Sheppard, E. W.; McCullen, S. B.; Higgins, J.
        B.; Schlenker, J. L. *J. Am. Chem. Soc.* **1992**, *114*, 10834-10843.

(9)   Beck, J. S.; Vartuli, J. C.; Kennedy, G. J.; Kresge, C. T.; Roth, W. J.; Schramm,
        S. E. *Chem. Mater.* **1994**, *6*, 1816-1821.

(10)   Zhao, D. Y.; Feng, J. L.; Huo, Q. S.; Melosh, N.; Fredrickson, G. H.; Chmelka, B.
        F.; Stucky, G. D. *Science* **1998**, *279*, 548-552.

(11)   Zhao, X. S.; Lu, G. Q. *J. Phys. Chem. B* **1998**, *102*, 1556-1561.

(12)   Zhao, D. Y. Q., Huo; Jianglin Feng; Bradley Chmelka; Galen D Stucky *J. Am.
        Chem. Soc.* **1998**, *120*, 6024-6036.

(13)   Tanev, P. T.; Pinnavaia, T. J. *Science* **1995**, *267*, 865-867.

(14)   Pauly, T. R.; Pinnavaia, T. J. *Chem. Mater.* **2001**, *13*, 987-993.

(15)   Bagshaw, S. A.; Prouzet, E.; Pinnavaia, T. J. *Science* **1995**, *269*, 1242-1244.

(16)   Bagshaw, S. A.; Pinnavaia, T. J. *Angew. Chem.-Int. Edit. Engl.* **1996**, *35*, 1102-1105.

(17)   Schmidt-Winkel, P.; Lukens, W. W.; Yang, P. D.; Margolese, D. I.; Lettow, J. S.; Ying, J. Y.; Stucky, G. D. *Chem. Mater.* **2000**, *12*, 686-696.

(18)   Fan, J.; Lei, J.; Wang, L.; Yu, C.; Tu, B.; Zhao, D. *Chem. Commun.* **2003**, 2140-2141.

(19)   Han, Y.-J.; Watson, J. T.; Stucky, G. D.; Butler, A. *J. Mol. Catal. B: Enzym.* **2002**, *17*, 1-8.

(20)   Yiu, H. H. P.; Wright, P. A.; Botting, N. P. *J. Mol. Catal. B: Enzym.* **2001**, *15*, 81-92.

(21)   Sing, K. S. W.; Everett, D. H.; Haul, R. A. W.; Moscou, L.; Pierotti, R. A.; Rouquerol, J.; Siemieniewska, T. *Pure Appl. Chem.* **1985**, *57*, 603-619.

(22)   Horvath, G.; Kawazoe, K. *J. Chem. Eng. Jpn.* **1983**, *16*, 470-475.

(23)   Huh, S.; Wiench Jerzy, W.; Trewyn Brian, G.; Song, S.; Pruski, M.; Lin Victor, S. Y. *Chem. Commun.* **2003**, 2364-2365.

(24)   Yoshitake, H.; Yokoi, T.; Tatsumi, T. *Chem. Mater.* **2002**, *14*, 4603-4610.

(25)   Clark, J. H.; Macquarrie, D. J. *Chem. Commun.* **1998**, 853-860.

(26)   Van Rhijn, W. M.; De Vos, D. E.; Sels, B. F.; Bossaert, W. D.; Jacobs, P. A. *Chem. Commun.* **1998**, 317-318.

(27)   Van Rhijn, W.; De Vos, D.; Jacobs, P. A. *Stud. Surf. Sci. Catal.* **1998**, 117, 183.

(28)   Mdoe, J. E. G.; Clark, J. H.; Macquarrie, D. J. *Synlett.* **1998**, 625-627.

(29)   Rao, Y. V. S.; De Vos, D. E.; Jacobs, P. A. *Angew. Chem., Int. Ed. Engl* **1997**, *36*, 2661-2663.

(30)   Bellocq, N.; Abramson, S.; Lasperas, M.; Brunel, D.; Moreau, P. *Tetrahedron-Asymmetr* **1999**, *10*, 3229-3241.

(31)   Johnson, B. F. G.; Raynor, S. A.; Shephard, D. S.; Mashmeyer, T.; Thomas, J. M.; Sankar, G.; Bromley, S.; Oldroyd, R.; Gladden, L.; Mantle, M. D. *Chem. Commun.* **1999**, 1167-1168.

(32)   Lei, C.; Shin, Y.; Liu, J.; Ackerman, E. J. *J. Am. Chem. Soc.* **2002**, *124*, 11242-11243.

(33)   Kulak, A.; Hall, S. R.; Mann, S. *Chem. Commun.* **2004**, 576-577.

(34)   Lai, C.-Y.; Trewyn, B. G.; Jeftinija, D. M.; Jeftinija, K.; Xu, S.; Jeftinija, S.; Lin, V. S. Y. *J. Am. Chem. Soc.* **2003**, *125*, 4451-4459.

(35)   Lin, V. S. Y.; Lai, C.-Y.; Trewyn, B. G. *Abstracts of Papers, 225th ACS National Meeting, New Orleans, LA, United States, March 23-27, 2003* **2003**, MTLS-029.

(36)   Dai, S.; Burleigh, M. C.; Shin, Y. *Angew. Chem., Int. Ed. Engl.***1999**. 38, 1235.

(37)   Macquarrie, D. J. *Philos. Trans. R. Soc. London, Ser. A* **2000**, *358*, 419-430.

(38)   Morey, M. S.; O'Brien, S.; Schwarz, S.; Stucky, G. D. *Chem. Mater.* **2000**, *12*, 898-911.

(39)   Schmidt-Winkel, P.; Lukens, W. W.; Zhao, D. Y.; Yang, P. D.; Chmelka, B. F.; Stucky, G. D. *J. Am. Chem. Soc.* **1999**, *121*, 254-255.

(40)   Walcarius, A.; Etienne, M.; Lebeau, B. *Chem. Mater.* **2003**, *15*, 2161-2173.

(41)   Lim, M. H.; Stein, A. *Chem. Mater.* **1999**, *11*, 3285-3295.

(42)   Yokoi, T.; Yoshitake, H.; Tatsumi, T. *J. Mater. Chem.* **2004**, *14*, 951-957.

(43)   Shah, J.; Kim, S.-S.; Pinnavaia, T. J. *Chem. Commun.* **2004**, 572-573.

(44)   Yu, N.; Gong, Y.; Wu, D.; Sun, Y.; Luo, Q.; Liu, W.; Deng, F. *Microporous Mesoporous Mater.* **2004**, *72*, 25-32.

(45)   Liu, C.; Naismith, N.; Fu, L.; Economy, J. *Chem. Commun.* **2003**, 2472-2473.

(46)   Liu, C.; Lambert, J. B. *Polym. Mater. Sci. Eng.* **2003**, *88*, 433-434.

33

(47)   Kruk, M.; Asefa, T.; Jaroniec, M.; Ozin Geoffrey, A. *J. Am. Chem. Soc.* **2002**, *124*, 6383-6392.

(48)   Lim, M. H.; Blanford, C. F.; Stein, A. *J. Am. Chem. Soc.* **1997**, *119*, 4090-4091.

(49)   Burkett, S. L.; Sims, S. D.; Mann, S. *Chem. Commun.* **1996**, 1367-1368.

(50)   Lim, M. H.; Blanford, C. F.; Stein, A. *Chem. Mater.* **1998**, *10*, 467-+.

(51)   Huh, S.; Wiench, J. W.; Yoo, J.-C.; Pruski, M.; Lin, V. S. Y. *Chem. Mater.* **2003**, *15*, 4247-4256.

(52)   Fowler, C. E.; Burkett, S. L.; Mann, S. *Chem. Commun.* **1997**, 1769-1770.

(53)   Joo, J.; Hyeon, T.; Hyeon-Lee, J. *Chem. Commun.* **2000**, 1487-1488.

(54)   Margolese, D.; Melero, J. A.; Christiansen, S. C.; Chmelka, B. F.; Stucky, G. D. *Chem. Mater.* **2000**, *12*, 2448-2459.

(55)   Markowitz, M. A.; Klaehn, J.; Hendel, R. A.; Qadriq, S. B.; Golledge, S. L.; Castner, D. G.; Gaber, B. P. *J. Phys. Chem. B* **2000**, *104*, 10820-10826.

(56)   Chong, A. S. M.; Zhao, X. S. *J. Phys. Chem. B* **2003**, *107*, 12650-12657.

(57)   Chong, A. S. M., Zhao, X.S., Kustedjo Angeline T., Qiao, S.Z. *Microporous Mesoporous Mater.* **2004**, *72*, 33-42.

(58)   Mori, Y.; Pinnavaia, T. J. *Chem. Mater.* **2001**, *13*, 2173-2178.

(59)   Bois, L.; Bonhomme, A.; Ribes, A.; Pais, B.; Raffin, G.; Tessier, F. *Colloids Surf., A* **2003**, *221*, 221-230.

(60)   Mercier, L.; Pinnavaia, T. J. *Chem. Mater.* **2000**, *12*, 188-196.

(61)   Macquarrie, D. J. *Chem. Commun.* **1996**, 1961-1962.

(62)   Macquarrie, D. J.; Jackson, D. B.; Tailland, S.; Utting, K. A. *J. Mater. Chem.* **2001**, *11*, 1843-1849.

(63)   Macquarrie, D. J.; Jackson, D. B.; Mdoe, J. E. G.; Clark, J. H. *New J. Chem.* **1999**, *23*, 539-544.

(64)   Macquarrie, D. J.; Rousseau, H. *Synlett.* **2003**, 244-246.

(65)   Corriu, R. J. P.; Mehdi, A.; Reye, C.; Thieuleux, C. *Chem. Mater.* **2004**, *16*, 159-166.

(66)   Beaudet, L.; Hossain, K.-Z.; Mercier, L. *Chem. Mater.* **2003**, *15*, 327-334.

(67)   Brown, J.; Richer, R.; Mercier, L. *Microporous Mesoporous Mater.* **2000**, *37*, 41-48.

(68)   Richer, R.; Mercier, L. *Chem. Commun.* **1998**, 1775-1776.

(69)   Richer, R.; Mercier, L. *Chem. Mater.* **2001**, *13*, 2999-3008.

(70)   Huh, S.; Chen, H.-T.; Wiench, J. W.; Pruski, M.; Lin, V. S. Y. *J. Am. Chem. Soc.* **2004**, *126*, 1010-1011.

(71)   Lee, B.; Kim, Y.; Lee, H.; Yi, J. *Microporous and Mesoporous Mater.* **2001**, *50*, 77-90.

(72)   Macquarrie, D. J. *Green Chem.* **1999**, *1*, 195-198.

(73)   Mel'nyk, I. V.; Zub, Y. L.; Chuiko, A. A.; Jaroniec, M.; Mann, S. *Stud. Surf. Sci. Catal.* **2002**, *141*, 205-212.

(74)   Zub, Y. L.; Seredyuk, I. V.; Chuiko, A. A.; Jaroniec, M.; Jones, M. O.; Parish, R. V.; Mann, S. *Mendeleev Commun.* **2001**, 208-210.

(75)   Stoeber, W.; Fink, A.; Bohn, E. *J. Colloid Interface Sci.* **1968**, *26*, 62-69.

(76)   Cai, Q.; Luo, Z.-S.; Pang, W.-Q.; Fan, Y.-W.; Chen, X.-H.; Cui, F.-Z. *Chem. Mater.* **2001**, *13*, 258-263.

(77)   Grun, M.; Unger, K. K.; Matsumoto, A.; Tsutsumi, K. *Microporous Mesoporous Mater.* **1999**, *27*, 207-216.

(78)   Nooney, R. I.; Thirunavukkarasu, D.; Chen, Y.; Josephs, R.; Ostafin, A. E. *Chem. Mater.* **2002**, *14*, 4721-4728.

(79)   Kosuge, K.; Singh, P. S. *Microporous Mesoporous Mater.* **2001**, *44-45*, 139-145.

(80) Boissiere, C.; van der Lee, A.; El Mansouri, A.; Larbot, A.; Prouzet, E. *Chem. Commun.* **1999**, 2047-2048.

(81) Etienne, M.; Lebeau, B.; Walcarius, A. *New J. Chem.* **2002**, *26*, 384-386.

(82) Ganesan, V.; Walcarius, A. *Langmuir* **2004**, *20*, 3632-3640.

(83) Kosuge, K.; Murakami, T.; Kikukawa, N.; Takemori, M. *Chem. Mater.* **2003**, *15*, 3184-3189.

(84) Sadasivan, S.; Khushalani, D.; Mann, S. *J. Mater. Chem.* **2003**, *13*, 1023-1029.

(85) McElroy, W. J.; Munthe, J. *Acta Chem. Scand.* **1991**, *45*, 254-257.

(86) Munthe, J.; Xiao, Z. F.; Lindqvist, O. *Water, Air, Soil Pollut.* **1991**, *56*, 621-630.

(87) Huang, C. P.; Blankenship, D. W. *Water Res.* **1984**, *18*, 37-46.

(88) Zamzow, M. J. E., B.R.; Sandgren, K.R.; Shanks, D.E. *Sep. Sci. Technol.* **1990**, *25*, 1555-1569.

(89) Prado, A. G. S.; Arakaki, L. N. H.; Airoldi, C. *Green Chem.* **2002**, *4*, 42-46.

(90) Ghazy, S. E. *Sep. Sci. Technol.* **1995**, *30*, 933-947.

(91) Chiarle, S.; Ratto, M.; Rovatti, M. *Water Res.* **2000**, *34*, 2971-2978.

(92) Dujardin, M. C.; Caze, C.; Vroman, I. *React. Funct. Polym.* **2000**, *43*, 123-132.

(93) Sikalidis, C. A.; Alexiades, C.; Misaelides, P. *Toxicological and Environmental Chemistry* **1989**, *20-1*, 175-180.

(94) Keizer, P., Bruggenwert, M. G. M. *NATO ASI Ser. E* **1991**, *190*, 177-203.

(95) Lagadic, I. L.; Mitchell, M. K.; Payne, B. D. *Environ. Sci. Technol.* **2001**, *35*, 984-990.

(96) Mercier, L.; Detellier, C. *Environ. Sci. Technol.* **1995**, *29*, 1318-1323.

(97) Mercier, L.; Pinnavaia, T. J. *Microporous Mesoporous Mater.* **1998**, *20*, 101-106.

(98)   Feng, X.; Fryxell, G. E.; Wang, L. Q.; Kim, A. Y.; Liu, J.; Kemner, K. M. *Science* **1997**, *276*, 923-926.

(99)   Liu, A. M.; Hidajat, K.; Kawi, S.; Zhao, D. Y. *Chem. Commun.* **2000**, 1145-1146.

(100)   Mercier, L.; Pinnavaia, T. J. *Adv. Mater.* **1997**, *9*, 500-503.

(101)   Mercier, L.; Pinnavaia, T. J. *Environ. Sci. Technol.* **1998**, *32*, 2749-2754.

(102)   Brown, J.; Mercier, L.; Pinnavaia, T. J. *Chem. Commun.* **1999**, 69-70.

(103)   Nooney, R. I.; Kalyanaraman, M.; Kennedy, G.; Maginn, E. J. *Langmuir* **2001**, *17*, 528-533.

(104)   Walcarius, A.; Delacote, C. *Chem. Mater.* **2003**, *15*, 4181-4192.

(105)   Kim, Y.; Lee, B.; Yi, J. *Sep. Sci. Technol.* **2004**, *39*, 1427-1442.

(106)   Antochshuk, V.; Jaronicc, M. *Chem. Commun.* **2002**, 258-259.

(107)   Antochshuk, V.; Olkhovyk, O.; Jaroniec, M.; Park, I.-S.; Ryoo, R. *Langmuir* **2003**, *19*, 3031-3034.

(108)   Abernathy, C. O.; Liu, Y.-P.; Longfellow, D.; Aposhian, H. V.; Beck, B.; Fowler, B.; Goyer, R.; Menzer, R.; Rossman, T.; Thompson, C.; Waalkes, M. *Environ. Health Perspect.* **1999**, *107*, 593-597.

(109)   Jain, C. K.; Ali, I. *Water Res.* **2000**, *34*, 4304-4312.

(110)   US EPA. www.epa.gov/tio/download/remed/542r02004/arsenic_report.pdf 2002.

(111)   Melamed, D.; Office of Superfund Remediation and Technology Innovation, 2004.

(112)   Yoshitake, H.; Yokoi, T.; Tatsumi, T. *Chem. Mater.* **2003**, *15*, 1713-1721.

(113)   Fryxell, G. E.; Liu, J.; Hauser, T. A.; Nie, Z.; Ferris, K. F.; Mattigod, S.; Gong, M.; Hallen, R. T. *Chem. Mater.* **1999**, *11*, 2148-2154.

(114)   Birnbaum, J. C.; Busche, B.; Lin, Y.; Shaw, W. J.; Fryxell, G. E. *Chem. Commun.* **2002**, 1374-1375.

(115) Fryxell, G. E.; Lin, Y.; Wu, H.; Kemner, K. M. *Stud. Surf. Sci. Catal.* **2002**, *141*, 583-590.

(116) Prout, W. E.; Russell, E. R.; Groh, H. J. *J Inorg. Nucl Chem.* **1965**, *27*, 473-479.

(117) Lin, Y.; Fryxell, G. E.; Wu, H.; Engelhard, M. *Environ. Sci. Technol.* **2001**, *35*, 3962-3966.

Chapter 2

Synthesis of spherical organo-functional wormhole mesoporous silicas using dodecylamine as the porogen.

2.1 Introduction

Polystyrene is widely used as a support or stationary phase for many types of chromatography and chemical reactions, due in part to low manufacturing cost. However, the polystyrene backbone can influence the behavior of the column in terms of solvent compatibility and reaction rate. Conventional functionalized polystyrene can be slow to react due to the long periods of time it takes for diffusion through the polymer and the reaction can be further slowed by the polymer's ability or inability to swell. Due to its chemical stability and the fact that it neither swells nor shrinks in the presence of solvents, silica can be a better choice of material for chromatography or supported chemical reactions.

Mesoporous metal oxides with their large surface areas, easily tunable pore sizes, and their ability to be functionalized for specific applications are an ideal support matrices for chromatography and supported chemical reactions. In addition to concern over the chemical composition of a support matrix, attention needs to be paid to the shape of the support particles. Spheres in the micron size range are very desirable due to their ability pack uniformly, as well as being easier to handle than powders. Aggregated as well as individual/monodispersed spherical mesoporous materials have been reported. Monodispersed spheres are more desirable since they have better packing properties than large aggregated spheres.

A myriad of mesoporous spheres have been synthesized by control of the condensation and hydrolysis of the silica source, typically tetraethylorthosilicate (TEOS). The isoelectric point of silica is at pH=2.0. Above this pH, silica particles are negatively charged. At pH values < 2.0, the particles become protonated and have a positive charge. By controlling the pH and concentration of silica reagents, spherical silica can be synthesized.

One example of a spherical mesoporous silica was synthesized by simply controlling the reaction stoichiometry of a wormhole framework HMS silica.[1] In a typical reaction, the silica : surfactant ratio (I^0/S^0) is equal to 4.0; this yields fractal or sponge-like particles.[2] However, when the (I^0/S^0) ratio was increased to 8.0, the TEM images showed non-uniform, monolithic, spherical particles ranging in size from 100 nm to 200 nm.

Boissiere[3,4] utilized a sodium fluoride catalyzed reaction in a mildly acidic medium to produce wormhole MSU-X with spherical particles ranging in size from 3-8 μm. This synthesis produces a spherical morphology by discriminating the assembly process from the tetraethylorthosilicate (TEOS) hydrolysis process. The silica source, TEOS, was dispersed in a non-ionic surfactant solution to obtain an emulsion. Hydrochloric acid was added to destroy the emulsion within minutes, giving a microemulsion composed of monodispersed particles containing both surfactant and silica oligomers. In a second step carried out 18 h later, the hydrolysis of TEOS was induced by the addition of a catalyst, sodium fluoride.

A second report of the synthesis of spherical forms of mesoporous silica also involved forming an emulsion precursor in acidic aqueous media.[5] Primary alkylamine

surfactants were used as the porogen under dilute acidic conditions to produce hard spheres, thick walled spheres, hollow spheres and thin walled hollow spheres. The type of sphere produced was dependent upon the chain length of the alkylamine surfactant, as well as the concentration and volume of the acidic aqueous solution.

Hollow spheres of silica with mesoporous walls were synthesized by dilution and neutralization of an aqueous reaction system.[6] The reaction began with a mixture of TEOS in an alkaline aqueous solution of cetyltrimethylammonium bromide (CTAB), which was quickly subjected to quenching by dilution, with a large amount of water, followed by pH neutralization with hydrochloric acid. A layer of white product slowly formed at the air-water interface.

Mesoporous solid spheres have also been synthesized through phase separation and emulsion chemistry.[7] The oil component in this case is the hydrophobic silicon source, tetrabutylorthosilicate (TBOS). The synthesis procedure simply involved adding TBOS with stirring to an alkaline aqueous solution of CTAB and controlling the stirring speed to vary the size and shape of the final product. The TBOS hydrolyzed to give butyl alcohol (BuOH), which is immiscible with water. Hydrogen bonding between BuOH and water provided a diffusion pathway for the surfactant and water to penetrate the TBOS/BuOH oil droplets. The hydrolysis of TBOS in the droplets form mesoporous spheres ranging in size from 0.2-0.5 mm.

Another emulsion system which has been used for the preparation of mesoporous microspheres utilizes kerosene.[8] Hollow silica spheres were synthesized by a sol-gel process of TEOS in a nonionic water-oil emulsion containing kerosene, sorbitan monooleate, and water.

Psuedomorphic synthesis has been used for the morphological control of MCM-41.[9] A pseudomorph is defined as an altered mineral phase having the outward appearance of another mineral species, and in this case, the MCM-41 grains are pseudomorphs of the silica gel grains (the silica source). Commercial silica gel spheres were mixed in an alkaline solution of CTAB and then autoclaved at 115 °C for 24 h. Although the parent silica was amorphous, the CTAB-treated solid showed X-ray diffraction properties and nitrogen isotherms consistent with MCM-41 mesoporous silica.

A final method for the formation of mesoporous silica spheres is the Stoeber method.[10] The Stoeber synthesis is an ammonia-catalyzed reaction of TEOS with water in low-molecular-weight alcohols which produces monodispersed spherical silica nanoparticles that range in size from 5-2000 nm. Under the dilute reaction conditions nucleation is competitive with propagation of particle growth. The spherical shape is favored because it minimizes the interface between silica and solution.

The ability to control sphere size is important for many applications. In order to achieve high speed and high resolution separation for HPLC (high performance liquid chromatography), the column packing should be less than 20 μm in diameter. Typically, 2-10 μm is desired. Packing of small diameter spheres reduces band broadening and gives narrow peaks. However, high pressure is required to move the eluent though the column. In addition to chromatographic applications, spherical nanoscale mesoporous materials are of interest for use in surface polishing, catalysis, medical implants, and drug delivery. Nanospherical mesoporous MCM-41 was first synthesized using a dilute solution catalyzed by ammonia.[11] The utilization of ammonia as a catalyst in a dilute

system is an adaptation of the Stoeber method. Other groups have also modified the Stoeber method to form nanospherical mesostructures.[12,13]

Add the advantages of spherical silica particles to the ability to organically functionalize the spheres and a very powerful media is born. Functionalized spherical mesoporous materials could open new opportunities in the fields of chromatography, catalysis, drug delivery, sensors, membrane technologies, among others. The ability to specifically tune adsorption columns for heavy metal adsorption, catalysis, or control hydrophobicity may allow for a innumerable of new applications to be developed.

The Stoeber and psuedomorphic synthetic methods have been utilized for the synthesis of organo-functionalized mesostructures via the grafting method. Grafting is the organic functionalization of silicas accomplished by surface anchoring of the organic moieties through the hydroxyls of the incompletely condensed silica. Aminopropyl (AP) and octyl (C_8) moieties have been grafted onto cubic MCM-48 silica to form functionalized MCM-48.[14] The water and acetaldehyde adsorption properties of these materials were examined. Octyl moieties have also been grafted onto hexagonal MCM-41 spheres prepared by the psuedomorphic method[15] and successfully used in reverse-phase liquid chromatography applications.

In addition to the grafting of organic groups to mesoporous silicas, some of the aforementioned methods for preparing non-functionalized mesoporous silicas have been adapted to form directly assembled functionalized mesoporous spheres. Direct-assembly is a process involving co-condensation of an organosilane with the inorganic precursor in the initial reaction mixture. One synthetic strategy that has been successful in forming functionalized mesoporous silicas is the Stoeber method. This process has also been used

to directly-assemble microspherical mercaptopropyl (MP) and aminopropyl (AP) functionalized MCM-41 mesoporous derivatives.[16-19]

Mercaptopropyl functionalized, monodisperse spheres of wormhole MSU-X silica have been synthesized by direct assembly methods under mild acid hydrolysis conditions using sodium fluoride as a catalyst.[20] It has been proposed that spheres are formed in a two-step fluoride assisted pathway.[21] In the first step a silicon alkoxide was hydrolyzed in a nonionic surfactant solution at pH = 2.0-4.0. In this pH range, TEOS quickly hydrolyzes, but is slow to condense. This solution contained hybrid objects composed of nonionic micelles and silica oligomers. The silica oligomers then were condensed in the PEO corona of the micelles by the addition of sodium fluoride. The mechanism of formation for organofunctionalized spheres is similar.

A third pathway for the direct-assembly of organofunctional mesoporous silica spheres having MCM-41 hexagonal framework topology has been reported.[22] Mercaptopropyl, aminopropyl, and vinyl functional groups were directly incorporated into hexagonal MCM-41 nanoparticle spheres. An electrostatic S^+I^- interaction between the cationic surfactant (S^+) and the anionic silica source (I^-) was achieved by initially mixing the surfactant (CTAB) at an alkaline pH. After 40 seconds, the mixture was diluted with water. After a few minutes, neutralization was accomplished by the addition of 2 M hydrochloric acid (HCl). Various nanoparticle shapes were formed depending on the time delay prior to acid quenching. Additionally, dinitrophenylaminopropyl (DNP) functionalized mesostructured nanoparticles prepared under dilution/neutralization conditions with CTAB as the surfactant have been reported.[23]

Direct-assembly has also been used to prepare mercaptan-functionalized spheres using a primary amine surfactant.[24] Amine surfactants have been previously used to synthesize highly functionalized MP-HMS wormhole framework structures under near neutral conditions.[25] Kosuge et al.[24] modified the HMS synthesis method and adapted the controlled growth mechanism of Boissiere[3,4] to form thiol-functionalized spheres using a primary amine surfactant. They suggested that a neutral S^0I^0 assembly was initially formed from a mixed suspension of alkoxides (TEOS and MPTMS) and the surfactant (dodecylamine). The addition of aqueous hydrochloric acid resulted in immediate nucleation and the assembly of a mesostructure by a $S^+X^-I^+$ pathway. The end result was the formation of the functionalized mesostructural spheres. As an aside, the stirring rate during both the initial S^0I^0 assembly, as well as after addition of the HCl, was instrumental in the determination of the sphere size.

One other class of interesting mesoporous organofunctional silica derivatives that have been prepared in spherical form, but are not mesostructured, are the silicas reported by the Waters Corporation.[26] These hybrid silica spherical particles have an integrated alcohol moiety on the surface. However, no XRD or TEM data were provided in support of the structural assignment. The method utilized is more likely to produce a xerogel rather than a MCM41-type material. A xerogel is the term used for dried forms of open structures which have passed through a gel stage during preparation (e.g. silica gel). The pore structure of a xerogel is not as ordered as a mesostructure, and the surface area is typically less than 100 m^2/g. The silicon alkoxides and organosilicon precursors were added to a solution of surfactant (Triton X), ethanol, and water under high shear mixing to form oil droplets in a continuous water/ethanol phase. The oil droplets were gelled to

form hybrid silicate spherical particles by the addition of ammonium hydroxide. The organofunctional reagent was [3-(methacryloxy)propyl]-trimethoxysilane [$(CH_3O)_3SiCH_2CH_2CH_2OC(O)C(CH_3)=CH_2$]. Through base-catalyzed ester hydrolysis and hydrothermal conditioning, the methacryloxypropyl group was reacted to produce hydroxypropyl moieties. The hydroxypropyl groups were further transformed through a series of classical alcohol reactions including bromination and esterification. Table 2.1 summarizes the various reported organo-functional mesoporous spheres and the method used for their synthesis.

The objective of the present work was to prepare functionalized mesostructured silica spheres using a primary alkylamine as the surfactant. The preparation of spheres in the nanoscale regime, as well as the micron size range, was examined. The resulting products have the anhydrous formula $(SiO_2)_{1-x}(LSiO_{1.5})_x$, where L is the organic group of interest and x is the fraction of framework silicon centers that are functionalized. The organofunctional group selected for this work was the mercaptopropyl group, because of its affinity for mercury and arsenite, as well as the ability of this group to be oxidized to sulfonic acid moieties. The latter functionality is potentially useful for acid catalyzed organic transformations.

For the synthesis of nanoscale functionalized mesoporous silicas, a modified Stoeber method was utilized. The preparation of nanoscale mesoporous silicas using dilute conditions and an alkylamine surfactant has been previously reported.[13] In order to expand on the utilization of the spheres, it was decided to prepare organically functionalized nanoscale mesoporous silica spheres following this method.

In order to synthesize micron-sized spheres, the electrically neutral pathway, S^0I^0, was utilized because of the ability to easily extract and recycle the surfactant. Also this pathway affords higher organic loading than other methods and yields a wormhole framework which is more accessible than hexagonal frameworks. At the time this work was begun, there were no reports of highly functionalized mesoporous nanospheres or microspheres. Reports of highly functionalized mesoporous nanospheres[22,23] and microspheres[24,16,19,27,26] have since been published and are given in Table 2.1. In addition to the report of the synthesis of these spherical mesoporous silicas, the adsorption properties of the structures have been examined.[14,15,24,16,19,27]

Table 2.1. Spherical forms of mesostructured $(SiO_2)_{1-x}$ $(LSiO_{1.5})_x$ compositions.

Mesostructure	Synthesis method	Assembly	Organic moiety	Functional group loading	Particle size	Predominant sphere type	Application
MCM-48[14]	Stoeber	Grafted	Octyl and AP		0.3-0.7 μm	Aggregates	Water and acetaldehyde adsorption
MCM-41[15]	Psuedomorphic	Grafted	Octyl		5 μm	Monodispersed	RP-HPLC
MCM-41[16,19,27]	Stoeber	DA	MP, SO_3H and AP	Up to x=0.50	0.4-0.6 μm	Aggregates	Heavy metal adsorption[17]
MSU-X[20]	Acidic with NaF	DA	MP	Up to x=0.06	2-10 μm	Monodispersed	
MCM-41 type[24]	Acidic	DA	MP	Up to x=0.40	100μm	Monodispersed	Water and benzene adsorption
MCM-41[22]	Dilution/neutralization	DA	MP, AP, and Vy	Up to x=0.15	0.2μm	Monodispersed	
MCM-41[23]	Dilution/neutralization	DA	DNP	x=0.10	10-50 nm	Monodispersed	
Waters Corporation[26]	Sol-gel	DA	Hydroxypropyl	Up to x=0.30	1-5μm	Monodispersed	HPLC

AP-aminopropyl, DNP-dinitrophenylaminopropyl, MP-mercaptopropyl, Octyl-C_8, Vy-vinyl

2.2 Experimental

2.2.1 Reagents

Mercaptopropyltrimethoxysilane, tetraethylorthosilicate, dodecylamine, and ammonia (a 2 M solution in 2-proponol) were purchased from Aldrich and used without further purification. Absolute ethanol was purchased in-house. Water used in the synthesis was double-exchanged to remove cations and anions via a Millipore filter apparatus.

2.2.2 Direct- assembly of mercaptopropyl functionalized Stoeber nanospheres.

Mercaptopropyl-functionalized nano-sized spheres with the composition $(SiO_2)_{1-x}$ $(LSiO_{1.5})_x$, were synthesized from tetraethylorthosilicate (TEOS) and mercaptopropyltrimethoxysilane (MPTMS) using the direct-assembly method of organic group incorporation. An amine surfactant was used as the structure – directing agent, under dilute conditions in the presence of ammonia. Ethanol was used to dissolve the surfactant, and dodecylamine (DDA). Then, water was added to this solution. Next a 2 M solution of ammonia in propanol was added drop wise with a syringe, and the mixture was equilibrated for 5 min. A mixture of TEOS and MPTMS, in absence of a solvent, then was added and the entire mixture was shaken for 24 h at room temperature. The mixture was centrifuged to collect the precipitate, which was then air-dried. The surfactant was removed by Soxhlet extraction in hot ethanol. The overall molar stoichiometry was: 1-x TEOS : x MPTMS : 0.29 DDA : 351 EtOH : 1143 H_2O : 3.79 NH_3 : 23.3 propanol. The x-values used in the synthesis were x=0.0, 0.10, 0.30, and 0.50.

2.2.3 Direct-assembly of mercaptopropyl functionalized HMS micron sized spheres

Mercaptopropyl-functionalized micron-sized spheres were synthesized using the direct-assembly method for organic group incorporation. An amine surfactant, with hydrodynamic forces applied during the beginning of the synthesis yielding the composition $(SiO_2)_{1-x}$ $(LSiO_{1.5})_x$. There were four different methods used to determine the optimal conditions for functionalized mesoporous microsphere formation.

Method I. A mixture of MPTMS and TEOS was added to a solution of surfactant and EtOH and shaken for 30 s. After the water was added to the silane surfactant solution, the reaction mixture was shaken for 2 min and aged statically. Ethanol, warmed to 65 °C, was used to dissolve the surfactant, dodecylamine. A premixed solution of 1-x TEOS and x MPTMS, was then added to the surfactant solution. The solution was vigorously shaken for 30 s and the silanes were allowed to prehydrolyze in the surfactant solution for 40 min. Next, water, pre-warmed to 65 °C, was rapidly added by volume to the surfactant silane solution. The entire mixture was then vigorously shaken for 2 min and left under static conditions in an oven at 65 °C for 36 h. Finally, the solution was filtered, the precipitate collected and air-dried, followed by Soxhlet extraction with ethanol to remove the surfactant. The overall molar stoichiometry employed was: 1-x TEOS : x MPTMS : 0.22 DDA : 6.7 EtOH : 160 H_2O.

Method II. The synthesis follows as in Method I, except that the reaction mixture is aged in a reciprocating water bath at 200 rpm at 65 °C instead of statically. Ethanol, warmed to 65 °C, was used to dissolve the surfactant, dodecylamine. A premixed solution of 1-x TEOS and x MPTMS, with x=0.10 or 0.50, was then added to the surfactant solution. The solution was vigorously shaken for 30 s, and the silanes were allowed to

prehydrolyze in the surfactant solution for 40 min. Next, water, pre-warmed to 65 °C, was rapidly added by volume to the surfactant silane solution. The entire mixture was then vigorously shaken for 2 min and aged in a reciprocating water bath at 65 °C for 36 h. Finally, the solution was filtered, the precipitate collected, and air-dried, followed by Soxhlet extraction with ethanol to remove the surfactant. The overall molar stoichiometry employed was: 1-x TEOS : x MPTMS : 0.22 DDA : 6.7 EtOH : 160 H_2O.

Method III. The synthesis follows as in Method II, except that the silanes were allowed to prehydrolyze in the surfactant solution for 40 min instead of 30 s and the shaking time after the addition of water was shortened. Ethanol, warmed to 65 °C, was used to dissolve the surfactant, dodecylamine. A premixed solution of 1-x TEOS and x MPTMS, with x values of x=0.10, 0.30, 0.50, 0.60, 0.70, or 0.80 was then added to the surfactant solution. The solution was vigorously shaken for 20 s and the silanes were allowed to prehydrolyze in the surfactant solution for 40 min. Next, water, pre-warmed to 65 °C, was rapidly added by volume to the surfactant silane solution. The entire mixture was then vigorously shaken for 20 s and aged at 65 °C and 200 rpm in a water bath for 36 h. Finally, the solution was filtered, the precipitate collected, and air-dried, followed by Soxhlet extraction with ethanol to remove the surfactant. The overall molar stoichiometry employed was: 1-x TEOS : x MPTMS : 0.22 DDA : 6.7 EtOH : 160 H_2O.

Method IV. The synthesis follows as in Method III, except that the order of the addition of water was altered. Ethanol, warmed to 65 °C, was used to dissolve the surfactant, dodecylamine. Next, water, pre-warmed to 65 °C, was rapidly added by volume to the surfactant solution. A premixed solution of 1-x TEOS and x MPTMS was then added to the surfactant-water mixture. The entire mixture was then vigorously shaken for 20 sec

and aged at 65 °C and 200 rpm in a water bath for 36 h. Finally, the solution was filtered, the precipitate collected, and air-dried, followed by Soxhlet extraction with ethanol to remove the surfactant. The overall molar stoichiometry employed was: 1-x TEOS : x MPTMS : 0.22 DDA : 5.0 EtOH : 160 H_2O.

2.3 Physical Measurements

The physical properties of the mercaptopropyl-functionalized Stoeber nanospheres were determined by nitrogen adsorption, powder XRD, and TEM. Nitrogen adsorption-desorption isotherms were measured at −196 °C on a Micrometrics ASAP 2010 sorptometer, the samples being outgassed at 80 °C and 10^{-6} Torr prior to measurement. Powder XRD patterns were collected on a Rigaku rotaflex diffractometer using Cu $K\alpha$ radiation. TEM images were obtained on a JOEL 100CX microscope with a CeB_6 filament and an accelerating voltage of 120 KV. Sample grids were prepared by sonicating samples in ethanol for 20 min, and evaporating one drop of the suspension onto a carbon coated, holey film supported on a 3 mm, 300 mesh copper grid.

The physical properties of the microspherical MP-HMS were determined by nitrogen adsorption, ^{29}Si magic angle spinning nuclear magnetic resonance (MAS-NMR), TEM, scanning electron microscopy (SEM), XRD, and Raman spectroscopy. ^{29}Si MAS-NMR spectra were collected on a Varian 400 solid state NMR spectrometer with a field strength of 400 MHz, under single-pulse mode with a zirconia rotor at a spinning frequency of 4 kHz. A pulse delay of 400 seconds was employed so that there was sufficient time for the nuclei to relax before application of another pulse. Talc was used as a reference. TEM images were obtained on a JOEL 100CX microscope with a CeB_6 filament and an accelerating voltage of 120 KV. Samples were microtomed for TEM via

two different methods. The first set of samples were embedded in LR White and cured for 2 days at 60 °C. The second method used a harder resin denoted Poly/Bed 812 embedding media, cured for 24 h. Two different microtomes were utilized for thin sectioning. SEM samples were gold coated for 4 min with a coating application of 7 nm/min. Imaging was done at an accelerating voltage of 15 kV on a JEOL JSM-6400V. For Raman spectroscopy, samples were packed into glass capillary tubes and analyzed with a Bio-Rad FT Raman Spectrometer equipped with a CCD camera detector using 633 nm radiation from a HeNe laser for excitation and a resolution of 4cm^{-1}. Laser power at the sample was estimated to be about 5mW, and the focused laser beam diameter was ~10 micrometer. A total of 200 scans was used to obtain the spectra.

2.4 Results and Discussion

2.4.1 Direct-assembly of mercaptopropyl functionalized Stoeber nanospheres

The equation for the formation of silica spheres via the Stoeber method is shown in Equation 2.1.

$$(2+y) \text{ H}_2\text{O} + \text{Si(OCH}_2\text{CH}_3)_4 \xrightarrow[\text{H}_2\text{O/EtOH}]{\text{NH}_3} \text{SiO}_2^* \text{ y H}_2\text{O} + \text{CH}_3\text{CH}_2\text{OH}$$
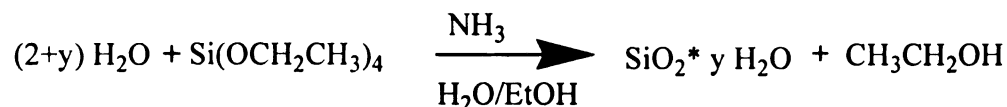
Equation 2.1

Under the dilute reaction conditions employed, nucleation is synchronous with propagation of particle growth. Thus, tiny particles are generated. In order to minimize the interface between silica and solution, spheres spontaneously form. Ammonia is used for the base catalyzed hydrolysis of TEOS. Monodisperse mesoporous silica nanospheres with a particle size of 60 nm have been recently reported for the reaction of TEOS and dodecylamine under modified Stoeber conditions.[13] In order to use these materials for different applications such as catalysis, medical implants, or drug delivery, organofunctionalization is necessary. The present work reports the direct assembly of mercaptopropyl-functionalized silica nanospheres prepared in the presence of an amine surfactant as a porogen and ammonia as a catalyst for TEOS hydrolysis under dilute reaction conditions. The anhydrous reaction for the formation of the nanospherical product is shown in Equation 2.2, where L equals the mercaptopropyl group.

$$1\text{-x Si(OCH}_2\text{CH}_3)_4 + \text{ x LSi(OCH}_3)_3 \xrightarrow[\text{DDA/H}_2\text{O/EtOH}]{\text{NH}_3} (\text{SiO}_2)_{1\text{-x}}(\text{SiO}_{1.5}\text{L})_x + \text{CH}_3\text{CH}_2\text{OH} + \text{CH}_3\text{OH}$$

Equation 2.2

54
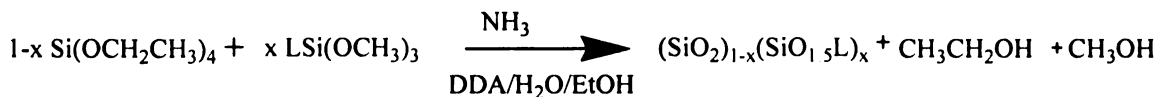
Increasing the organosilicon content (x) of the reaction mixture greatly influenced the structure of the nanospheres. As evident from the TEM images (Figures 2.1 and 2.2), the mesostructure formed at x=0.10 exhibited a beautiful wormhole structure, quite similar to that of the non-functionalized nanospheres. Increasing the organic content of the reaction mixture to x=0.30 and x=0.50 produces more dense spheres, as observed in the TEM micrographs (Figures 2.3 and 2.4). For both the x=0.0 and 0.10 compositions, the TEM images show the presence of non-spherical particles, in addition to the spheres. Only spherical silica particles were observed by Nooney et al.[13] The x=0.30 and 0.50 compositions are totally spherical. The lack of non-spherical powder is most probably due to the increased hydrophobicity of the system from the increased organic content. The tendency to minimize the silica-solution interface is increased by the additional organic groups present. Sphere sizes up to 3,000 nm were observed for the x=0.30 and 0.50 compositions. This is substantially larger that the nanoscale sphere size of ≤100 nm that was previously reported for nanospherical mesoporous structures.[13] Due to the organic content of the functionalized spheres, the growth of the silica particles was faster than the nucleation, thus the larger size spheres.
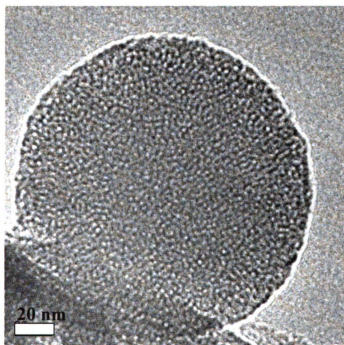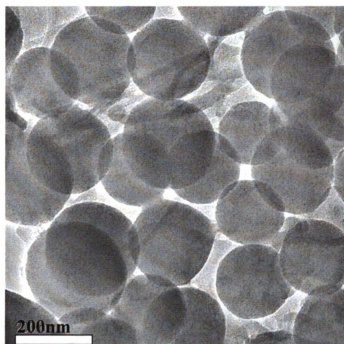
Figure 2.1. Transmission electron microscope image of pure silica (x=0.0) nanospheres at low and high magnification.
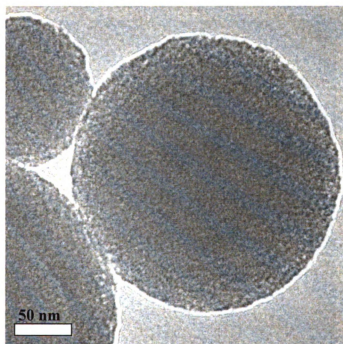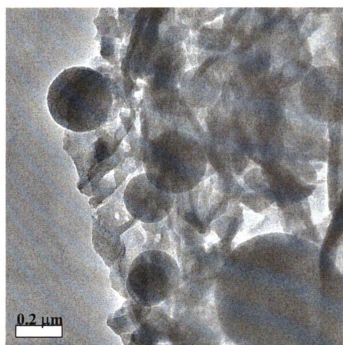
Figure 2.2. Transmission electron microscope image of functionalized $(SiO_2)_{1-x}$ $(LSiO_{1.5})_x$ compositions (L=mercaptopropyl) with x=0.10 and a wormhole framework structure at low and high magnification.
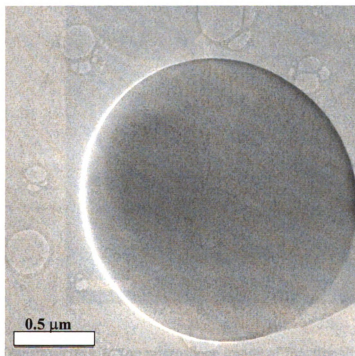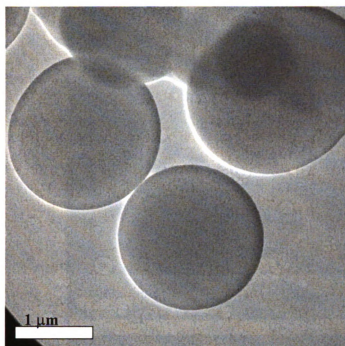
Figure 2.3. Transmission electron microscope image of functionalized $(SiO_2)_{1-x}$ $(LSiO_{1.5})_x$ compositions (L=mercaptopropyl) with x=0.30 at low and high magnification.
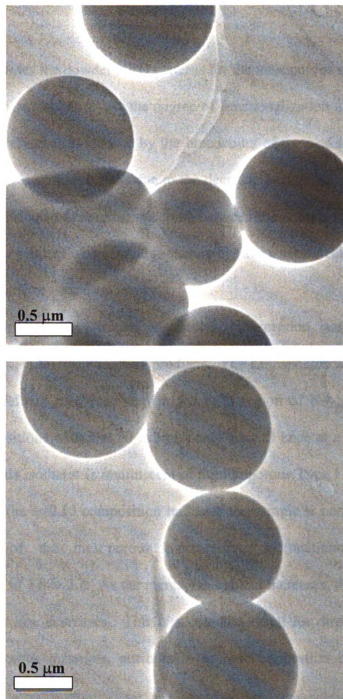
Figure 2.4. Transmission electron microscope image of functionalized $(SiO_2)_{1-x}$ $(LSiO_{1.5})_x$ compositions (L=mercaptopropyl) with x=0.50 at low and high magnification.

Figure 2.5 provides the powder XRD patterns for the mesoporous mercaptopropyl functionalized Stoeber nanospheres. As the degree of functionalization increases, a loss of mesoporosity is observed as evidenced by the broadening of the peaks. The increase in 2Θ for the nanospheres with x=0.30 is due to the decrease in pore size. The intensity decrease can also be attributed to contrast matching between the organic moieties and the silicon framework. The product with x=0.50 (not shown) gave a very weak and broad 2Θ reflection, indicating little or no mesoporosity.

Figure 2.6 provides the nitrogen adsorption – desorption isotherms for the mesostructured $(SiO_2)_{1-x}(LSiO_{1.5})_x$ reaction products. The nanospheres with x=0.00 and 0.10 display a well defined mesopore step in the P/Po region of 0.4 and a Type IV isotherm. The compositions with x=0.30 exhibits only a small knee at a very low P/Po value, below 0.20. This isotherm is reminiscent of a microporous Type I isotherm. The nitrogen isotherm for the x=0.50 composition indicates the sample is non-porous. The physical properties of the mesoporous mercaptopropyl functionalized Stoeber nanospheres are given in Table 2.2. As the mercaptan content increases, the surface area, pore volume and pore size decreases. This is a common result for directly assembled functionalized mesoporous materials, attributable to pore congestion by the organic moieties.
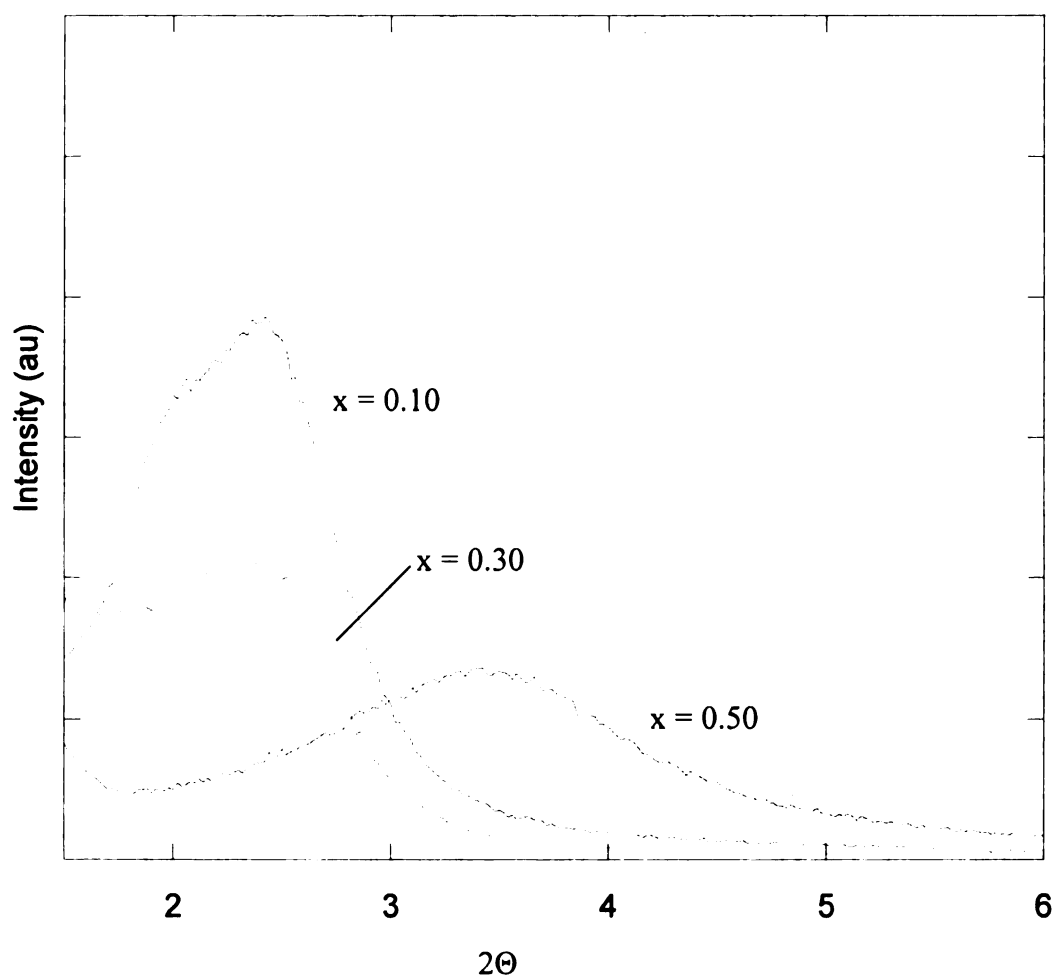
Figure 2.5. XRD patterns of functionalized $(SiO_2)_{1-x}(LSiO_{1.5})_x$ Stoeber nanospheres (L=mercaptopropyl) with x=0.10, 0.30, 0.50.
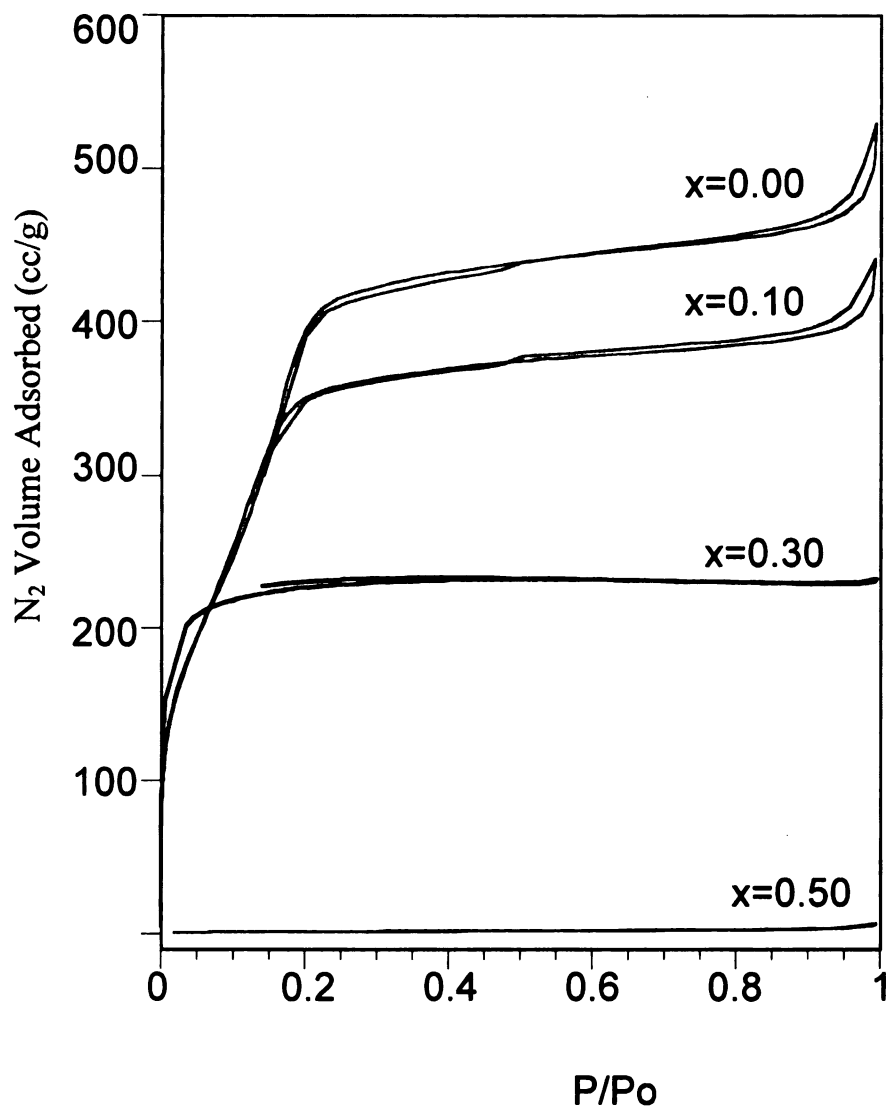
Figure 2.6. Nitrogen Isotherm for functionalized $(SiO_2)_{1-x}(LSiO_{1.5})_x$ Stoeber nanospheres (L=mercaptopropyl) with x=0.0, 0.10, 0.30, and 0.50.

To date there has been no report of a nanospherical organically functionalized mesoporous material assembled with an amine surfactant under dilute conditions using ammonia as a catalyst. However, a mercaptopropyl functionalized MCM-41 material has been reported which was synthesized from TEOS and CTAB as a porogen following a modified Stoeber method.[18] Table 2.3 gives a direct comparison between the mercaptopropyl functionalized Stoeber nanospheres using an alkylamine surfactant and nanospherical MP-MCM-41. As illustrated in Figures 2.1-2.4, the mercaptopropyl functionalized Stoeber nanospheres are predominately individual spheres as opposed to the aggregated spheres reported for the MP-MCM-41.[18] Walcarius[18] was able to incorporate a greater amount of organic functionality, up to x=0.50 for the MP-MCM-41 nanospheres, as opposed to a maximum of x=0.30 with mercaptopropyl functionalized Stoeber nanospheres in this work. Nitrogen adsorption measurements of the nanospherical MP-MCM-41 obtained from fractions of organosilane larger than x=0.25 yielded type I microporous isotherms.[18] The XRD patterns for the compositions with x=0.40 and 0.50 are very weak and have high 2 theta values.[18] The molar ratio of the reagents was different for the two nanospheres; the ratio in this work was more dilute than in Walcarius.[18] The nanospherical molar ratio was: 1.0 SiO_2: 0.41 CTAB: 11.8 ammonia: 65 EtOH:175 H_2O . The nanospherical molar ratio used in this work was: 1.0 SiO_2: 0.29 DDA: 351 EtOH: 1143 H_2O: 3.79 NH_3: 23.3 propanol. Under the more dilute reaction system of this work large aggregated particles were not observed as with the other reported work.[18]

Table 2.2. Physical properties of mercaptopropyl functionalized mesoporous Stoeber nanospheres, synthesized by direct-assembly with an alkylamine porogen.

x_{theo}	SA^a m^2/g	mol SiO_2/L rxn mix	V_{fr}^b cm^3/g	V_t^c cm^3/g	Pore diameter^d (nm)	Spheres from TEM
0.0	1752	0.0052 mol/0.182L	0.655	0.74	2.4	Wormhole, 200 nm ± 25 nm rather uniform
0.10	1507	0.029	0.562	0.60	2.2	Wormhole, 0.2μm-0.6μm, not uniform
0.30	777	0.029	Isotherm type I	0.356	<2.0	Solid, 2μm-3μm, some grown together
0.50	6.0	0.029	Non-porous	-	-	1μm rather uniform some intergrowth present

^{a}Calculated from nitrogen adsorption isotherms by BET method. ^{b}Framework pore volume determined at P/Po = 0.55. ^{c}Total pore volume determined at P/Po = 0.98. ^{d}Determined by the Horvath-Kawazoe model.

Table 2.3. Comparison of physical properties of mercaptopropyl functionalized Stoeber nanospheres synthesized with an alkylamine structure director and nanospherical MP-MCM-41.

Author	x_{theo}	SA^a m^2/g	Sphere size μm	Aggregate size μm
Walcarius[18]	0.00	1264	0.56	5.8 ± 1.4
McKimmy	0.00	1752	0.2 TEM	
Walcarius[18]	0.10	1598	0.62	6.5 ± 1.9
McKimmy	0.10	1507	0.2-0.6 TEM	
Walcarius[18]	0.20	1073	0.58	6.4 ± 1.1
Walcarius[18]	0.30	757	0.55	9.3 ± 1.4
McKimmy	0.30	777	2-3 TEM	
Walcarius[18]	0.50	340	0.5	15.9 ± 1.1
McKimmy	0.50	6.0	1.0 TEM	
Walcarius[18]	0.70	3.4	0.51	14.8 ± 0.7
Walcarius[18]	1.00	2.5	0.44	22.0 ± 2.0

[a]Calculated from nitrogen adsorption isotherms by BET method.

2.4.2 Direct-assembly of mercaptopropyl functionalized HMS microspheres

After examining the results of the mercaptopropyl functionalized Stoeber nanospheres and observing phase segregation in the reaction mixture at high organosilane loadings, a second method for forming functionalized mesoporous spheres was examined. It was hypothesized that due to the presences of organosilanes, there was phase separation between the silanes and water. Vigorous shaking of the phase-segregated reaction mixture will induce the silanes to form mesosphere reagents to minimize the interface between the silica and solution. By increasing the amount of organic functionality in the system, the hydrophobicity of the system is increased. This increased hydrophobicity aides in the formation of spheres by forming an emulsion-like system. As a result of applying vigorous shaking to an emulsion-like system as described in each of the four Methods, mesoporous microspheres form. This would allow spheres to form without the necessity of using very dilute reaction conditions as is typical of a Stoeber reaction system.

Mercaptopropyl-functionalized microspheres have been prepared using direct-assembly organic incorporation in the presence of an amine surfactant as a porogen. These spheres are denoted as microspherical MP-HMS and have the anhydrous formula $(SiO_2)_{1-x}(LSiO_{1.5})_x$ where L is the mercaptopropyl moiety. By simply vigorously shaking the initial reaction mixture for 20 seconds, beautiful mesoporous spheres with varying levels of organic group incorporation were synthesized. The spherical shape is more easily prepared at organic loadings of x=0.30 values and above, as illustrated in Figures 2.7 and 2.8. The microspherical MP-HMS with x=0.10 resulted in the formation of spheres which are predominantly aggregated. Also, at x=0.10 a bulk powder is present in

addition to the silica spheres, whereas the mesostructure compositions with x=0.30, 0.50, and 0.60 are totally spherical, with no bulk powder present. The fact that the higher the organic incorporation, the more spherical the product, indicates that the hydrophobicity of the organic group does play a role in the formation of spheres. The organosilane does not dissolve in ethanol to the extent TEOS does, therefore as the organic component increases, the two different alkoxysilanes (MPTMS and TEOS) form isolated droplets and have a greater interaction with the micelle than the bulk solution.

In synthetic Method I and II, all the reagents are added in the same order and in the same molar quantity. The only difference between the two methods is in the degree of agitation used after all the reagents are mixed, spheres prepared by Method I are aged under static conditions and spheres prepared by Method II are aged with stirring in a reciprocal water bath. Figure 2.9 shows microspherical MP-HMS with x=0.50 made by syntheses Method I and Method II. The sizes of the spheres, as well as the distribution of the spheres' sizes, are quite comparable, indicating that spheres form in the initial part of the synthesis, and that the aging conditions are not a factor for sphere formation. SEM micrographs (not shown) for microspherical MP-HMS with x=0.10, 0.30, and 0.60 prepared by Method I versus Method II illustrate the same results, that spheres are formed in the beginning of the synthesis.
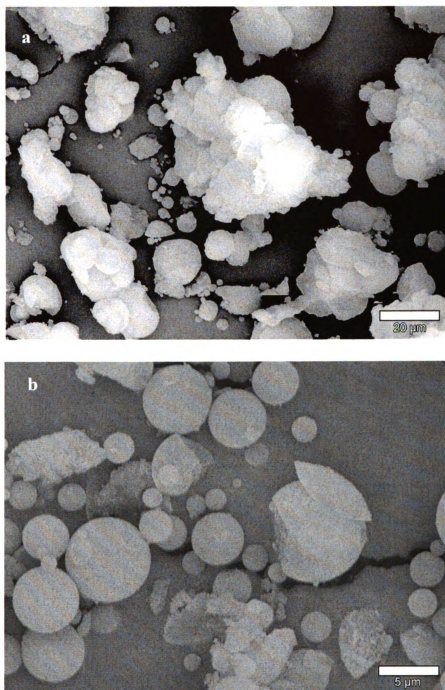
Figure 2.7. SEM image of microspherical functionalized $(SiO_2)_{1-x}(LSiO_{1.5})_x$ (L=mercaptopropyl), denoted microspherical MP-HMS a. x=0.10 prepared by Method I b. x=0.30 prepared by Method I.
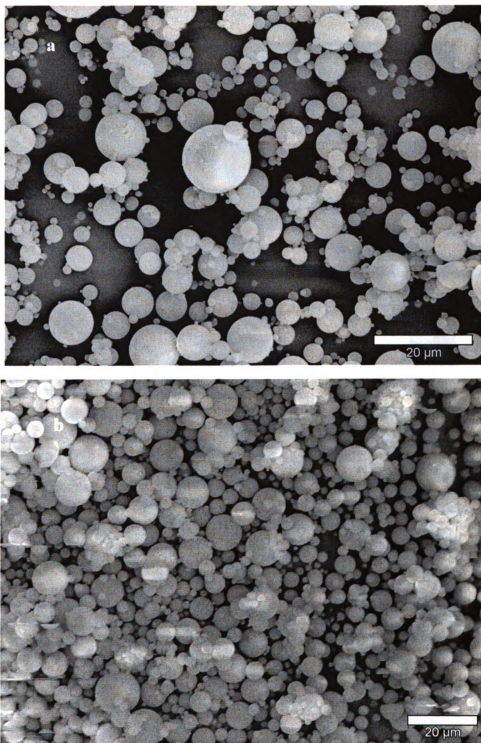
Figure 2.8. SEM image of microspherical functionalized $(SiO_2)_{1-x}(LSiO_{1.5})_x$
(L=mercaptopropyl), denoted microspherical MP-HMS a. x=0.50 prepared by Method I
b. x=0.60 prepared by Method I.
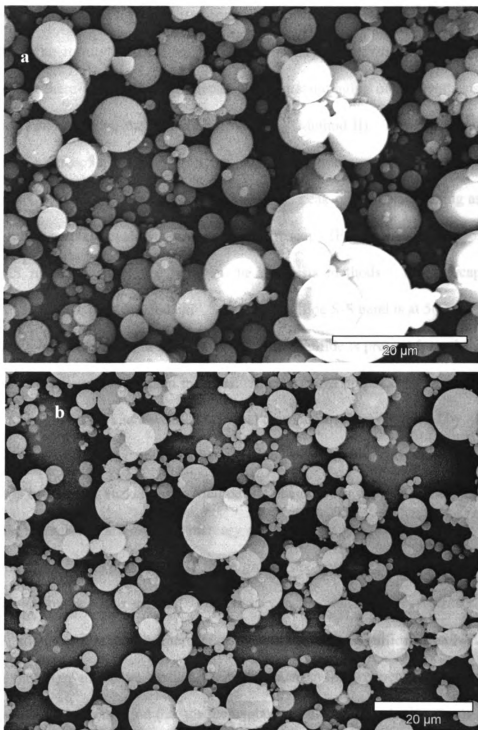
Figure 2.9. SEM image of microspherical functionalized $(SiO_2)_{1-x}(LSiO_{1.5})_x$ (L=mercaptopropyl), denoted microspherical MP-HMS a. x=0.50 prepared by Method I b. x=0.50 prepared by Method II.

In addition to SEM micrographs, nitrogen isotherms, XRD, and Raman spectroscopy were used for the characterization of the microspheres prepared by Methods I and II. The results of the nitrogen isotherm analysis, shown in Table 2.4, further indicate that there is very little difference between static aging of the synthesis mixture (Method I) and agitating the mixture during aging (Method II). The XRD patterns (not shown) of microspherical MP-HMS are characteristic of wormhole MP-HMS XRD structure. One low angle peak is observed with the peak intensity decreasing as organic incorporation increases. However, Raman spectroscopy (Figure 2.10) of microspherical MP-HMS reveals a difference between the synthesis methods. The mercaptan S-H stretch is an intense band at 2560 cm^{-1}.[28,29] The disulfide S-S band is at 500 cm^{-1}, and the C-H stretch is an intense band 2900 cm^{-1}.[28,29] The disulfide is present from the oxidation by air of two adjacent mercaptan moieties. Microspheres prepared by Method I have a more intense S-H band and a weaker S-S band than microspheres prepared by Method II. Thus, more mercaptan is oxidized by dioxygen to form disulfide when the reaction mixture is continually shaken, as in Method II. The concern with disulfide occurrence is that if these materials are used for mercury or arsenite trapping, high disulfide presence will compromise adsorption because these groups are not expected to be active toward reaction with mercury or arsenic. For mercaptan-functionalized mesostructures to be utilized, it is important that the mercaptan not be oxidized to disulfide. The NMR results indicate that more of the organosilane is incorporated in the product prepared by Method II, but one must keep in mind that the mercaptan and disulfide both give rise to T^3 bands of the same chemical shift in the ^{29}Si NMR. Thus, the ^{29}Si NMR results do not differentiate between mercaptan and disulfide linkages. Furthermore, by comparing the

Q^4/Q^3- fully cross-linked silicon centers $Si(OSi)_4$ /incompletely condensed silicon centers $Si(OSi)_3(OH)$- the ratios are the same for products of both Method I and Method II (Q^4/Q^3=1.5); indicating the cross-linking is the same for both synthetic methods.

Table 2.4. Physical properties of functionalized $(SiO_2)_{1-x}(LSiO_{1.5})_x$ (L=mercaptopropyl), denoted microspherical MP-HMS synthesized by Method I static aging and Method II aging with shaking.

Method	x_{theo}	x_{obs}	mmol SH/g	SA^a (m^2/g)	Pore diameter^b (nm)	V_t^c (cm^3/g)	V_{fr}^d (cm^3/g)	V_{tx}^e (cm^3/g)	SH/SS from Raman	Sphere Size Range^f (μm)
I	0.10			951	3.2	1.02	0.66	0.36	8	Spheres plus bulk powder
II	0.10			1042	3.2	1.01	0.64	0.37	3.25	Spheres plus bulk powder
I	0.30			1119	<2.0	1.21	0.53	0.68	26	Primarily Spherical (1-10)
II	0.30			1078	<2.0	1.10	0.51	0.59	11.5	Primarily Spherical (2-10)
I	0.50	0.46	5.00	550	<2.0	0.28	0.26	0.02	27.5	0.85 – 15
II	0.50	0.48	5.10	627	2.1	0.30	0.29	0.01	10	0.2 – 20
I	0.60			196	<2.0	0.10	0.10	0.00	27	1 – 10
II	0.60			337	<2.0	0.17	0.16	0.01	11	0.8 – 14

^{a}Calculated from nitrogen adsorption isotherms by BET method. ^{b} Determined by the Horvath-Kawazoe model. ^{c}Total pore volume determined at P/Po = 0.98. ^{d}Framework pore volume determined at P/Po = 0.55. ^{e}Textural pore volume determined from the difference between V_t and V_{fr}. ^{f}Sphere size calculated from SEM image.
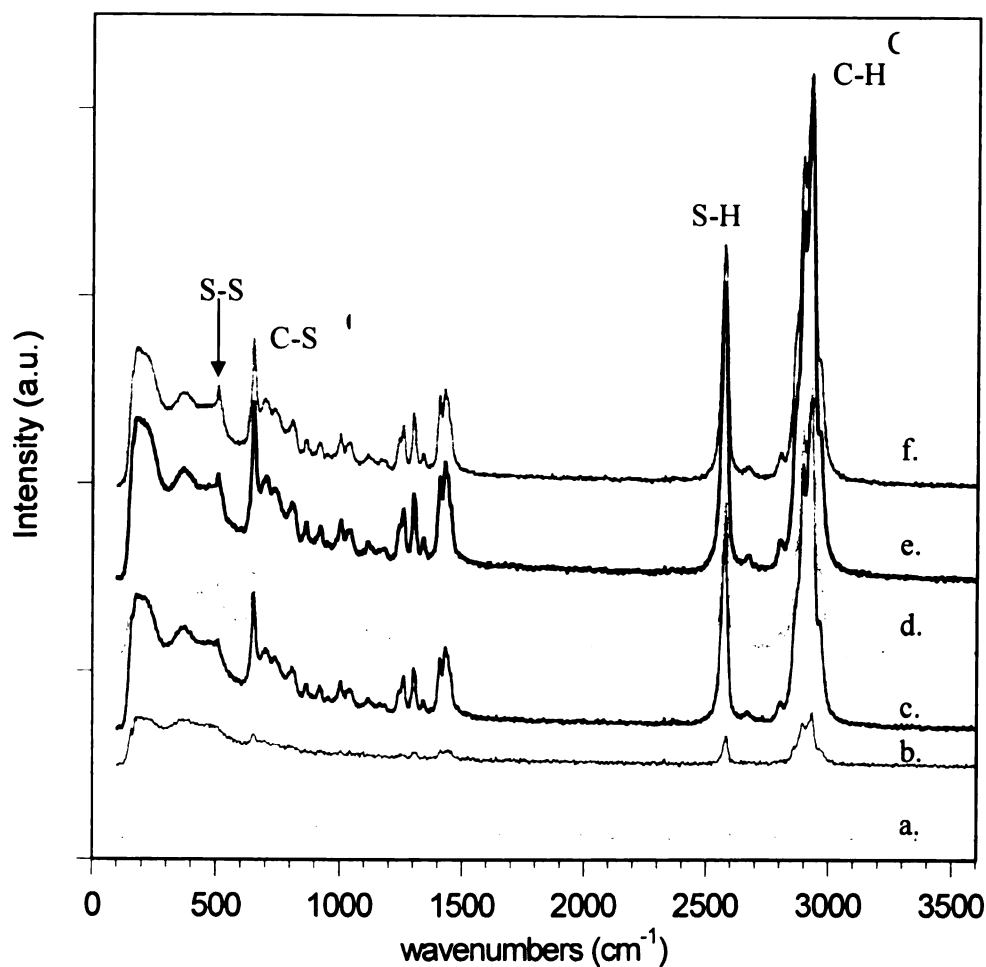
Figure 2.10. Raman spectra of functionalized $(SiO_2)_{1-x}(LSiO_{1.5})_x$ (L=mercaptopropyl), denoted microspherical MP-HMS. a. x=0.30 prepared by Method II (aging with shaking), b. x=0.30 prepared by Method I (static aging) c. x=0.50 prepared by Method I d. x=0.50 prepared by Method II e. x=0.60 prepared by Method I f. x=0.60 prepared by Method II. The spectra are offset on the y-axis for clarity.

The results of microsphere MP-HMS formation by Methods I and II indicate that spheres are formed at the beginning of the reaction. But if the order of addition of the reagents changed, would that affect the formation of spheres? Alkoxysilanes begin polymerizing once they come into contact with water. Therefore, it would be prudent to examine the timing of the addition of water on the formation of spheres. The effects of the order of addition of reagents on sphere formation were examined by comparing synthesis Method III to Method IV. In Method III water is added to a surfactant silane reaction mixture, whereas in Method IV the silanes are added to a water-surfactant mixture. The physical properties of microspherical MP-HMS synthesized by method III and IV are given in Table 2.5. The physical properties for each product are very similar and essentially, there is no difference in the surface area, pore volume, and pore diameter between mesostructures synthesized by the two methods. The nitrogen isotherms show nearly identical Type I isotherms for microspherical MP-HMS with x=0.50. However, the isotherms for microspherical MP-HMS with x=0.30 are slightly different for the two preparation methods. The microspherical MP-HMS with x=0.3 made by Method IV has no textural porosity while, the microspherical MP-HMS with x=0.3, synthesized by Method III, has textural porosity as evidenced in the nitrogen isotherm. Framework mesoporosity is the porosity within the silica particles created by the alkylamine porogen, whereas, textural porosity is the porosity between the silica particles. In addition, both synthetic methods yield spheres, as shown in the SEM images of the microspherical MP-HMS in Figures 2.11 and 2.12. Nonetheless, there is a difference between the products synthesized by the two different methods of the microspherical MP-HMS as seen by the Raman spectra. The Method IV synthesis of microspheres produces higher disulfide

content than Method III spheres, as shown in Figure 2.12. It is fascinating that synthesis

Method IV yields spheres so similar in shape and physical properties to synthesis Method

III.

Table 2.5. Physical properties of functionalized $(SiO_2)_{1-x}(LSiO_{1.5})_x$ (L=mercaptopropyl), denoted microspherical MP-HMS prepared by two different synthesis methods.

Method[a]	x_{theo}	SA[b] m^2/g	V_t^c cm^3/g	V_{fr}^c cm^3/g	Pore diameter[e] (nm)	Spheres from SEM
III	0.3	1090		0.68	2.1	2-20 μm clusters
III	0.5	600	Type I isotherm	0.30	<2.0	2-20 μm
IV	0.3	1289	0.58	0.61	2.2	15-50 μm
IV	0.5	625	Type I isotherm	0.30	<2.0	10-40 μm

[a]In Method I water is added to a mixture of silanes in presence of the porogen; Method IV reverses the order of addition. [b]Calculated from nitrogen adsorption isotherms by BET method. [c]Framework pore volume determined at P/Po = 0.55. [d]Total pore volume determined at P/Po = 0.98. [e]Determined by the Horvath-Kawazoe model.

77
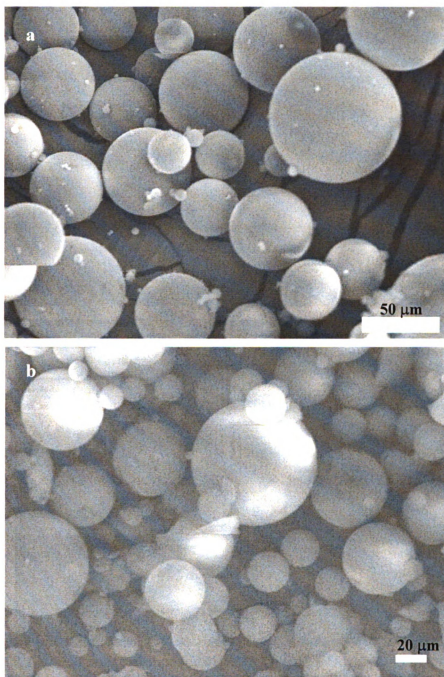
Figure 2.11. SEM image of microspherical functionalized $(SiO_2)_{1-x}(LSiO_{1.5})_x$ (L=mercaptopropyl), denoted microspherical MP-HMS a. x=0.30 prepared by Method III b. x=0.30 prepared by Method IV.
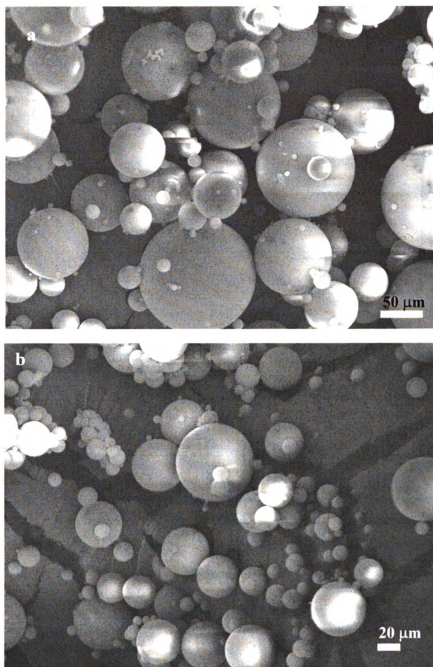
Figure 2.12. SEM image of functionalized $(SiO_2)_{1-x}(LSiO_{1.5})_x$ (L=mercaptopropyl), denoted microspherical MP-HMS a. x=0.50 prepared by Method III b. x=0.50 prepared by Method IV.
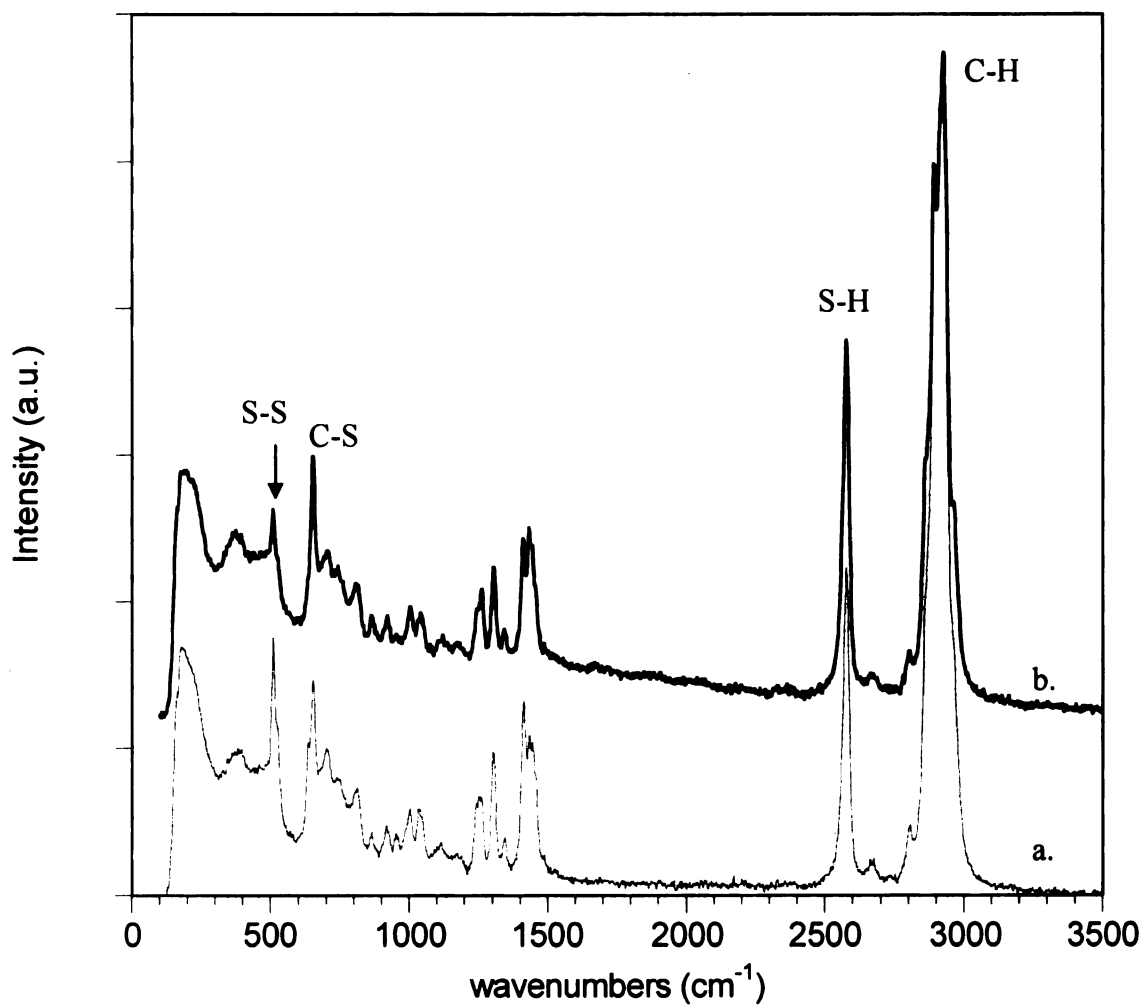
Figure 2.13. Raman spectra of microspherical functionalized $(SiO_2)_{1-x}(LSiO_{1.5})_x$ (L=mercaptopropyl), denoted microspherical MP-HMS a. x=0.50 synthesized by Method III b. x=0.50 synthesized by Method IV.

Of interest is the inside of the spheres; are they hollow or solid? In order to examine the inside of the microspherical MP-HMS with x=0.50, thin-sectioning was done. Thin-sectioning consists of embedding the sample in a resin or epoxy and microtoming nm thick sections to examine by TEM microscopy. The TEM and SEM images of the thin-sectioning are shown in Figure 2.14. From Figure 2.14 b it would appear that the microspheres are solid and have a lamellar pore structure. Yet the spacings of the lamellae are much larger size than the pore size indicated from the nitrogen isotherm results. These lines are actually artifacts[30] produced during the microtoming. To further verify this hypothesis, a sample was made by condensing only TEOS and MPTMS, without any porogen. With no surfactant present, there shouldn't be any pores, so if the lines are present in this sample, the "lamellae" are truly artifacts. Figure 2.16 illustrates that the lamellae are indeed artifacts from the microtoming process. The determination of the spheres being hollow or solid must be made from the SEM images. Both hollow and solid spheres are seen in various SEM images. But hollow spheres appear more numerous than the hollow ones.

This is the first reported example of using near neutral synthesis conditions for assembling functionalized mesoporous spheres. There has been one recent report of mercaptopropyl functionalized spheres synthesized using an electrostatic pathway.[24] Table 2.6 gives a comparison of this work and Kosuge's reported work.[24] The present work is able to incorporate higher organic loading, has better cross-linking, and provides a more facile synthesis method. Higher organic loadings are important for heavy metal trapping, catalysis, and other uses. The increased cross-linking is significant because the

greater the cross linking, the greater the stability of the material. Both methods form monodispersed spheres of comparable size.
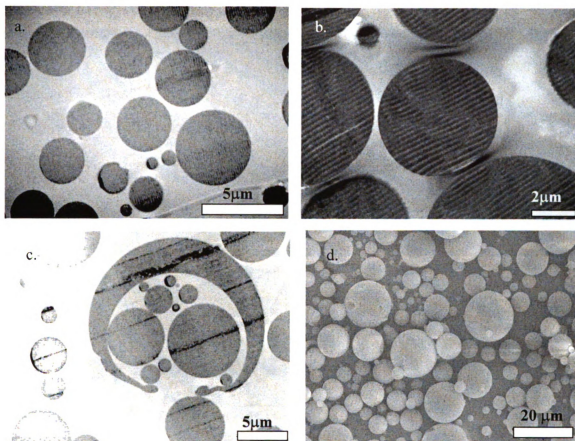
Figure 2.14. Functionalized $(SiO_2)_{1-x}(LSiO_{1.5})_x$ (L=mercaptopropyl), denoted microspherical MP-HMS prepared by Method III with x=0.50. a. b. and c. thin-section TEM micrographs and d. SEM micrograph.
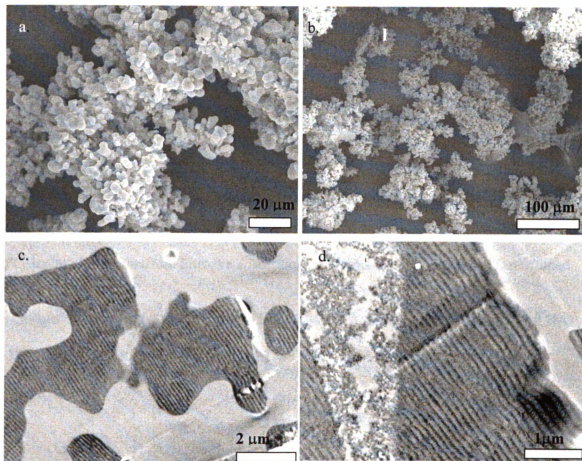
Figure 2.15. Functionalized $(SiO_2)_{1-x}(LSiO_{1.5})_x$ (L=mercaptopropyl) composite synthesized in absence of a surfactant, using the synthesis order of Method III. a. and b. SEM images for the powdered samples. c and d. thin-section TEM images.

Table 2.6. Comparison of physical properties of microspherical MP-HMS made by Method III and a microspherical mercaptopropyl functionalized MCM-41 type mesoporous silica prepared under acidic conditions according to Kosuge.[24]

Author	x_{theo}	SA^a (m^2/g)	mmol SH/g^b	Sphere size (μm) from SEM
McKimmy	0.10	1042	1.3	Spheres plus bulk powder
Kosuge[24]	0.10	810		5-20
Kosuge[24]	0.20	847		5-30
McKimmy	0.30	1090	3.21	2-20
Kosuge[24]	0.40	807		5-25
McKimmy	0.50	600	5.03	2-20
McKimmy	0.60	368	4.64	0.8-14

^{a}Calculated from the from nitrogen adsorption isotherms by BET method. ^{b}Determined from ^{29}Si MAS NMR.

Kosuge[24] mol ratio: 1-x TEOS: x MPTMS : 0.35 DDA: 0.004 HCl: 0.9 EtOH: 39.0 H_2O

McKimmy mol ratio: 1-x TEOS : x MPTMS : 0.22 DDA : 6.7 EtOH : 160 H_2O

85

2.5 Conclusion

2.5.1 Direct-assembly of mercaptopropyl-functionalized Stoeber nanospheres

Mercaptopropyl functionalized mesoporous nanospheres have been successfully synthesized using a modified Stoeber process in the presence of dodecylamine as a surfactant. Up to 30% of the silicon centers were functionalized with retention of a high specific surface area. Nonetheless, the highly diluted reaction system, which is necessary for nanospheres formation, is not desirable for large scale or commercial applications. Also the large quantities of solvents used are in opposition to the "green chemistry" approach that industry is moving towards. Furthermore, the level of mercaptopropyl functionalization is not as high as can be achieved using other synthetic methods.

2.5.2 Direct-assembly of mercaptopropyl functionalized HMS microspheres

Microspherical mercaptopropyl functionalized HMS silica with a wormhole framework structure has been successfully synthesized from TEOS, MPTMS, and dodecylamine. By simply applying vigorous shaking once all the reagents were added, mesoporous microspheres with functionalization levels of up to 60% have been prepared. This is the first report of mesoporous spheres being made in this simple, one-step manner. Furthermore, these spheres have the highest incorporation of organo-functional groups reported to date. Additionally, the use of a near neutral assembly pathway allows for simple extraction and recyclability of the surfactant. Microspherical MP-HMS has great potential for use in chromatography, heavy metal adsorption, and drug delivery. Mercury trapping column studies by microspherical MP-HMS have been examined and will be discussed in Chapter 4.

2.6 References

(1)   Pauly, T. R.; Pinnavaia, T. J. *Chem. Mater.* **2001**, *13*, 987-993.

(2)   Pauly, T. R.; Liu, Y.; Pinnavaia, T. J.; Billinge, S. J. L.; Rieker, T. P. *J. Am. Chem. Soc.* **1999**, *121*, 8835-8842.

(3)   Boissiere, C.; Larbot, A.; Prouzet, E. *Stud. Surf. Sci. Catal.* **2001**, *135*, 1298-1304.

(4)   Boissiere, C.; van der Lee, A.; El Mansouri, A.; Larbot, A.; Prouzet, E. *Chem. Commun.* **1999**, 2047-2048.

(5)   Kosuge, K.; Singh, P. S. *Microporous Mesoporous Mater.* **2001**, *44-45*, 139-145.

(6)   Fowler, C. E.; Khushalani, D.; Mann, S. *Chem. Commun.* **2001**, 2028-2029.

(7)   Huo, Q.; Feng, J.; Schueth, F.; Stucky, G. D. *Chem. Mater.* **1997**, *9*, 14-17.

(8)   Li, W.; Sha, X.; Dong, W.; Wang, Z. *Chem. Commu.* **2002**, 2434-2435.

(9)   Martin, T.; Galarneau, A.; Di Renzo, F.; Fajula, F.; Plee, D. *Angew. Chem., Int. Ed. Engl* **2002**, *41*, 2590-2592.

(10)   Stoeber, W.; Fink, A.; Bohn, E. *J. Colloid Interface Sci.* **1968**, *26*, 62-69.

(11)   Cai, Q.; Luo, Z.-S.; Pang, W.-Q.; Fan, Y.-W.; Chen, X.-H.; Cui, F.-Z. *Chem. Mater.* **2001**, *13*, 258-263.

(12)   Grun, M.; Unger, K. K.; Matsumoto, A.; Tsutsumi, K. *Microporous Mesoporous Mater.* **1999**, *27*, 207-216.

(13)   Nooney, R. I.; Thirunavukkarasu, D.; Chen, Y.; Josephs, R.; Ostafin, A. E. *Chem. Mater.* **2002**, *14*, 4721-4728.

(14)   Matsumoto, A.; Tsutsumi, K.; Schumacher, K.; Unger, K. K. *Langmuir* **2002**, *18*, 4014-4019.

(15)   Martin, T.; Galarneau, A.; Di Renzo, F.; Brunel, D.; Fajula, F.; Heinisch, S.; Cretier, G.; Rocca, J.-L. *Chem. Mater.* **2004**, *16*, 1725-1731.

(16)   Etienne, M.; Lebeau, B.; Walcarius, A. *New J.Chem.* **2002**, *26*, 384-386.

(17)   Etienne, M.; Sayen, S.; Lebeau, B.; Walcarius, A. *Stud. Surf. Sci. Catal.* **2002**, *141*, 615-622.

(18)   Walcarius, A.; Delacote, C. *Chem. Mater.* **2003**, *15*, 4181-4192.

(19)   Ganesan, V.; Walcarius, A. *Langmuir* **2004**, *20*, 3632-3640.

(20)   Beaudet, L.; Hossain, K.-Z.; Mercier, L. *Chem. Mater.* **2003**, *15*, 327-334.

(21)   Prouzet, E.; Boissiere, C.; Hovnanian, N.; Larbot, A. *Stud. Surf. Sci. Catal.* **2001**, *135*, 1329-1336.

(22)   Sadasivan, S.; Khushalani, D.; Mann, S. *J. Mater. Chem.* **2003**, *13*, 1023-1029.

(23)   Fowler, C. E.; Khushalani, D.; Lebeau, B.; Mann, S. *Adv. Mater.* **2001**, *13*, 649-652.

(24)   Kosuge, K.; Murakami, T.; Kikukawa, N.; Takemori, M. *Chem. Mater.* **2003**, *15*, 3184-3189.

(25)   Mori, Y.; Pinnavaia, T. J. *Chem. Mater.* **2001**, *13*, 2173-2178.

(26)   Ding, J.; Hudalla, C. J.; Cook, J. T.; Walsh, D. P.; Boissel, C. E.; Iraneta, P. C.; O'Gara, J. E. *Chem. Mater.* **2004**, *16*, 670-681.

(27)   Walcarius, A.; Etienne, M.; Lebeau, B. *Chem. Mater.* **2003**, *15*, 2161-2173.

(28)   Yuan, Z.-Y.; Six-Boulanger, M.-F.; Su, B.-L. *Angew. Chem., Int. Ed. Engl* **2003**, *42*, 1572-1573.

Chapter 3

Synthesis of bi-functional mesoporous organo-functionalized silicas with a wormhole framework structure.

3.1 Introduction

A host of organo-functionalized mesoporous materials have been synthesized and examined for use in catalysis,[1,2 3,4] heavy element trapping,[5,6 7,8] chromatography,[9-12] and sensing.[13] The interest in these materials is due to their high surface area, the ability to specifically tune the organic group and the loading of organic moiety, and control of particle morphology. In an attempt to further expand the versatility of organo-functionalized mesoporous materials, multi-functionalized materials have been synthesized. These functionalized mesostructures contain two or more different organic groups. The incorporation of various organic groups within the same framework allows for those properties unique to each functional group to be imparted to the material. For example, one functional group might serve as a catalyst (covalent/active site), and the second might provide noncovalent interactions (change hydrophobicity/hydrophilicity). In addition to imparting different chemical properties to the same framework, bi-functionality can be used to control particle morphology.[14,15]

As with the incorporation of a single functional group types in a mesostructured framework, bi-functionality can be accomplished by grafting, or direct assembly, or a combination of both. Grafting is the incorporation of organic moieties into a silica network accomplished by surface anchoring through the hydroxyls of the incompletely condensed silica. The direct assembly procedure entails the direct co-condensation of the

89

organosilane with the inorganic precursor in the initial reaction mixture to incorporate the organic moiety. Lin et al. synthesized mercapto-functionalized hexagonal MCM-41 by direct-assembly and then grafted propyl, phenyl, or pentafluorophenyl groups to the mercapto-functionalized mesostructure.[13] The mercaptan moieties were used to anchor phthalic dicarboxaldehyde thus forming an amine-sensitive *o*-phthalic hemithioacetal (OPTA)-derived material to be used for sensing of dopamine, a hormone-like substance and an important neurotransmitter. A schematic representationof the *o*-phthalic hemithioacetal (OPTA) functionalized mesoporous silica material and their fluorescent detection of amines (R = siloxy, propyl, phenyl, or pentafluorophenyl groups; R'-NH$_2$ = dopamine or glucosamine) is shown in Scheme 3.1.[13]

Scheme 3.1[13]

90
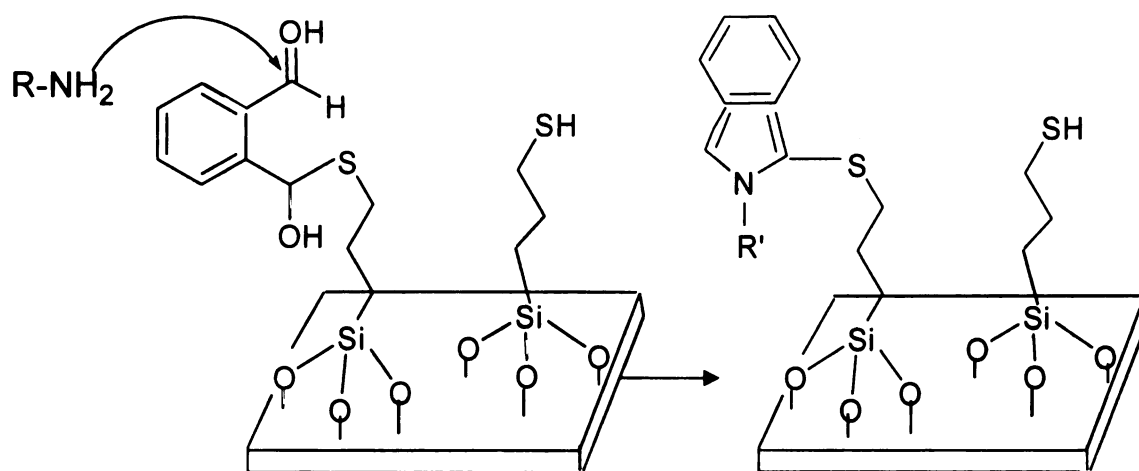
The mesostructures with a second functional group of pentafluorophenyl were more reactive towards dopamine than the structures with propyl or phenyl moieties.[13] The increase in reactivity was attributed to the better π-π donor/acceptor stacking of the catechol rings of dopamine molecules and the pentafluorophenyl groups than was possible with the propyl or phenyl moieties.

Hexagonal framework MCM-41 functionalized by grafting with amines or polyamines have been used effectively as catalysts for nitroaldol reactions to produce nitroalkenes in high yields.[16] The mono-functionalized MCM-41 was able to catalyze the reaction of 4-hydroxybenzaldehyde with nitromethane to produce nitroalkenes. Yet when a series of three competitive nitroaldol reactions, consisting of various chain length alkoxybenzaldehyde and 4-hydroxybenzaldehyde were performed with the propyldiethylenetriamine (NNN) MCM-41, there was no reaction selectivity observed for the desired product, the alkoxy 4-(2-nitro-vinyl) benzene.[17] Rather 4-(2-nitrovinyl) phenol and the alkoxy 4-(2-nitrovinyl) benzene were produced in nearly a 1:1 ratio. Yet, by introducing a secondary functional group, specifically a mercaptopropyl (MP) or vinyl (Vy) group to the NNN functionalized MCM-41, an increase of reaction selectivity towards the alkoxy 4-(2-nitrovinyl) benzene product was observed. Both organic moieties were incorporated simultaneously by direct-assembly. The results suggested that the hydrophobic secondary groups (MP and Vy) played a significant role in preferentially allowing the more hydrophobic reactants to penetrate into the mesopores and react with the triamine functionality. The competitive nitroaldol reaction using a bi-functionalized mesostructure is shown below in Scheme 3.2.[17]
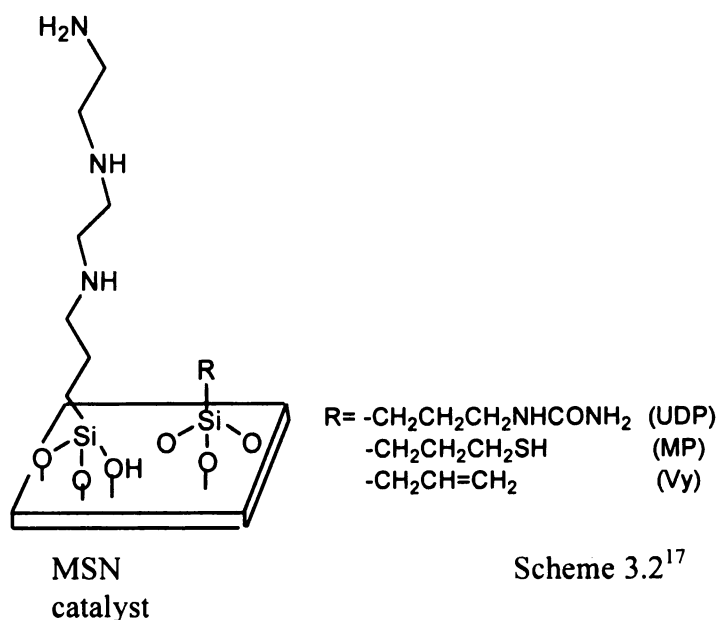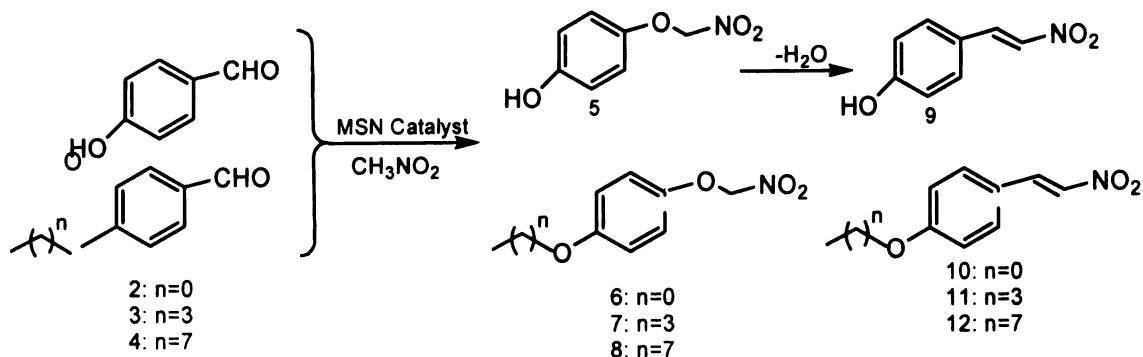
Scheme 3.2[17]

The variation of particle morphology with the direct incorporation of two different functional groups (bi-functionality) has been reported by Lin.[14] By using two different organosilanes and varying the ratio between the organosilanes (the total organosilane amount was held constant at 1 mole organosilane to 8 moles of tetraethylorthosilicate (TEOS) added), different shaped mesostructures were formed. A combination of a NNN and mercaptopropyl moieties created spherical particles with diameters around 1.5 μm. By changing the ratio of NNN to MP groups, the size of the

spheres were varied. Combining the functional groups cyanopropyl and mercaptopropyl produced an oblong rod-like mesostructure.

Other groups have also synthesized multi-functional mesostructures by direct-assembly. Table 3.1 summarizes the materials prepared, as well as some of the applications that have been examined. Electrostatic and hydrogen-bonded synthesis conditions are useful for the direct synthesis of multi-functional mesoporous materials. However, all loadings of organic groups are limited to a maximum of 20 mole percent. There is mention of only one attempt to incorporate higher organic group loadings.[18] It was reported that increasing organic incorporation from 20 to 40% gave structures in which T^2 ($RSi(OSi)_2OH$) and Q^2 ($Si(OSi)_2(OH)_2$) sites were predominant. Significant amounts of uncondensed Si-OH centers typically result in weak or collapsed structures. It is likely that other endeavors to synthesize higher functional dual mesostructures have also been attempted, but resulted in collapsed structures.

The intention of the present work is to develop a synthesis strategy to incorporate high loadings of two different organic moieties in a wormhole mesostructure prepared through a direct supramolecular assembly pathway. The resulting products have the anhydrous formula $(SiO_2)_{1-(x+y)}(LSiO_{1.5})_x(L'SiO_{1.5})_y$, where L and L' are the organic groups of interest and (x+y) is the fraction of framework silicon centers that are functionalized. The organofunctional groups selected for this work were mercaptopropyl and aminopropyl groups. The former organic moiety was chosen because of its affinity for mercury and arsenite and the latter for its ability to trap arsenate. Although dual functionalized HMS wormhole structures have been synthesized,[19] the loadings of the

organic groups was limited to x+y=0.25, and the only application examined was trapping of mercury.

The US Environmental Protection Agency (EPA) has set a limit of 10 parts per billion (ppb) for the amount of total arsenic that is allowable in drinking water. The possibility of utilizing a dual-functionalized mesostructure with high organic loadings for the remediation of both arsenite and arsenate will be examined in Chapter 5.

Table 3.1. Summary of multi-functional mesoporous organosilicas prepared by direct-assembly (DA) and grafting method and their applications.

Mesostructure	Organo-functional groups	Incorporation	Organic group loading added mmol/g	Applications Examined
MCM-41[13]	MP+propyl MP+Ph MP+pentafluorophenyl	DA for MP, second group grafted	1.5 + 1.5 1.5 + 1.0 1.5 + 1.2	Fluorescence sensory system for biogenic molecules
MCM-41 and MCM-48[18]	Ph + MP Ph + AP Ph +allyl	DA	1.5 + 1.5 1.5 + 1.5 1.5 + 1.5	
MCM-41[17]	NNN + UDP NNN + MP NNN + allyl	DA	0.54 + 0.46 0.71 + 0.69 0.69 + 0.61 actual	Competitive catalytic nitroaldol reactions
SBA-15[20]	SO₃H* + benzyl SO₃H* + methyl	DA	1.5 + 0.85	Adsorption of triethylphosphineoxide to determine solid acid properties
HMS[21,22]	AP + MP MP+AP+Ph NN + MP + Ph BTMPA + MP+ methyl	DA	1.16 + 0.97 0.67 + 0.65 + 5.87 (C) 1.55 + 0.70 + 7.05 (C) 0.65 + 0.54 + 3.99 (C)	
HMS[19]	MP + AP MP + AP MP + AP	DA	0.12 + 1.85 1.06 + 1.07 1.70 + 0.17	Mercury adsorption
HMS[23]	AP + Ph AP + methyl	DA	1.15 +1.15 1.1 + 1.1	Tested in Knoevenagel reaction
MSU-X[24,25]	UDP + methyl UDP + Ph	DA	0.80 + 0.80 0.80 + 0.80	

*SO₃H from oxidation of MP. AP-aminopropyl, BTMPA-bis[3-(trimetholxysilyl)propyl]amine, MP-mercaptopropyl, NN-ethylenediamine, NNN-diethylenetriamine, Ph-phenyl, UDP-ureidopropyl

3.2 Experimental

3.2.1 Reagents

Mercaptopropyltrimethoxysilane, tetraethylorthosilicate, dodecylamine, and aminopropyltrimethoxysilane were purchased from Aldrich and used without further purification. Absolute ethanol was purchased in-house. Water was double-exchanged to remove cations and anions via a Millipore filter apparatus.

3.2.2 Direct assembly of dual mercaptopropyl and aminopropyl functionalized HMS

Mercaptopropyl and aminopropyl-functionalized HMS with the composition formula $(SiO_2)_{1-(x+y)}(LSiO_{1.5})_x(L'SiO_{1.5})_y$, were synthesized from tetraethylorthosilicate (TEOS), mercaptopropyltrimethoxysilane (MPTMS), and aminopropyltrimethoxysilane (APTMS) using the direct-assembly method of organic group incorporation. An amine surfactant was used as the structure – directing agent, specifically dodecylamine (DDA), and the synthesis conditions were that of an electrostatically neutral one, S^0I^0. There were five different methods used to determine the optimal conditions for dual functionalized mesoporous silica formation.

Method I. A mixture of MPTMS, APTMS, TEOS was added to a solution of surfactant, EtOH, and water to form the reaction mixture. Ethanol, dodecylamine (DDA) surfactant, and water were mixed and warmed to 35 °C. A x : y : 1-(x+y) molar mixture of x MPTMS, y aminopropyltrimethoxysilane (APTMS), and 1-(x+y) TEOS was added drop wise to the surfactant water mixture. The entire mixture was shaken for 48 h at 35 °C. Finally, the solution was filtered, the precipitate collected and air-dried, followed by

96

Soxhlet extraction with ethanol to remove the surfactant. The overall molar stoichiometry was:

1-(x+y) TEOS : x MPTMS : y APTMS : 0.22 DDA : 5.0 EtOH : 160 H_2O

Method II. A partially hydrolyzed solution of MPTMS, APTMS, TEOS in EtOH was added to an ethanol and surfactant solution, and water was added to complete the reaction mixture. A x : y : 1-(x+y) molar mixture of x MPTMS, y aminopropyltrimethoxysilane (APTMS), and 1-(x+y) TEOS was added to one-half of the total ethanol needed for the reaction. This silane ethanol solution was aged at 35 °C for 1 h. After this 1 h of pre-hydrolysis time, the remaining ethanol and the surfactant, dodecylamine (DDA), were added. The silane, surfactant, and ethanol mixture was allowed to react for 5 min before the water was added. The entire mixture was shaken for 48 h at 35 °C. Finally, the solution was filtered, the precipitate collected and air-dried, followed by Soxhlet extraction with ethanol to remove the surfactant. The overall molar stoichiometry was:

1-(x+y) TEOS : x MPTMS : y APTMS : 0.22 DDA : 5.0 EtOH : 160 H_2O

Method III. A partially hydrolyzed solution of MPTMS and TEOS in EtOH was added to an ethanol and surfactant solution with APTMS being added in this step. Then, water was added to complete the reaction mixture. A x : 1-(x+y) molar mixture of x MPTMS and 1-(x+y) TEOS was added to one-half of the ethanol and aged at 35 °C for 1 h. After this 1 h of pre-hydrolysis time, the y APTMS, remaining ethanol, and surfactant, DDA, were added. The silane, surfactant and ethanol mixture was allowed to react for 5 min before the water was added. The entire mixture was shaken for 48 h at 35 °C. Finally, the solution was filtered, the precipitate collected and air-dried, followed by Soxhlet

97

extraction with ethanol to remove the surfactant.   The overall molar stoichiometry employed was:

1-(x+y) TEOS : x MPTMS : y APTMS : 0.22 DDA : 5.0 EtOH : 160 H_2O

Method IV.   TEOS, MPTMS, APTMS were sequentially added to ethanol.   The surfactant solution and then water was added to complete the reaction mixture.   Each silane was added dropwise one by one, beginning with the molar quantity 1-(x+y) TEOS, followed by x MPTMS, and finally y APTMS to the surfactant, DDA, ethanol mixture, which had been pre-warmed to 35 °C.   This silane, surfactant, and ethanol mixture was allowed to react for 5 min before the water was added.   The entire mixture was shaken for 48 h at 35 °C.   Finally, the solution was filtered, the precipitate collected and air-dried, followed by Soxhlet extraction with ethanol to remove the surfactant.   The overall molar stoichiometry was:

1-(x+y) TEOS : x MPTMS : y APTMS : 0.22 DDA : 5.0 EtOH : 160 H_2O

Method V.   A mixture of TEOS, MPTMS, and APTMS was added to a surfactant solution, and water was added to form the reaction mixture.   A x : y : 1-(x+y) molar mixture of x MPTMS, y APTMS, and 1-(x+y) TEOS was added to a surfactant, DDA, ethanol mixture, which had been pre-warmed to 35 °C.   This silane, surfactant, and ethanol mixture was allowed to react for 5 minutes before the water was added.   The entire mixture was shaken for 48 h at 35 °C.   Finally, the solution was filtered, the precipitate collected and air-dried, followed by Soxhlet extraction with ethanol to remove the surfactant. The overall molar stoichiometry employed was:

1-(x+y) TEOS : x MPTMS : y APTMS : 0.22 DDA : 5.0 EtOH : 160 H_2O

3.3 Physical Measurements

The physical properties of the dual mercaptopropyl and amino functionalized HMS were determined by nitrogen adsorption, powder X-ray diffraction (XRD), ^{29}Si magic angle spinning nuclear magnetic resonance (MAS-NMR), Raman spectroscopy, Transmission Electron Microscopy (TEM), and Infrared Spectroscopy. Nitrogen adsorption-desorption isotherms were measured at -196 °C on a Micrometrics ASAP 2010 sorptometer, the samples being outgassed at 80 °C and 10^{-6} Torr prior to measurement. Powder XRD patterns were collected on a Rigaku rotaflex diffractometer using Cu Kα radiation. ^{29}Si MAS-NMR spectra were collected on a Varian 400 solid state NMR spectrometer with a field strength of 400 MHz, under single-pulse mode with a zirconia rotor at a spinning frequency of 4 kHz. A pulse delay of 400 seconds was employed so that there was sufficient time for the nuclei to relax before application of another pulse. Talc was used as a reference. For Raman spectroscopy, samples were packed into glass capillary tubes and analyzed with a Bio-Rad FT Raman Spectrometer equipped with a germanium CCD camera detector and 633 nm radiation from a HeNe laser for excitation with a resolution of 4 cm^{-1}. Laser power at the sample was estimated to be about 5mW, and the focused laser beam diameter was ~10 micrometer. A total of 200 scans was accumulated for each spectrum. TEM images were obtained on a JOEL 100CX microscope with a CeB$_6$ filament and an accelerating voltage of 120 KV. Sample grids were prepared by sonicating samples in ethanol for 20 min and evaporating one drop of the suspension onto a carbon coated, holey film supported on a 3 mm, 300 mesh copper grid. Infrared spectra were recorded in the 4000-500 cm^{-1} range using a

Nicolet FTIR Protégé 460 spectrometer equipped with a diffuse reflectance accessory (DRIFTS).

3.4 Results and Discussion

3.4.1 Method I MP+AP-HMS Low Organic Loading

Wormhole mesostructures with two different organic moieties incorporated by direct-assembly have been prepared under near neutral pH conditions with an amine surfactant as the porogen. The mesostructures, denoted MP+AP-HMS, have high surface areas as well as high level of incorporation of the organic groups. The low angle powder x-ray diffraction patterns (XRD) are shown in Figure 3.1 for the mesostructures prepared by Method I. Method I synthesis involved adding two organosilanes and one silicon precursor to a surfactant, ethanol, and water solution. This is essentially the preparation method used for the assembly of monofunctional MP-HMS[26] with aminopropyltrimethoxysilane added as a second organosilane. For each structure, a single broad peak was observed, indicative of a wormhole mesostructure. Variations in the amount of functional groups lead to changes in the intensity of the diffraction peak. The decrease in the intensity of the XRD peak with increased organic group loading is attributed to contrast matching.[27] X-rays scattered in phase cause an increase in diffraction intensity. The scattering from the pore walls is in phase (constructive scattering), whereas, the organosilicon scattering from within the pores is out of phase with the wall scattering. This results in lower intensity XRD patterns. Increasing the organic functionality also causes a shift to a higher 2Θ, indicative of smaller pore sizes. The MP+AP-HMS with x=0.15 y=0.13 has the highest organic loading, highest 2Θ value, and broadest peak. The decrease in pore size with increased functionality is not

100

unexpected and is attributed to a greater interaction of the hydrophobic organic moieties with the hydrophobic center of the micelle. The increase in broadness with increase of functionality indicates perturbation of the micelle by the organic groups due to the greater interaction between the organic moieties and the hydrophilic core of the micelle.

The MP+AP-HMS nitrogen isotherms for the products made by Method I are shown in Figure 3.2. Each mesostructure has a Type IV isotherm.[28] However, as the functionality increases the mesopore step occurs at a lower P/P_0, which is further evidence of a decrease in the pore size with increased organic loading. In order to determine the amount of incorporation of the organic groups, ^{29}Si MAS-NMR was done. The T^3 band, indicative of a silane with three hydrolyzable groups and one Si-C bond, increases as the functionalization increases. However, the Q^3 band, which signifies incompletely cross-linked SiO_4 centers, also increases with the increased functionality. The ^{29}Si MAS-NMR cannot differentiate between silicon centers that are functionalized with the mercaptopropyl moiety or aminopropyl moiety. Instead, the technique provides the information on the total degree of organo-functionalization. MP-HMS quantatively incorporates the mercaptopropyl group, typically 95% of the organic group added is incorporated. For MP+AP-HMS, there was generally less than quantative incorporation of the organic group. The MP+AP-HMS with x=0.15 y=0.12 was the only dual–functional composition with near quantative incorporation at 90%. The other structures incorporated about 80% incorporation of the organic groups. Since MP-HMS exhibits nearly quantative incorporation of the mercaptopropyl moiety, it is presumed the incorporation of the aminopropyl group being only partially incorporated at about the 60% level. By elemental analysis, (C, H, N) it was determined that only 60-70% of the

aminopropyl added was integrated into the mesostructure depending on the composition. Table 3.2 provides the physical properties of the mercaptopropyl and aminopropyl functionalized mesostructured silica prepared by Method I.
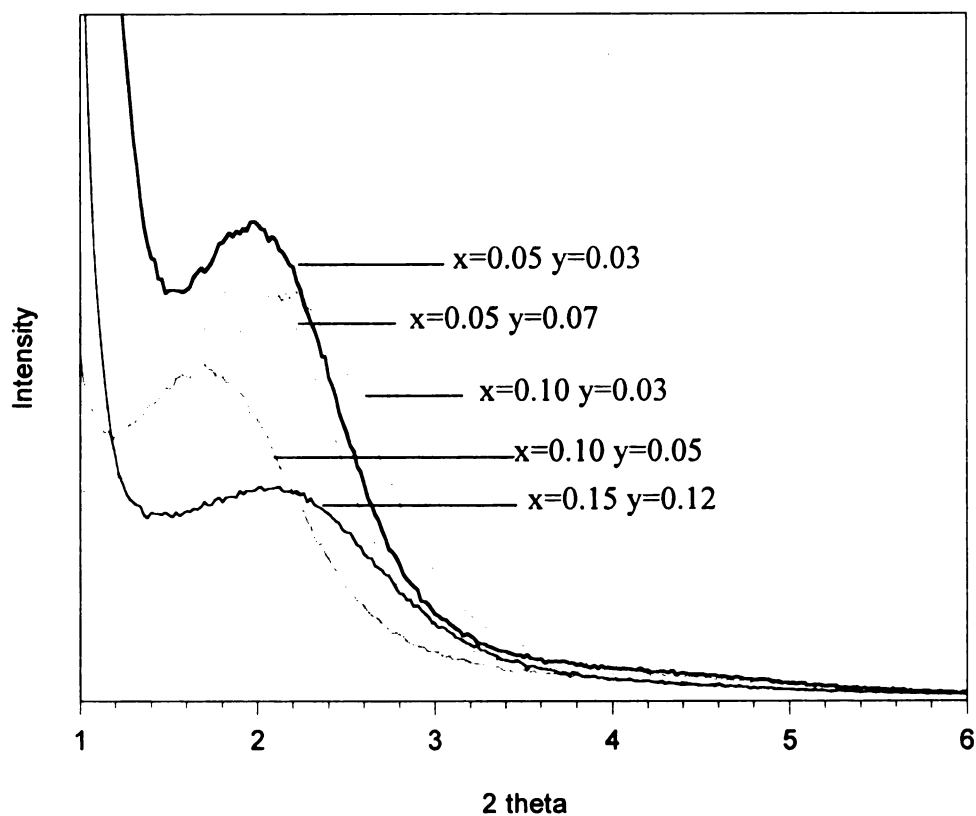
Figure 3.1. XRD pattern for functionalized $(SiO_2)_{1-(x+y)} (LSiO_{1.5})_x (L'SiO_{1.5})_y$ compositions (L=mercaptopropyl, L'=aminopropyl) with a wormhole framework structure, denoted MP+AP-HMS and assembled according to Method I.

Figure 3.2. Nitrogen adsorption-desorption isotherm for functionalized $(SiO_2)_{1-(x+y)}$ $(LSiO_{1.5})_x$ $(L'SiO_{1.5})_y$ compositions (L=mercaptopropyl, L'=aminopropyl) with a wormhole framework structure, denoted MP+AP-HMS and assembled according to Method I. The isotherms are offset on the y-axis for clarity.
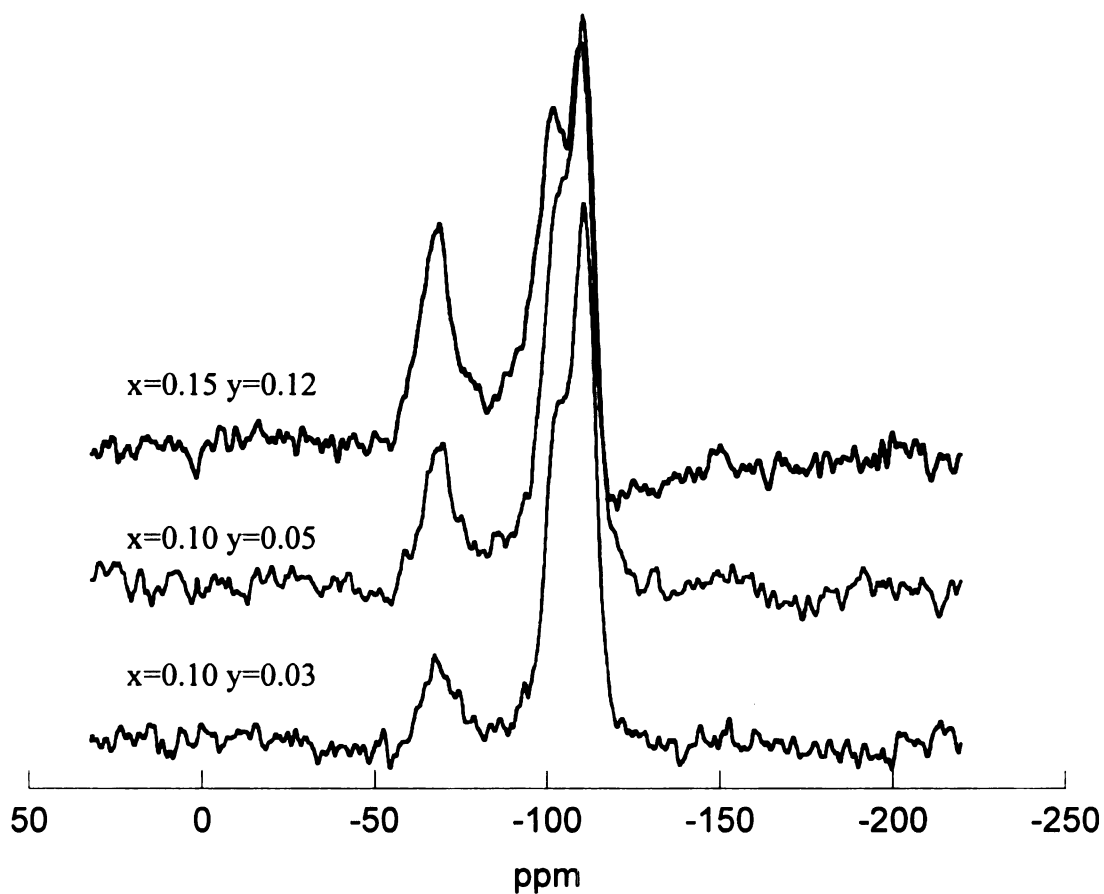
Figure 3.3. ^{29}Si MAS NMR spectra for functionalized $(SiO_2)_{1-(x+y)} (LSiO_{1.5})_x (L'SiO_{1.5})_y$ compositions (L=mercaptopropyl, L'=aminopropyl) with a wormhole framework structure, denoted MP+AP-HMS and assembled according to Method I.

Table 3.2. Textural properties of $(SiO_2)_{1-(x+y)}(LSiO_{1.5})_x(L'SiO_{1.5})_y$ compositions (L=mercaptopropyl, L'=aminopropyl) with a wormhole framework structure, denoted MP+AP-HMS and assembled according to Method I.

MP+AP-HMS	d_{100}	SA^a cm²/g	Pore^b diameter (nm)	Pore^c volume cm³/g	$x+y_{theo}$	$x+y_{obs}^d$	Q^4/Q^3	mmol ligands/g	Elemental analysis N content (wt%) theoretical/observed
x=y=0.05	45.1	945	3.6	0.78	0.10				
x=y=0.10	42.5	1030	3.1	0.64	0.20	0.15	1.13	2.05	
x=y=0.15	42.1	971	2.0	0.67	0.30	0.27	0.80	3.41	2.6/1.9
x=0.10 y=0.05	40.9	1203	3.1	0.74	0.15	0.12	1.01	1.67	1.1/0.72
x=0.05 y=0.10	44.6	853	3.6	0.78	0.15				

^{a}Calculated from nitrogen adsorption isotherms by BET method. ^{b}Determined by the Horvath-Kawazoe model.
^{c}Total pore volume determined at P/Po = 0.98. ^{d}Calculated from ^{29}Si MAS NMR.
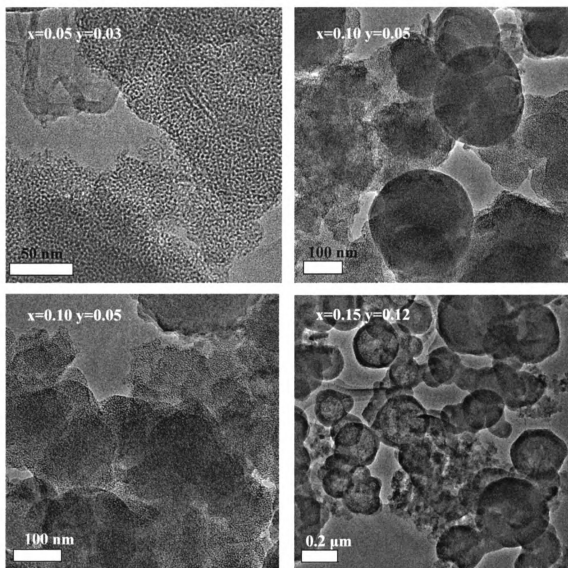
Figure 3.4. TEM images for functionalized $(SiO_2)_{1-(x+y)} (LSiO_{1.5})_x (L'SiO_{1.5})_y$ compositions (L=mercaptopropyl, L'=aminopropyl) with a wormhole framework structure, denoted MP+AP-HMS and assembled according to Method I.

All dual-functional compositions have high surface areas (853-1203 cm^3/g). The pore volume decreases with increasing functionality indicating the organic group is indeed being incorporated. It is interesting to note the difference between the samples where x and y are not equal. The MP+AP-HMS with x=0.10 MP and y=0.03 AP has a very large surface area, 1203 cm^3/g, whereas, for the structure with the greater amine loading, x=0.05 MP and y=0.07 AP, the surface area drops to 853 cm^3/g. Yet, with the surface area decrease, an unexpected pore diameter increase is observed. The two samples have the similar total organic moiety loading, but the derivative with the higher amine loading has different physical properties than the composition with higher mercaptan loading.

The TEM images for MP+AP-HMS in Figure 3.4 show typical HMS wormhole structures for the compositions with lower organic group loading (x=0.05 y=0.03), but with increasing organic moiety loading (x=0.15 y=0.12), the derivatives form predominately spheres. The formation of spheres by the dual functionalized HMS was not unexpected. Differences in particle morphology caused by direct incorporation of two different organofunctional groups had been previously reported by Lin.[14] In his work, spheres were formed by mesostructures with a propyldiethylenetriamine (NNN) and mercaptopropyl moieties, by changing the ratio of NNN to MP groups, the size of the spheres could be varied. Additionally, combining the cyanopropyl and mercaptopropyl functional groups produced an oblong rod-like mesostructure. No explanation was given as to why the dual functionalized mesostructure formed spheres or rods.[14]

After the initial success of the preparing MP+AP-HMS with up to 30% of the silicon centers being functionalized, an attempt was made to prepare a mesostructure with

50% of the silicon sites having functional groups. Since no other work had reported dual functionalized mesostructures with such high loadings of organic groups, four different synthesis methods were examined. The syntheses varied in the sequence of the addition of the silanes. There has been great success in synthesizing MP functionalized mesostructures, MP-HMS, with up to 50% of the silicon centers being functionalized has been reported.[26] However, functionalization with AP has proven to be more difficult with the highest reported loading of the amine group being 40% of the total silicon centers for a hexagonal MCM-41. But only 24% AP functionalization was actually achieved.[29] The difficultly in synthesizing directly assembled aminopropyl functionalized mesostructures lies in the hydrolysis rate of APTMS, basicity of the amines, and hydrophilicity of APTMS. The amine groups enhance water solubility as well as catalyze rapid hydrolysis, making the synthesis of a mesostructure functionalized with amines more difficult.

3.4.2 Method II-V Higher Bi-Functional Organic Incorporation

Four additional methods were used to prepare MP+AP-HMS with theoretical loading of x=y=0.25 where x and y are the fraction of the silicon centers being functionalized. For Method II, all silanes were mixed together and prehydrolyzed with half of the total ethanol needed for the reaction. The ethanol is anhydrous. However, trace amounts of water are presumably present upon exposure to the atmosphere, but not enough to completely hydrolyze the silanes. The silane ethanol mixture was added to the remaining ethanol and surfactant mixture, followed by the addition of water. Method III involves the prehydrolysis of only MPTMS and TEOS with half the total ethanol. Then the silane ethanol mixture was added to the rest of the ethanol and surfactant, followed by

the addition of APTMS. Water was then added to complete the reaction mixture. For Method IV, each silane was added one at a time, TEOS, MPTMS, and then APTMS to the surfactant ethanol mixture. This was done to see if the "prehydrolysis" had any effect on the resulting structure. The order of the reagents was chosen because APTMS hydrolyzes at a faster rate than the other silanes, by adding it after the other silanes, better incorporation of both the organosilanes might occur. Water was then added to the silane surfactant ethanol mixture. Method V was the same as Method IV except the silanes were premixed, not added individually.

The low angle powder x-ray diffraction patterns (XRD) are shown in Figure 3.5 for the MP+AP-HMS with x=y=0.25 prepared by Methods II-V. All powder patterns have a single broad peak of low intensity similar to MP-HMS with x=0.50.[26] The broadness is due in part to the presence of small particles, and the low intensity is due to contrast matching. But there are differences in the 2Θ value between each synthesis method. The silicas prepared by Method III have the highest 2Θ value, indicating the smallest pore size. The X-ray pattern for the mesostructures prepared by Method II, were very broad and of lower intensity than the others indicating substantial framework disorder.

Each mesostructure, regardless of the synthesis method, had a Type I isotherm[28] (not shown). The almost horizontal plateau of a Type I isotherm is generally considered to be an indication of a very small external surface area and of the absence of any significant mesoporosity. The physical properties calculated from the nitrogen isotherms are given in Table 3.3. The products have surface areas in the range of 338-654 m^2/g, less than that of the functionalized MP+AP-HMS compositions with smaller x and y

values, but comparable to the surface area of 695 m^2/g reported for MP-HMS with x=0.50 using dodecylamine as the porogen.[26] Pore volumes for MP+AP-HMS with theoretical loadings of x=y=0.25 range from 0.16-0.31 cm^3/g which are again comparable to the reported MP-HMS with x=0.50 pore volume of 0.35 cm^3/g. The pore diameter for all samples was < 2.0 nm.
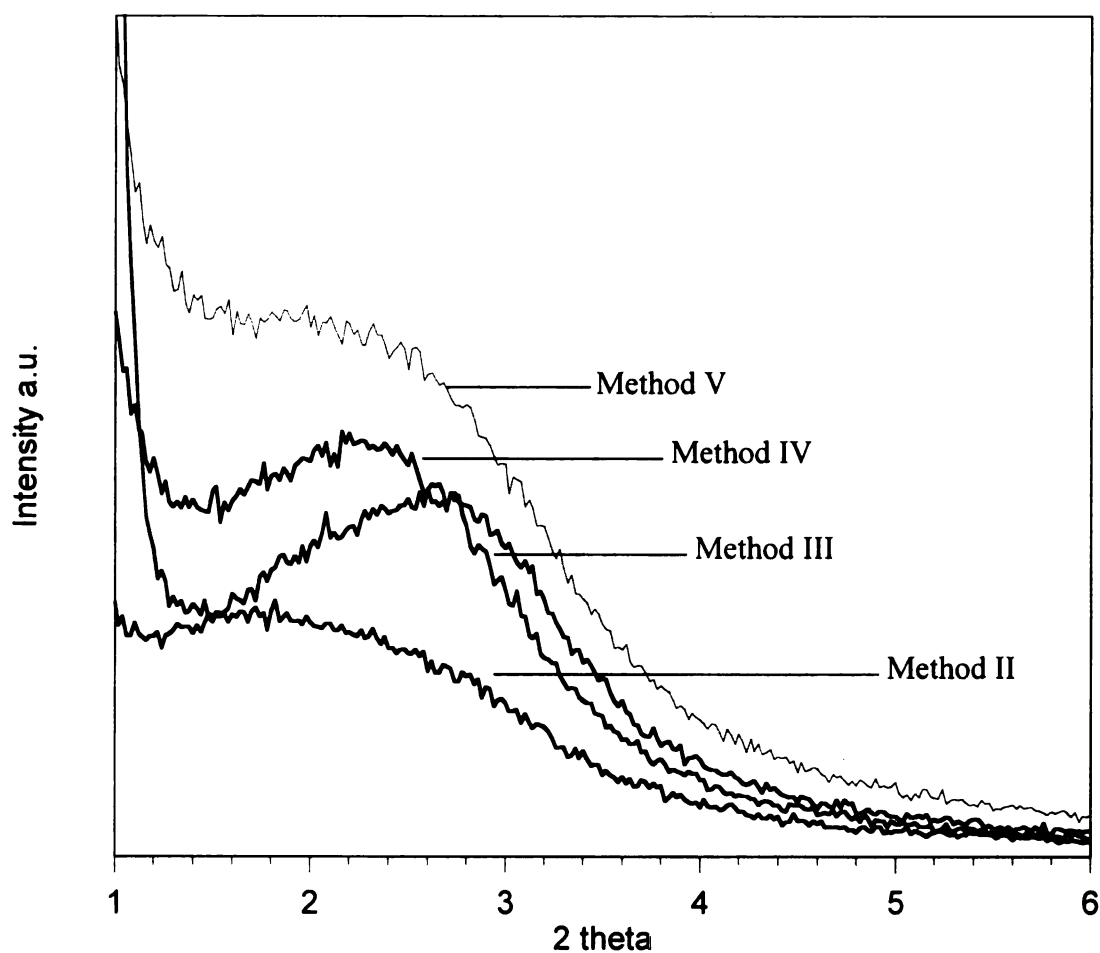
Figure 3.5. XRD pattern for functionalized $(SiO_2)_{1-(x+y)}$ $(LSiO_{1.5})_x$ $(L'SiO_{1.5})_y$ compositions (L=mercaptopropyl, L'=aminopropyl) where the theoretical organic loading is x=y=0.25 with a wormhole framework structure, denoted MP+AP-HMS and assembled to the method indicated.
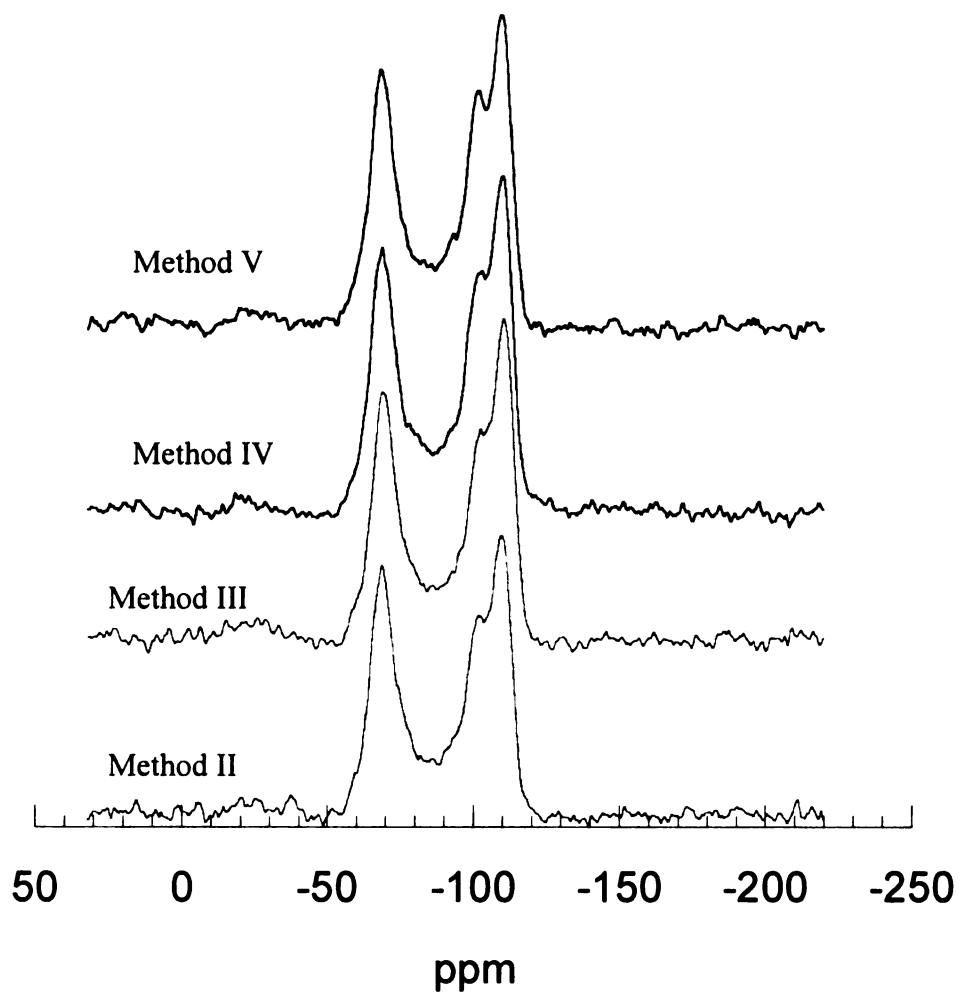
Figure 3.6. ^{29}Si MAS NMR spectra for functionalized $(SiO_2)_{1-(x+y)}(LSiO_{1.5})_x(L'SiO_{1.5})_y$ compositions (L=mercaptopropyl, L'=aminopropyl) where the theoretical organic loading is x=y=0.25 with a wormhole framework structure, denoted MP+AP-HMS and assembled according to the method indicated.
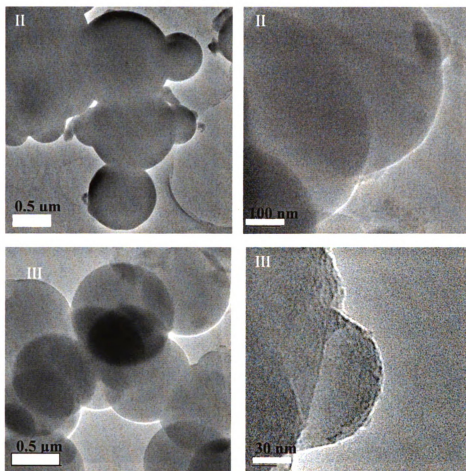
Figure 3.7. TEM images for functionalized $(SiO_2)_{1-(x+y)}(LSiO_{1.5})_x(L'SiO_{1.5})_y$ compositions (L=mercaptopropyl, L'=aminopropyl) where the theoretical organic loading is x=y=0.25 with a wormhole framework structure, denoted MP+AP-HMS. The Roman numeral indicates the synthesis method.
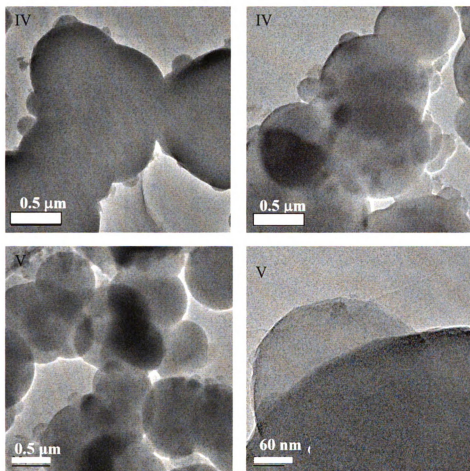
Figure 3.8. TEM images for functionalized $(SiO_2)_{1-(x+y)}(LSiO_{1.5})_x(L'SiO_{1.5})_y$ compositions (L=mercaptopropyl, L'=aminopropyl) where the theoretical organic loading is x=y=0.25 with a wormhole framework structure, denoted MP+AP-HMS. The Roman numeral indicates the synthesis method.

Table 3.3. Textural properties of functionalized $(SiO_2)_{1-(x+y)}(LSiO_{1.5})_x(L'SiO_{1.5})_y$ compositions (L=mercaptopropyl, L'=aminopropyl) where x=y=0.25 with a wormhole framework structure, denoted MP+AP-HMS and assembled according to the method indicated.

Synthesis Method	d_{100}	Pore[a] diameter	SA[b] cm^2/g	Pore volume[c] cm^3/g	$x+y_{theo}$	$x+y_{obs}$[d]	Q^4/Q^3	mmol ligands/g theoretical	mmol ligands/g observed	mmol SH/g	mmol NH_2/g
II	39.8	<2.0	388	0.19	0.5	0.49	0.83	5.60	5.38	2.74	2.64
III	33.5	<2.0	637	0.30	0.5	0.44	0.94	5.60	4.96	2.82	2.14
IV	39.1	<2.0	654	0.31	0.5	0.33	0.74	5.60	3.96	2.64	1.32
V	38.1	<2.0	338	0.16	0.5	0.35	0.99	5.60	4.15	2.72	1.42

[a]Determined by the Horvath-Kawazoe model. [b]Calculated from nitrogen adsorption isotherms by BET method. [c]Total pore volume determined at P/Po = 0.98. [d]Determined from ^{29}Si MAS NMR.
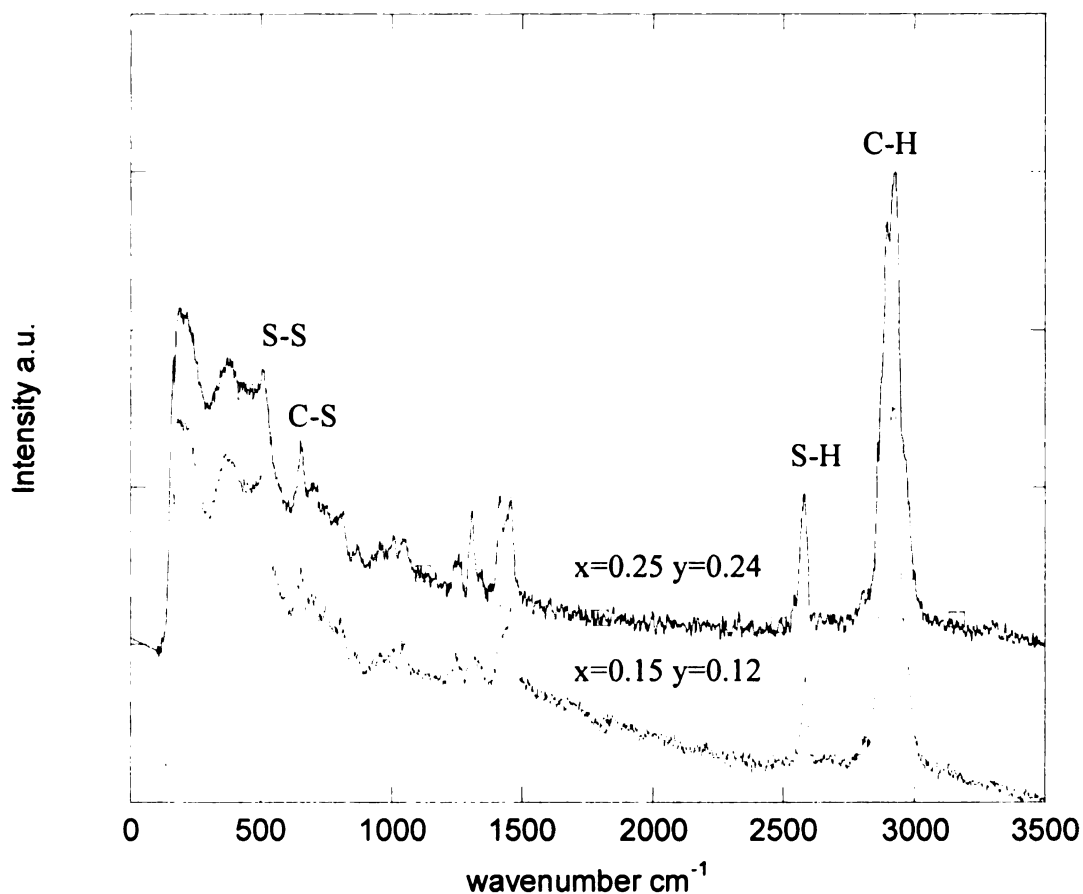
Figure 3.9. Raman spectra of functionalized $(SiO_2)_{1-(x+y)}(LSiO_{1.5})_x(L'SiO_{1.5})_y$ compositions (L=mercaptopropyl, L'=aminopropyl) with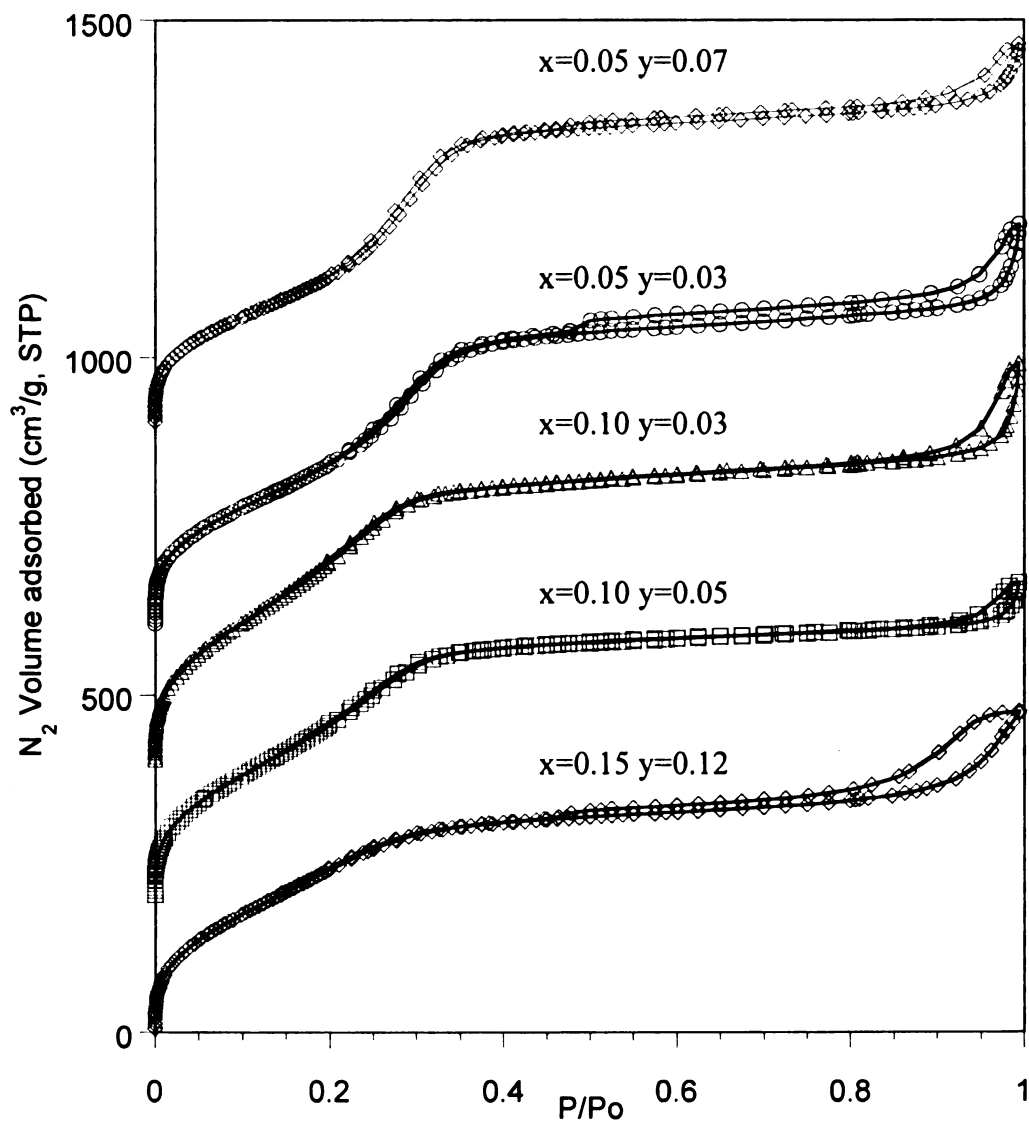 a wormhole framework structure, denoted MP+AP-HMS. The mesostructure with x=0.15 y=0.12 was assembled using Method I and the mesostructure with x=0.25 y=0.24 according to Method II. The spectra are offset on the y-axis for clarity.

In order to determine the amount of incorporation of the organic group, ^{29}Si

MAS-NMR was done, the results are shown in Figure 3.6. The T^3 band, indicative of a

silane with three hydrolyzable groups and one Si-C bond, was nearly equal in intensity to

the Q band intensity, demonstrating high organic incorporation. However, the Q^3 band,

which signifies incompletely cross-linked silica, changed with the different synthetic

methods. The framework cross-linking and the organosilane mole fractions were

calculated from the deconvoluted ^{29}Si MAS NMR spectroscopic data, and the results are

given in Table 3.3. The products of the synthetic Methods II and V had a 1:1 Q^4/Q^3 ratio.

Mesostructures prepared by Methods III and IV had a greater amount of incompletely

condensed silicon centers and thus a smaller Q^4/Q^3 ratio signifying less framework cross-

linking. Methods II and III produced the structures with the highest degree of organic

group incorporation with 98 and 88% of the organosilanes added being incorporated into

the framework, respectively. These results indicate that prehydrolysis of the silanes does

indeed have a positive effect on the quality of the products. The two samples made by

Methods IV and V for which the silanes were not prehydrolyzed, had around 70%

incorporation of the organic moieties. By elemental analysis, it was determined that less

than quantative organic group incorporation was due to low amine incorporation. Even

though Methods II and III for the synthesis of MP+AP-HMS with theoretical value of

x=y=0.25 had nearly quantative incorporation of the organosilanes, there were other

physical differences between the two products. The mesostructure prepared by Method

II, in which the all the silanes were simultaneously mixed and prehydrolyzed, had a lower

surface area (388 vs. 637 m^2/g) area and lower pore volume (0.19 vs. 0.30 cm^3/g) than the

product of Method III, where only the MPTMS and TEOS were prehydrolyzed and

APTMS was added later. Since MPTMS is the most hydrophobic reagent in the system and APTMS is quite hydrophilic, differentiating their addition to the reaction mixture allows for improved pore volume and surface area properties.

The TEM images for the products of each synthesis method are shown in Figures 3.7 and 3.8. All synthetic methods for MP+AP-HMS with theoretical values of x=y=0.25 formed spheres. The change of the morphology from sponge-like particles to spheres was observed for MP+AP-HMS with x=0.15 y=0.12. The change to a purely spherical morphology was not unexpected with the increase of functionality. The formation of spheres is due to the tendency of the system to minimize the interface between the silica and solution. Synthesis Methods III and V produced more individualized spheres than did synthesis Methods II and IV.

The presence of the thiol in the samples is easily confirmed by Raman spectroscopy (Figure 3.9). An attempt was made to use diffuse reflectance infrared spectroscopy (DRIFTS) to characterize the amine portion of the MP+AP-HMS (Figure not shown). The N-H bend in primary amines results in a broad band in the range from 1640-1560 cm^{-1}.[30] Primary amines have two bands in the range of 3500-3300 cm^{-1} from the N-H stretch.[30] There were bands present in these ranges observed in the DRIFTS spectra of MP+AP-HMS with x=y=0.25. However, there were also bands observed in the non-functionalized HMS composition in these regions. There was a very broad band observed in both the amine-functionalized mesostructure as well as the non-functionalized mesostructure in the 3500-3300 cm^{-1} region. Nonetheless, the band was not a doublet as would indicate the presence of a primary amine. The amine stretch was most likely overlapped by the O-H stretch in this region. Hydroxyl groups (Si-OH) are

known to be present in both samples. The band observed at 1610 cm^{-1} could be due to the bending mode of molecular water. Thus, elemental analysis was the only way to quantify amine incorporation.

3.5 Conclusion

Dual-functionalized mesostructured organosilica compounds with high organic incorporation have been assembled via the direct assembly methodology in the presence of a neutral amine surfactant as a structure director has been accomplished. The compositions synthesized, denoted MP+AP-HMS, have the anhydrous formula $(SiO_2)_{1-(x+y)}$ $(LSiO_{1.5})_x$ $(L'SiO_{1.5})_y$ where (L=mercaptopropyl, L'=aminopropyl) . The derivatives had a wormhole or spherical morphology depending on the organic loading level. The functional group loading of 5.38 mmol ligand/g, is the highest reported for a multifunctional mesostructure. Depending on the synthesis method, quantative incorporation of both the amine and the mercaptan could be achieved. In other cases, only 70% of the amine added was incorporated into the structure. Additionally, the dual-functionalized mesostructures had surface areas in the range of 1203-338 m^2/g and pore sizes of 3.6-2.0 nm. The physical properties for MP+AP-HMS are analogous to those reported for MP-HMS prepared with dodecylamine. The utilization of these mesostructures for arsenic adsorption will be examined in Chapter 5.

3.6 References

(1) Van Rhijn, W. M.; De Vos, D. E.; Sels, B. F.; Bossaert, W. D.; Jacobs, P. A. *Chem. Commun.* **1998**, 317-318.

(2) Van Rhijn, W.; De Vos, D.; Jacobs, P. A. *Stud. Surf. Sci. Catal.* **1998**, 117, 183.

(3) Mdoe, J. E. G.; Clark, J. H.; Macquarrie, D. J. *Synlett* **1998**, 625-627.

(4) Rao, Y. V. S.; De Vos, D. E.; Jacobs, P. A. *Angew. Chem., Int. Ed. Engl.* **1997**, 36, 2661-2663.

(5) Feng, X.; Fryxell, G. E.; Wang, L. Q.; Kim, A. Y.; Liu, J.; Kemner, K. M. *Science* **1997**, 276, 923-926.

(6) Mercier, L.; Pinnavaia, T. J. *Adv. Mater.* **1997**, 9, 500-&.

(7) Yoshitake, H.; Yokoi, T.; Tatsumi, T. *Chem. Mater.* **2002**, 14, 4603-4610.

(8) Fryxell, G. E.; Liu, J.; Hauser, T. A.; Nie, Z. M.; Ferris, K. F.; Mattigod, S.; Gong, M. L.; Hallen, R. T. *Chem. Mater.* **1999**, 11, 2148-2154.

(9) Boissiere, C.; Kummel, M.; Persin, M.; Larbot, A.; Prouzet, E. *Adv. Func. Mater.* **2001**, 11, 129-135.

(10) Ma, Y.; Qi, L.; Ma, J.; Wu, Y.; Liu, O.; Cheng, H. *Colloids Surf., A* **2003**, 229, 1-8.

(11) Martin, T.; Galarneau, A.; Di Renzo, F.; Brunel, D.; Fajula, F.; Heinisch, S.; Cretier, G.; Rocca, J.-L. *Chem. Mater* **2004**, 16, 1725-1731.

(12) Salesch, T.; Bachmann, S.; Brugger, S.; Rabelo-Schaefer, R.; Albert, K.; Steinbrecher, S.; Plies, E.; Mehdi, A.; Reye, C.; Corriu, R. J. P.; Lindner, E. *Adv. Func. Mater.* **2002**, 12, 134-142.

(13)   Lin, V. S.; Lai, C. Y.; Huang, J.; Song, S. A.; Xu, S. *J. Am. Chem. Soc.* **2001**, *123*, 11510-11511.

(14)   Huh, S.; Wiench Jerzy, W.; Trewyn Brian, G.; Song, S.; Pruski, M.; Lin Victor, S. Y. *Chem. Commun.* **2003**, 2364-2365.

(15)   Huh, S.; Wiench, J. W.; Yoo, J.-C.; Pruski, M.; Lin, V. S. Y. *Chem. Mater.* **2003**, *15*, 4247-4256.

(16)   Deratani, A.; Sebille, B. *Anal. Chem.* **1981**, *53*, 1742-1746.

(17)   Huh, S.; Chen, H.-T.; Wiench, J. W.; Pruski, M.; Lin, V. S. Y. *J. Am. Chem. Soc.* **2004**, *126*, 1010-1011.

(18)   Hall, S. R.; Fowler, C. E.; Mann, S.; Lebeau, B. *Chem. Commun.* **1999**, 201-202.

(19)   Lee, B.; Kim, Y.; Lee, H.; Yi, J. *Microporous Mesoporous Mater.* **2001**, *50*, 77-90.

(20)   Margolese, D.; Melero, J. A.; Christiansen, S. C.; Chmelka, B. F.; Stucky, G. D. *Chem. Mater.* **2000**, *12*, 2448-2459.

(21)   Zub, Y. L.; Seredyuk, I. V.; Chuiko, A. A.; Jaroniec, M.; Jones, M. O.; Parish, R. V.; Mann, S. *Mendeleev Commun.* **2001**, 208-210.

(22)   Mel'nyk, I. V.; Zub, Y. L.; Chuiko, A. A.; Jaroniec, M.; Mann, S. *Stud. Surf. Sci. Catal.* **2002**, *141*, 205-212.

(23)   Macquarrie, D. J. *Green Chem.* **1999**, *1*, 195-198.

(24)   Gong, Y. J.; Li, Z. H.; Wu, D.; Sun, Y. H.; Deng, F.; Luo, Q.; Yue, Y. *Microporous Mesoporous Mater.* **2001**, *49*, 95-102.

(25)   Gong, Y.; Li, Z.; Wu, D.; Sun, Y.; Dong, B.; Deng, F. *Stud. Surf. Sci. Catal.* **2003**, *146*, 461-465.

(26)   Mori, Y.; Pinnavaia, T. J. *Chem. Mater.* **2001**, *13*, 2173-2178.

(27)   Mercier, L.; Pinnavaia, T. J. *Chem. Mater.* **2000**, *12*, 188-196.

(28)   Sing, K. S. W.; Everett, D. H.; Haul, R. A. W.; Moscou, L.; Pierotti, R. A.;
         Rouquerol, J.; Siemieniewska, T. *Pure Appl. Chem.* **1985**, *57*, 603-619.

(29)   Yokoi, T.; Yoshitake, H.; Tatsumi, T. *J. Mater. Chem.* **2004**, *14*, 951-957.

(30)   Kriz, D. P. G. L. G. *Introduction to Spectroscopy: A guide for students of organic
         chemistry*; COMPress: Wentworth NH, 1987.

Chapter 4

Mercury Trapping by Functionalized Wormhole Mesostructures

4.1 Introduction

Mercury is a ubiquitous toxic heavy metal known to cause neurological impairment in humans and is of great environmental concern. According to the United States Environmental Protection Agency (EPA) the greatest source of anthropogenic mercury is from coal-fired power plants, other sources include chlor-alkali plants, and incineration of waste.[1] During combustion, the mercury in coal is volatilized and converted to elemental mercury (Hg^0) vapor in the high temperature regions of coal-fired boilers. As the flue gas is cooled, a series of complex reactions begin to convert Hg^0 to vapor phase ionic mercury (Hg^{2+}) compounds and/or solid phase or particulate-bound mercury (Hg_p).[1] Atmospheric deposition of mercury is a primary route of transport of mercury to water. Mercury is also found naturally in the environment from the eruption of volcanoes, and it is also present in ores such as cinnabar (HgS). Leaching of these ores contributes to the presence of mercury in water. Mercury has been listed as a pollutant of concern to the EPA's Great Water Program due to its persistence in the environment, potential to bioaccumulate, and toxicity to humans and the environment. Due to this toxicity and the prevalence of mercury in water, in 2003 45 states issued mercury fish advisories to limit the human consumption of fish in those states.[2] Although most waterways in the US contain mercury in the parts per trillion (ppt) range of concentration, Superfund sites, the Everglades, and countries such as India, have much higher concentrations of mercury in water. The EPA has set a maximum contaminant

level (MCL) of 0.002 ppm for the concentration of mercury allowable in drinking water and a MCL of 0.020 ppm for hazardous waste.

According to the EPA, well-established and widely reported full-scale technologies for aqueous mercury treatments are precipitation, coagulation/co-precipitation, and activated carbon adsorption.[3] Ion-exchange is also a viable technique. Co-precipitation and ion-exchange achieve the lowest effluent mercury concentrations for many waste streams, ranging from 0.5 to 5.0 ppb.

Remediation of mercury via the precipitation method involves the addition of a sulfide salt to the waste stream to convert the soluble mercury to insoluble HgS. This process is usually combined with pH adjustment and flocculation, followed by solids separation. This method is not able to reduce mercury below 10 -100 ppb, and the formation of soluble mercury sulfide species at excess dosage of sulfide, due to the common ion effect, is possible.[3] Another drawback is the need to dispose of the sulfide sludge.

Coagulation/co-precipitation is a process in which one ion is adsorbed into another bulk solid formed in situ. Alum (aluminum sulfate) is a common coagulant used. The alum precipitates to form aluminum hydroxide which in turn adsorbs the mercury. Effluent levels of mercury achieved by alum treatment range from 1.5 to 102 ppb, with a value of 5 to 10 ppb being typical.[3] As with other treatments, pH adjustments and filtration are necessary steps for this treatment to be effective.

According to the US Department of Energy (DOE), granular activated carbon is the most commonly used adsorbent system for treating industrial waste. Pretreatment or modification of activated carbon with a carbon disulfide solution before use has been

shown to improve mercury removal from waste. Activated carbon can reduce mercury levels from 10 ppm to 4 ppm. The sulfur-modified activated carbon can reduce mercury effluent from 10 ppm to 0.2 ppb.[3]

Ion–exchange resins have a higher loading capacity than activated carbon. The initial trapping capacity typically is 150 g Hg(II)/L of resin, and the effluent concentration can be reduced to below 10 μg/L.[3] This technique has historically been limited to the use of anion resins to process industrial wastewater that contains inorganic mercury in the complex mercuric chloride form. Furthermore, most available resins are not easily regenerated and thus need to be deposited in waste storage sites and replaced after loading.

One promising technique for achieving the removal of low levels of mercury from ground water is to trap it using complexing ligands (e.g. thiols) that are covalently linked to porous structures. Thiol functionalized mesoporous silicas have been examined as candidates for mercury remediation.[4-7] The advantages of functionalized mesoporous silicas are their high surface areas, well-defined pore size, framework structure that is stable under regeneration conditions, and ability to covalently link organic groups to the framework to allow for selective adsorption of toxic heavy metals such as mercury. This linkage of the organic moiety to the mesostructure can be accomplished by two different means, grafting or direct-assembly. Grafting is the process by which an organic moiety is anchored onto a silica surface though condensation of surface silanols with alkoxy groups of an organosiloxane. This process has been used to functionalize wormhole HMS,[4,8] hexagonal MCM-41,[5] and hexagonal SBA-15[6] mesostructures. Each of these mesostructures has been utilized for mercury trapping. The direct-assembly pathway for

the functionalization of a mesostructure entails the direct co-condensation of an organosilane with a silica precursor in the initial reaction mixture to form a product with the anhydrous composition $(SiO_2)_{1-x} (LSiO_{1.5})_x$, where L is the organic group and x is the fraction of the framework silicon centers that are functionalized. Both hexagonal MCM-41[7,9] and wormhole MSU-X[10] have been functionalized by direct-assembly and used for mercury adsorption.

The focus of this work is to examine Hg^{2+} remediation with a functionalized mesoporous silica, denoted MP-HMS, which has the anhydrous composition $(SiO_2)_{1-x}$ $(LSiO_{1.5})_x$ where L is the mercaptopropyl group and x is the fraction of framework silicon centers that are functionalized. Since the process of direct-assembly allows for a greater loading of the organic group, fewer steps in the overall synthesis, recovery of the surfactant, greater accessibility to the organic groups, and a more homogenous distribution of the organic groups, this was the desired method for functionalization chosen in the present work. Additionally, the morphology of the trapping agent is an important factor to be considered. The wormhole framework motif of MP-HMS assembled through a hydrogen bonding interaction between the surfactant and silica source provides a 3-D channel network and allows for more facile accessibility to the trapping sites than the 1-D pore structure of hexagonal frameworks formed an electrostatically directed assembly pathway.[11]   In addition to the trapping of mercury by MP-HMS, regeneration of the spent adsorbent, leaching of the trapped mercury, and coordination of the bound mercury by pair distribution function (PDF) analysis of synchrotron X-ray scattering data will be examined in this chapter.

4.2 Experimental

4.2.1 Reagents

Mercaptopropyltrimethoxysilane, tetraethylorthosilicate, and dodecylamine, were purchased from Aldrich and used without further purification. Absolute ethanol, nitric acid, ammonium hydroxide, and carbon tetrachloride were purchased in-house. A standardized mercuric nitrate solution in water with a known concentration was used as the Hg^{2+} source. The mercuric nitrate solution and the indicator, diphenylthiocarbazone, were purchased from Aldrich. Water used in the synthesis was double-exchanged to remove cations and anions via a Millipore filter apparatus.

4.2.2 Material Synthesis

4.2.3 Material for Mercury Adsorption

MP-HMS mesostructures with wormhole frameworks structures were synthesized by the direct-assembly method using dodecylamine as the porogen. The mesostructures which have the anhydrous composition $(SiO_2)_{1-x}$ $(LSiO_{1.5})_x$, where L equals mercaptopropyl (MP), were examined for viability in mercury adsorption. Two different mesostructures forms of MP-HMS were used. A powdered MP-HMS was synthesized by direct-assembly as previously reported.[12] The second mesostructure was micron-sized spheres prepared by Method III as described in Chapter 2. Mercaptopropyl-functionalized micron-sized spheres were synthesized by the application of vigorous shaking at the beginning of the synthesis followed by aging in a reciprocating water bath shaker.

4.2.4 Functionalized Wormhole Structures

MP-HMS. In accord with the previously reported method,[12] ethanol, warmed to 65 °C, was used to dissolve the surfactant, dodecylamine. A (1-x) : x molar mixture of tetraethylorthosilicate (TEOS) and mercaptopropyltrimethoxysilane (MPTMS) was then added to the surfactant solution. The silanes were allowed to prehydrolyzed 40 min with a small amount of water present in the ethanol-surfactant solution. Next, water pre-warmed to 65 °C was rapidly added to the surfactant-silane solution. The resulting mixture was then aged in a reciprocating water bath shaker at 65 °C for 36 h. Finally, the solution was filtered, the precipitate collected and air-dried, followed by Soxhlet extraction with ethanol to remove the surfactant. The overall molar stoichiometry employed was: 1-x TEOS : x MPTMS : 0.22 DDA : 6.7 EtOH : 160 H_2O.

Micron-sized spherical MP-HMS. The samples were made according to Method III described in Chapter 2. Ethanol, warmed to 65 °C, was used to dissolve the surfactant, dodecylamine. A premixed solution of 1-x TEOS and x MPTMS was then added to the surfactant solution. The solution was vigorously shaken for 30 s, and the silanes were allowed to prehydrolyze in the surfactant solution for 40 min. Next, water, pre-warmed to 65 °C, was rapidly added to the surfactant silane solution. The entire mixture was then vigorously shaken for 2 min and aged in a reciprocating water bath shaker at 65 °C for 36 h. The solution was filtered, the precipitate collected and air-dried, followed by Soxhlet extraction with ethanol to remove the surfactant. The overall molar stoichiometry employed was: 1-x TEOS : x MPTMS : 0.22 DDA : 6.7 EtOH : 160 H_2O.

4.3 Physical Measurements

The physical properties of the functionalized mesostructures were determined by nitrogen adsorption, powder X-ray diffraction (XRD), ^{29}Si Magic Angle Spinning Nuclear Magnetic Resonance spectroscopy (^{29}Si MAS-NMR), and Transmission Electron Microscopy (TEM). The binding of mercury to the mesostructures was examined by Raman spectroscopy and Pair Distribution Function (PDF) analysis of synchrotron X-ray scattering data. For obtaining the mercury uptake curves, the amount of mercury in the filtrate before and after adsorption was analyzed by UV-VIS spectroscopy and cold vapor atomic absorption spectroscopy (AAS).

Nitrogen adsorption-desorption isotherms were measured at -196 °C on a Micrometrics ASAP 2010 sorptometer. The samples were outgassed at 80 °C and 10^{-6} Torr prior to measurement. Powder XRD patterns were collected on a Rigaku rotaflex diffractometer using Cu Kα radiation. ^{29}Si MAS-NMR spectra were collected on a Varian 400 solid state NMR spectrometer with a field strength of 400 MHz, under single-pulse mode with a zirconia rotor at a spinning frequency of 4 kHz. A pulse delay of 400 s was employed so that there was sufficient time for the nuclei to relax before application of another pulse. Talc was used as a reference. TEM images were obtained on a JOEL 2200FS microscope with an accelerating voltage of 200 KV. Sample grids were prepared by sonicating samples in ethanol for 20 min and evaporating one drop of the suspension onto a carbon coated, holey film supported on a 3 mm, 300 mesh copper grid. For Raman spectroscopy, samples were packed into glass capillary tubes and analyzed with a Bio-Rad FT Raman Spectrometer equipped with a germanium CCD camera detector and 633 nm radiation from a HeNe laser for excitation with a resolution of 4 cm^{-1}. Laser

power at the sample was estimated to be about 5mW, and the focused laser beam diameter was ~10 μm. A total of 200 scans was accumulated for each spectrum. The x-ray scattering experiments were conducted on the powder samples using x-rays of energy 76 keV (λ=0.16248 Å) at the 6-IDD beam line at the Advanced Photon Source (APS) at Argonne National Laboratory. Diffraction data were collected using the recently developed rapid acquisition pair distribution function (RA-PDF) technique.[13] The UV-VIS absorbance measurements for the colorimetric analysis of mercury were carried out on an IBM 9430 UV-Visible double beam spectrometer at a set wavelength of 485 nm using diphenylthiocarbazone as an indicator.

4.3.1 Batch Studies of Mercury Adsorption. A 200-mg quantity of MP-HMS with x=0.30 or x=0.50 was added to a specific volume of 1000 ppm $Hg(NO_3)_2$ solution. The volume of solution was varied to achieve specific Hg^{2+}:SH molar ratios. The ratios of Hg^{2+}:SH were varied from 0.1 up to 2.0 by adjusting the weight ratio of solution to solid from 100 to 2,000. The suspensions were agitated for 48 ± 3 h, and the filtrate was analyzed by colorimetric assay using diphenylthiocarbazone as a complexant.[14] The spectrophotometric analysis procedure for determination of residual mercury in the filtrate was governed by the ratio of Hg^{2+}: diphenylthiocarbazone. The maximum mole ratio that can be accurately measured is 0.5 mol of Hg^{2+}:1 mol indicator. To ensure that there was excess indicator, the filtrate was diluted. After the filtrate was diluted to a total volume of 10 mL, 10 drops of concentrated nitric acid were added to ensure that all mercury was in the 2+ oxidation state. Next 5 g of indicator solution (8.2 mg of diphenylthiocarbazone in 500 g of carbontetrachloride) was added as well as an additional 5 g quantity of carbon tetrachloride. The mixture was vigorously shaken, and

the liquids were allowed to separate. All of the mercury is in the aqueous phase. To release any excess indicator from the aqueous phase, 20 drops of concentrated ammonium hydroxide were then added to the mixture. The aqueous phase was then analyzed by UV-VIS at 485 nm. Using a linear calibration curve and Beer's Law, the concentration of the mercury in the filtrate was determined. The amount of mercury adsorbed by the MP-HMS mesostructure is then the difference of the known amount added to the initial reaction and the final amount in the filtrate.

5.3.2 Column Studies of Mercury Adsorption. Micron sized spherical MP-HMS synthesized by Method III (described in Chapter 2) with x=0.30 or 0.50 were used for mercury adsorption in packed column geometry. A 50 mL plastic pipet, with glass wool in the bottom, was packed with 10-20 cc of pre-wetted solid. A plastic buret was chosen because a glass column caused the solid to creep, disturbing the packing. In order to optimize the flow of the column, the spherical MP-HMS was sieved (using either a 38 or 45 μm sieve) to exclude small spheres. A solution of 50 ppm, 5 ppm, or 0.1 ppm mercuric nitrate was passed through the column. The effect of different bed heights and flow rates on mercury adsorption was examined. The effluent was acidified with 1.4 mL of concentrated HCl and 0.4 mL of HNO_3 and analyzed by cold-vapor atomic absorption spectroscopy. The MSU toxicology laboratory provided cold vapor AAS analysis for the mercury content of the samples obtained in the column studies.

4.3.3 PDF. These studies were carried out by the research group of Professor Simon Billinge in the Department of Physics and Astronomy, Michigan State University and professor Valeri Petkov, Department Physics and Astronomy, Central Michigan University. A 500-mg quantity of MP-HMS with x=0.50 was added to 1000 ppm

$Hg(NO_3)_2$ solutions with Hg^{2+}:SH ratios equal to 0.5 and 2.0. The suspensions were agitated for 48 h ± 3, and the filtrate was analyzed by colorimetric assay using diphenylthiocarbazone as an indicator.[14] The air-dried solids were examined by PDF the data were extracted from X-ray scattering data obtained at the Advanced Photon Source (APS) at Argonne National Laboratory.

4.3.4 Regeneration Experiments. MP-HMS compositions with x = 0.10, 0.30, and 0.50 were loaded with varying amounts of mercury per mole of immobilized thiol by equilibrating the solids with known amounts of $Hg(NO_3)_2$ solution. The slurry was agitated for 20 h and then filtered. The solid was allowed to air-dry for 20 h and then was washed with a 6 M HCl solution to displace the coordinated mercury. This mixture was stirred until the material was fully wetted and sank to the bottom of the container. The acid washed material was filtered and air-dried for 20 h. The regenerated MP-HMS was again loaded with the same amount of $Hg(NO_3)_2$ to determine the adsorption capacity after regeneration.

4.3.5 Leaching of mercury from MP-HMS. Mercury was loaded onto MP-HMS compositions with x=0.10 and x=0.50 at both room temperature and at 65 °C using a Hg^{2+}:SH ratio greater than one. After being filtered, the mercury-saturated material was then rinsed with water to remove any surface mercury and air-dried. A 1:100 mixture of sample to water was stirred for 5 min with a magnetic stir bar, and the resultant pH was measured. Since the pH of the mixture was found to be less than 5, an acetic acid-sodium acetate buffer extraction fluid of pH = 5 was used, according to the EPA method number 1311 protocol. A sample containing 50 milligrams of the dried mercury-laden material was then added to the acetate buffer extraction fluid. This mixture was agitated at room

temperature at 100 rpm for 18 hr ± 2 hr. After stirring, the solid was removed by filtration and rinsed with 5 mL of deionized water. The filtrate analyzed by UV-VIS spectroscopy.[14]

4.4 Results and Discussion

4.4.1 MP-HMS Material Characterization

Wormhole mesostructures with mercaptopropyl organic moieties incorporated by direct-assembly have been prepared under near neutral pH conditions with an amine surfactant as the porogen. The mesostructures denoted, MP-HMS, have high surface areas as well as a high level of incorporation of the thiol groups. Within experimental uncertainty, all of the thiol initially present in the assembly reaction is incorporated into the framework of the mesostructure. The low angle powder x-ray diffraction patterns (XRD) for the powder form of MP-HMS are shown in Figure 4.1. For each structure, a single broad diffraction peak was observed, indicative of a wormhole mesostructure. Variations in the amount of functional groups lead to changes in the intensity of the peak. MP-HMS silica with no thiol functionality (x=0.00) has the most intense XRD peak. MP-HMS with x=0.50 exhibits the least intense XRD peak and the highest level of thiol. This decrease in the intensity of the XRD peak with increased organic group loading is attributed to contrast matching.[15] There is also a marked increase in broadness of the XRD peaks with increase in the thiol functionality. This broadness indicates increased variation in the pore-pore correlation distances due to perturbation of the micelle by the organic groups due to the greater interaction between the organic moieties and the hydrophobic core of the micelle.

The powder form of MP-HMS nitrogen isotherms are shown in Figure 4.2. The MP-HMS with x=0.00 and 0.10 exhibit a well-defined mesopore filling step in the $P/P_0 =$ 0.4 region of theType IV isotherms.[16] The MP-HMS with x=0.30 exhibits a small knee at a lower P/P_0, near 0.2, and an uptake of nitrogen a P/P_0 region above 0.8 indicative of textural porosity. Textural porosity is generated by the void space between primary particles. MP-HMS with x=0.50 displays a Type I isotherm characteristic of a microporous material.[16] The long, almost horizontal plateau of a Type I isotherm is generally considered to be an indication of a very small external surface area and of the absence of any significant mesoporosity.

The thiol loadings for MP-HMS powder with x values of 0.10 to 0.50 ranged from 1.4 to 5.2 mmol/g as calculated from the ^{29}Si MAS NMR spectra (Figure 4.3). The thiol incorporation of each MP-HMS composition as determined by ^{29}Si MAS NMR was quantative, the x values expected on the basis of the reaction stoichiometry used in the preparation were equal to the x values in the final products. The framework cross-linking parameters and mercaptan incorporation for MP-HMS with x=0.10, 0.30, and 0.50 are given in Table 4.1. In addition to quantative inclusion of the organic moiety, the structures also have highly cross-linked frameworks.

The TEM images for the powder MP-HMS compositions are shown in Figure 4.4. The wormhole morphology expected from the XRD patterns is indeed verified by the TEM image.
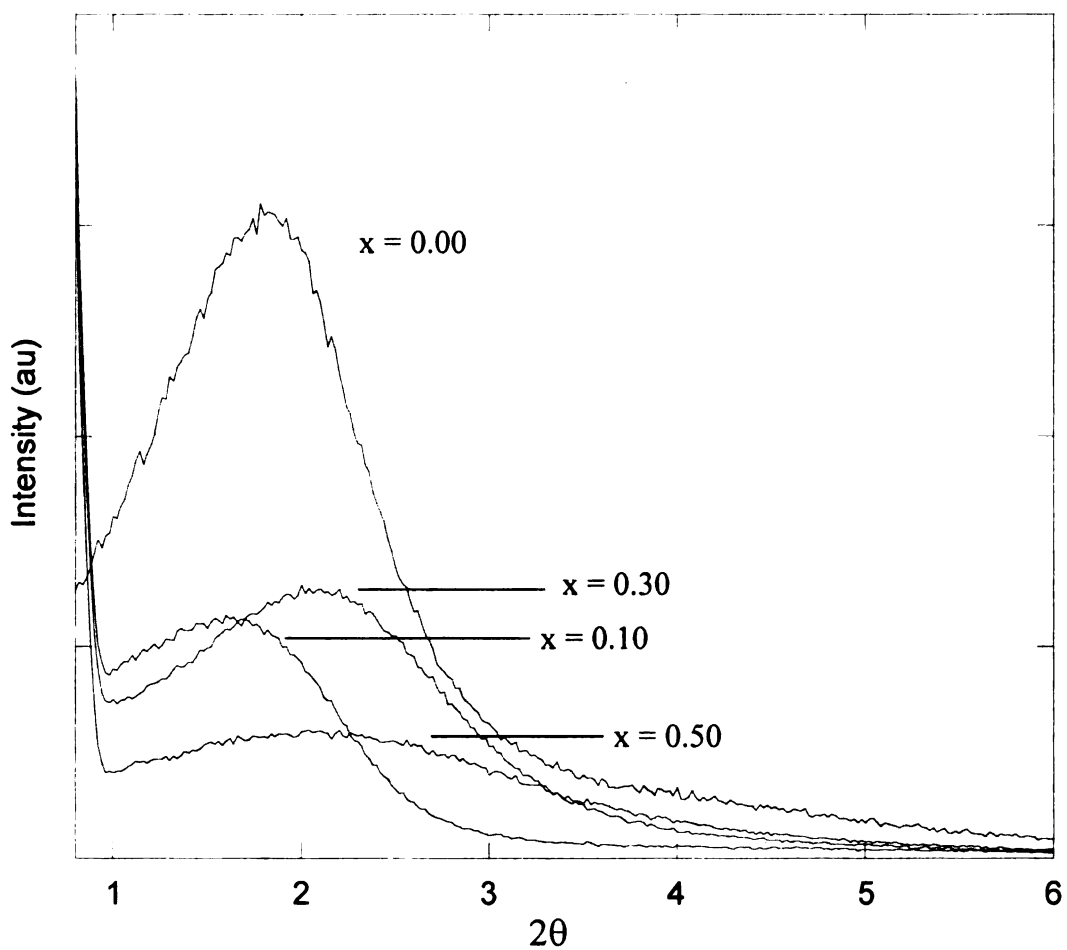
Figure 4.1. XRD patterns for powder form of functionalized $(SiO_2)_{1-x}(LSiO_{1.5})_x$ compositions (L=mercaptopropyl) with a wormhole framework structure denoted, MP-HMS.
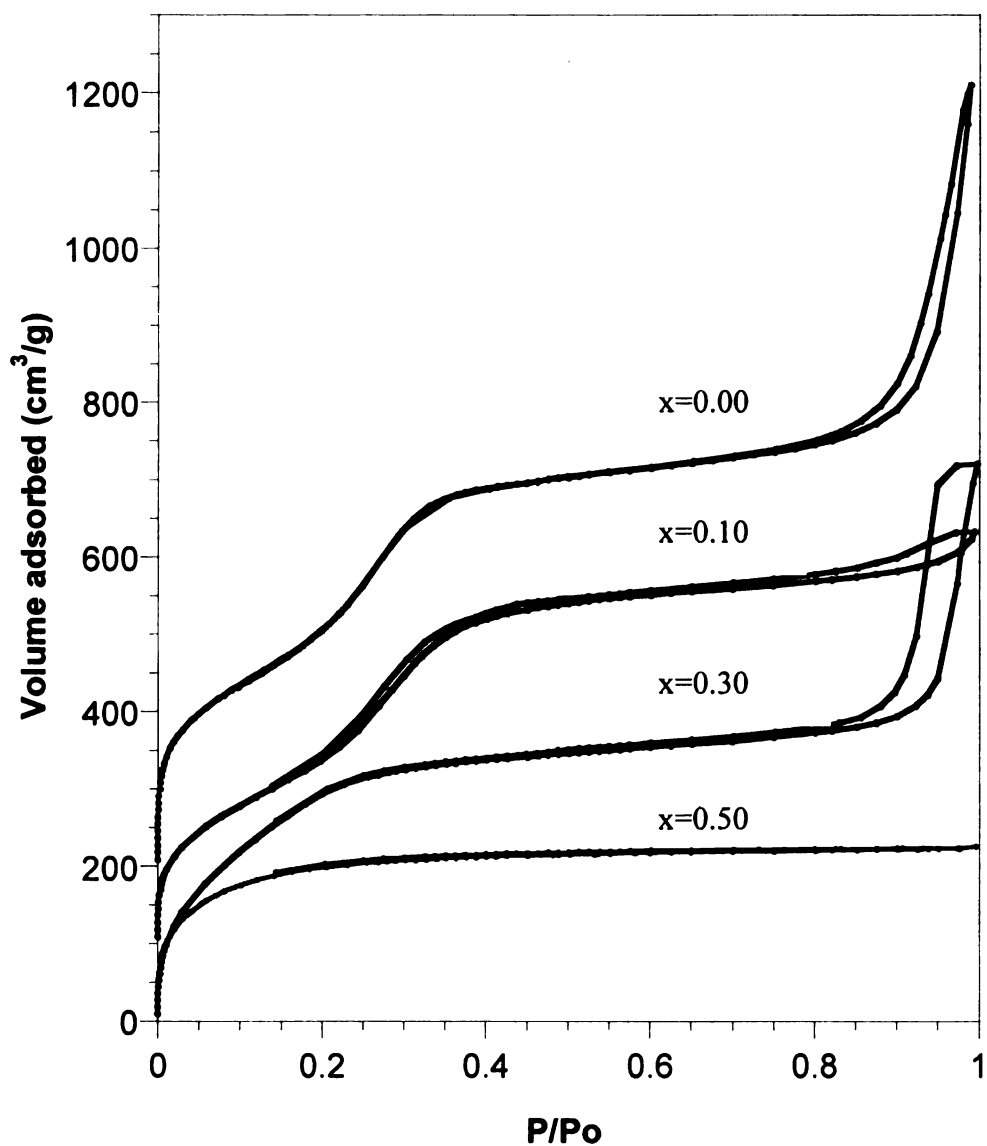
Figure 4.2. Nitrogen adsorption-desorption isotherm for the powder form of functionalized $(SiO_2)_{1-x}(LSiO_{1.5})_x$ compositions (L=mercaptopropyl) with a wormhole framework structure, denoted MP-HMS. The isotherm of x = 0.00 is offset vertically by 200 cm^3/g and the isotherm of x = 0.10 is offset vertically by 100 cm^3/g for clarity.

137
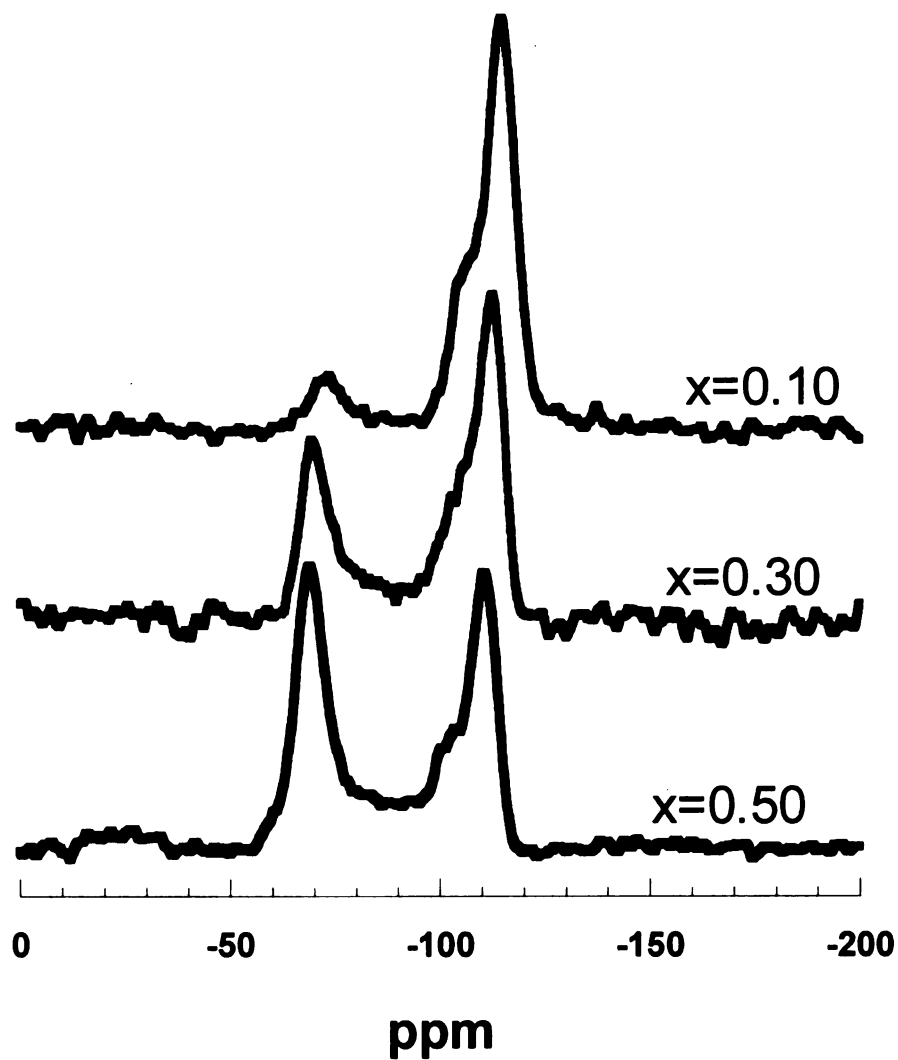
Figure 4.3. ^{29}Si MAS NMR spectra for the powdered form of functionalized $(SiO_2)_{1-x}$ $(LSiO_{1.5})_x$ compositions (L=mercaptopropyl) with a wormhole framework structure, denoted MP-HMS.

Table 4.1. Cross-linking parameters and the equivalent weight of the powdered form of functionalized $(SiO_2)_{1-x}(LSiO_{1.5})_x$ compositions (L=mercaptopropyl) with a wormhole framework structure denoted, MP-HMS. The data were obtained from the deconvoluted solid state 29Si NMR spectra.

x_{theo}	x_{obs}	d_{100} (nm)	% Q^4 cross-linking	$(Q^4+T^3)/(Q^3/T^2)$	Calculated Formula Weight g/mol Si	mmol SH/g
0.10	0.08	4.8	74	2.18	68.7	1.43
0.30	0.28	4.2	74	2.64	81.7	3.63
0.50	0.46	3.6	77	2.89	94.6	5.28
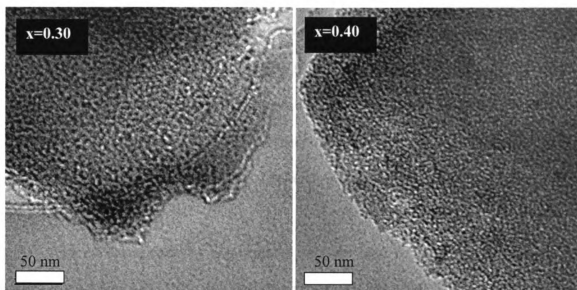
Figure 4.4. TEM images for the powdered form of functionalized $(SiO_2)_{1-x}(LSiO_{1.5})_x$ compositions (L=mercaptopropyl) with a wormhole framework structure denoted, MP-HMS.

4.4.2 Batch Studies of Mercury Uptake by MP-HMS

As previously stated, MP-HMS with two different topologies, spherical and powdered particles, were used for mercury trapping. The micron-sized spherical form of MP-HMS was only used in column experiments. For all other experiments, the sponge-like particle compositions of MP-HMS were used. Both the powder and spherical forms of MP-HMS have comparable physical properties, and only differ in particle morphology. The MP-HMS derivatives in powder or spherical form with x=0.50 have the highest mercaptan content of any reported mesostructure.[12] Therefore, it would be expected to have the highest mercury adsorption capacity. To determine the mercury adsorption capacity of MP-HMS, uptake curves were carried out with the powder form of MP-HMS. Different volumes of 1,000 ppm solution and different overall Hg^{2+}:SH molar ratios were equilibrated with MP-HMS powder with x=0.30 and 0.50 for 48 h at ambient temperature. The mercury uptake was determined by difference of initially added and the final concentration in the filtrate. The uptake curves for MP-HMS with x=0.30 and 0.50 are shown in Figure 4.5.

The uptake of mercury is quantative until the total Hg^{2+}:SH molar ratio reaches nearly 1:1 for both MP-HMS with x=0.30 and x=0.50. For MP-HMS compositions with x=0.30 this corresponds to quantative uptake until 0.73 g Hg^{2+}/g. The MP-HMS compositions with x=0.50 have quantative uptake of total mercury until 1.03 g Hg^{2+}/g. Above a total mercury to sulfur ratio of 0.9: 1, mercury uptake is no longer quantative, yet mercury continues to bind in the presence of excess mercury in solution.

As expected, the mesostructure with the higher organic loading does indeed adsorb the greatest amount of mercury. Yet what was unexpected was the maximum

uptake of mercury. At saturation, MP-HMS compositions with x=0.30 were capable of binding a maximum of 5.0 mmol Hg^{2+}/g (1.0 g Hg^{2+}/g), and the MP-HMS with x=0.50 trapped 7.3 mmol Hg^{2+}/g (1.46 g Hg^{2+}/g). Each composition was able to adsorb an amount of mercury in excess to the mercaptan quantity when the adsorption system was equilibrated with an excess of mercury in solution.

In addition to determination of the loading capacity of MP-HMS as a trapping agent, the ability of a MP-HMS to effectively uptake mercury in a column system was studied. A spherical shape is desirable for column packing because spheres pack more uniformly than powders and provide more uniform flow of solution through the column. For this reason micron-sized spheres of MP-HMS with x=0.30 and 0.50 were used for column studies of mercury uptake. The spherical MP-HMS with x=0.30 has a surface area of over 1200 m^2/g, comparable to that of the powdered form of MP-HMS with x=0.30. Nonetheless, the spherical MP-HMS with x=0.30 does not exhibit the textural porosity of the powdered form. Both the spherical and powdered forms of MP-HMS with x=0.50 exhibit a Type I isotherm with no textural porosity.
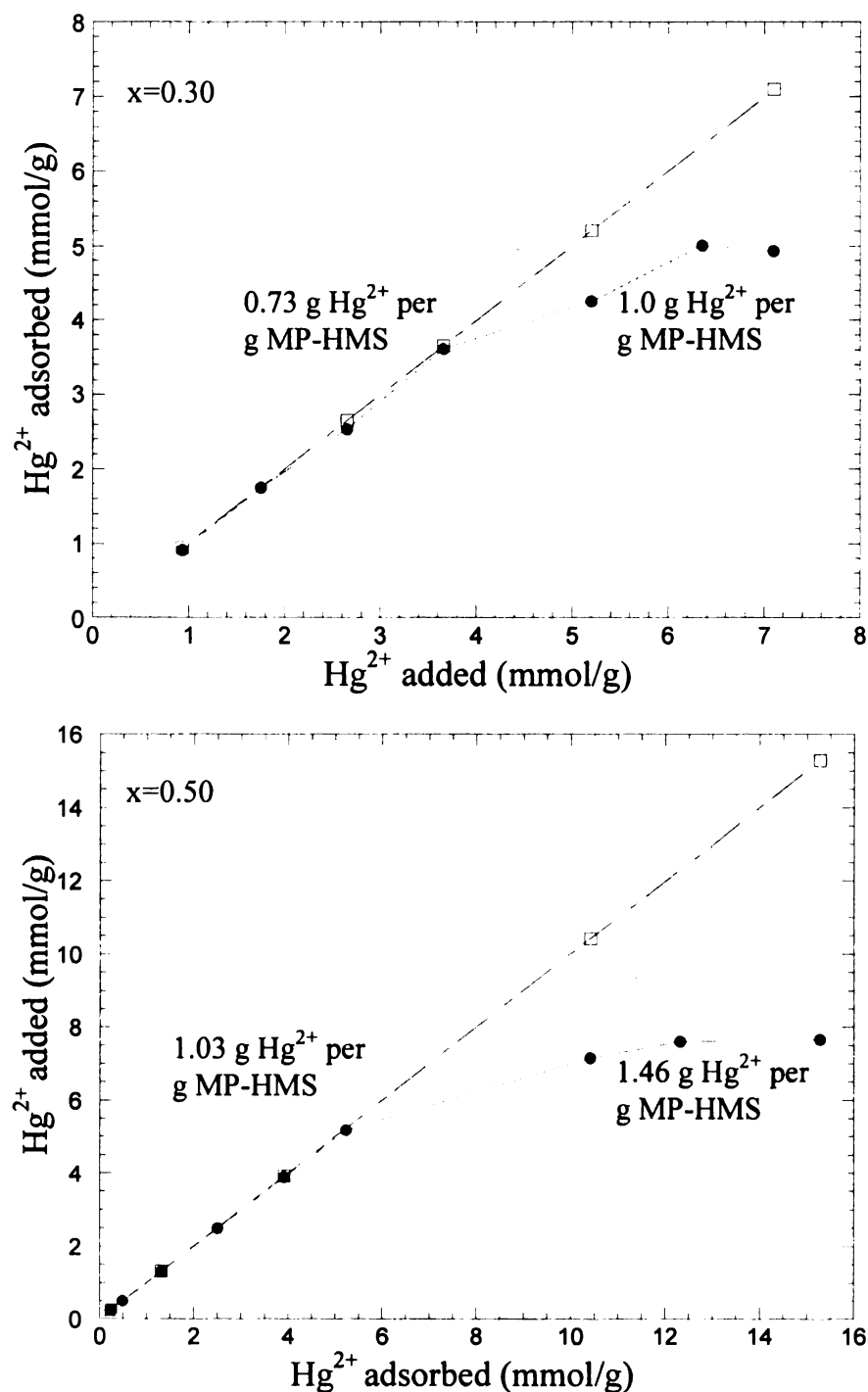
Figure 4.5. Mercury uptake curves for the powdered forms of functionalized $(SiO_2)_{1-x}$ $(LSiO_{1.5})_x$ compositions (L=mercaptopropyl) with a wormhole framework structure denoted, MP-HMS. The initial concentration of the mercury solution was 1000 ppm. The mass of MP-HMS was 200 mg. The volume of solution was varied to achieve different amounts of added Hg^{2+}. The loading of SH/g for each mesostructure is given in Table 4.1. The dashed line indicates quantative uptake of mercury.

4.4.3 Column Studies of Mercury Adsorption by Spherical MP-HMS

The spherical form of MP-HMS synthesized by Method III packed uniformly in a plastic buret with a diameter of 1.7 cm and a total column height of 50 cm. The resulting columns were able to reduce mercury effluent to EPA drinking water standards. The results are shown in Table 4.2. Two separate reactions were run using the same contact time of 4.0 min, but different initial mercury concentrations of 50 and 5 ppm. Both flow rates reduced the effluent to essentially the same final mercury concentration, 0.022 and 0.018 ppm, respectively. When the bed volume was doubled, which in turn increased the contact time to 10 min, the concentration of mercury in the effluent was reduced further from 50 ppm to 0.011 ppm. This demonstrates that the effluent concentration was highly dependent upon the contact time (column length/flow rate). The longer the contact time of the solution in the column, the greater the reduction of mercury concentration.

A parallel experiment was run to determine whether the level of functionalization of the matrix played a significant role in the column performance. For a 50 ppm initial mercury solution and a 20 cc bed volume, MP-HMS with x=0.50 reduced the effluent to 0.011 ppm whereas MP-HMS with x=0.30 was only able to reduce the effluent concentration to 0.097 ppm, indicating the increased functionalization does enhance adsorption properties. The maximum reduction in mercury concentration was in the range of 0.010 ppm for contact times 4.0-13 min, it was not until the contact time was increased to 18 min and the initial concentration reduced to 0.11 ppm that the optimum results were obtained. By using the aforementioned conditions, the Hg^{2+} concentration of the effluent was reduced to 24 ppt, far below the EPA drinking water standard of 2 ppb. An initial concentration of 0.11 ppm is significantly lower than the other concentrations

143

used, 5 and 50 ppm. However, this lower concentration is still on the high end of what is found in the natural environment. Thus, it is not an unreasonable approximation of the levels of mercury found in some drinking water. The MP-HMS was sieved in some experiments to separate particles smaller than 38 or 45 μm. However, there was no performance change in the instances when the silica was sieved and when it was not, thus the sphere size did not play a major role in determining column efficiency. All mercury solutions used for column experiments were at neutral pH to best simulate natural water systems. The desired pH was achieved by dilution of the acidic standard mercuric nitrate solution with water.

As indicated in the introduction of this chapter, there has been extensive work done on mercury adsorption using mercaptan functionalized mesoporous materials. Table 4.3 is a summary of the previous works that make use of immobilized thiols groups for mercury trapping. Studies based on other organic groups are included in the table for comparison purposes. Overall, the direct-assembly method of thiol incorporation yields the highest level of functionalization, up to 3.2 mmol SH/g for grafting versus 5.3 mmol SH/g for direct-assembly. Concomitantly, the directly assembled mesostructures have the highest mercury binding capacity. A 1:1 ratio of Hg^{2+}: SH has been achieved for both grafted as well as directly-assembled mesostructures, indicating that both types of functionalized silicas have highly accessible ligands. It is interesting to note that the structures that do bind 1:1 are assembled through H-bonding interactions at the micelle-solution interface. All of the electrostatically-assembled mesostructures reached maximum binding capacity when there was still an excess of mercaptan ligands present.[4,5,17,18]

There are three silica structures, which are not mercaptan functionalized mesostructures that are included in Table 4.3. The first is a mercaptan functionalized organo-ceramic adsorbent synthesized by sol-gel techniques,[19] denoted MP-Sol-Gel. The synthesis conditions consisted of TEOS and MPTMS being independently condensed in a mixture of acidic water and alcohol before being mixed together and gelled by the addition of triethylamine. Since no porogen is used, the silica does not have ordered mesopores and is not mesostructured. Yet, the MP-Sol-Gel was included because of its high mercury binding capacity, 6.4 mmol/g. Also, it is the only other mercaptan-functionalized silica to have been used in column studies.

The second mercury trapping agent is a mesostructure containing a thioether functionality organic-inorganic mesoporous composite,[20] denoted "tetrasulfide SBA-15". A procedure similar to that used to prepare SBA-15 was used to prepare the thioether mesostructure. TEOS and (1,4)-bis(triethoxysilyl)propane tetrasulfide, $(CH_3CH_2O)_3Si(CH_2)_3S$-S-S-$S(CH_2)_3Si(OCH_2CH_3)$, were condensed and hydrolyzed under acidic conditions with a tri-block copolymer (P123) as the structure director. The mesostructure had a hexagonal morphology like that of SBA-15. The composition is of interest because it is reported to adsorb the highest amount of mercury namely, 13.5 mmol/g. The achievement of this extremely high adsorption results in a 3:1 Hg^{2+} to S ratio. This excess of mercury to ligand "could be attributed to the stereo-coordination chemistry of S with Hg^{2+}."[20] Despite its high mercury binding capacity, the tetrasulfide SBA-15 was not able to reduce the mercury effluent to low concentrations, from 10.76 to 0.23 ppm, well above the EPA drinking water and even the hazardous waste limit.

An attempt to replicate the synthesis of tetrasulfide SBA-15 following the reported method failed to produce an SBA-15 mesostructure, rather a wormhole derivative was produced. Moreover, the replicated tetrasulfide SBA-15 composition was able to adsorb mercury but not to the extent reported.

The third non-mercaptopropyl functionalized mesostructure in Table 4.3 is MCM-41 grafted initially with aminopropyl ligands. The amine functionalized mesostructure was then reacted with benzoyl isothiocyanate to yield MCM-41 functionalized with 1-benzoyl-3-thiolpropylurea,[21] denoted BTP-MCM-41. A schematic illustration of the ligand present on the mesostructure is shown below.
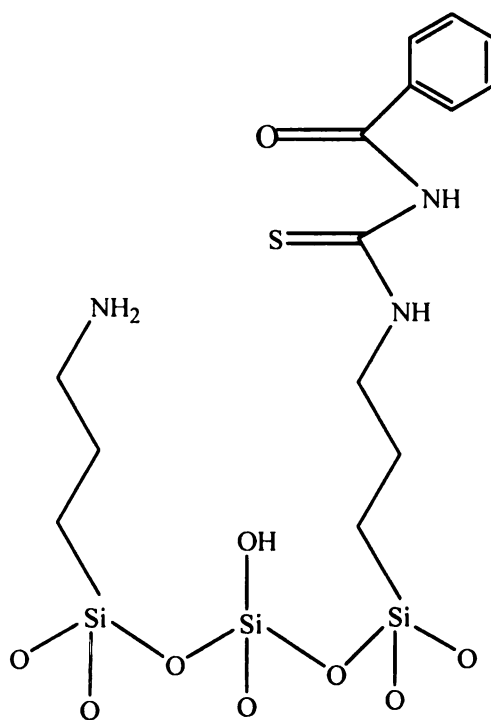
The aminopropyl moiety is depicted in the schematic because only around 70% of the amines were chemically accessible. Thus, the final product had 0.65 mmol NH_2/g and 1.5 mmol/g of 1-benzoyl-3-thiolpropylurea. The MCM-41 functionalized with 1-benzoyl-3-thiolpropylurea was able to adsorb a maximum of 5.00 mmol Hg/g, an excess

coordination of over 3 Hg: 1 ligand.[21] The excess binding of mercury was attributed to the formation of bonds to mercury with ligands other than sulfur. After saturation of the sulfur sites, it was proposed that the mercury formed mercury-nitrogen, mercury-oxygen, and polymeric chains due to the binding of one ligand to two adjacent mercury ions.[21] No studies were done to determine the true coordination of the mercury trapped by 1-benzoyl-3-thiolpropylurea MCM-41.

Of all the reported mesostructures, directly-assembled MP-HMS has the highest thiol loading with 5.3 mmol/g. Concomitantly, MP-HMS also has the greatest mercury binding capacity with 7.3 mmol/g, of a mercaptan-functionalized mesostructure. Furthermore, MP-HMS with x=0.50 was able to perform well in column studies and reduce mercury concentration to 24 ppt, well below the EPA drinking water limit of 2 ppb.

Table 4.2. Performance of functionalized $(SiO_2)_{1-x}(LSiO_{1.5})_x$ compositions (L=mercaptopropyl) with a wormhole framework structure denoted, MP-HMS in column studies of mercury adsorption.

MP-HMS	Column ID cm	Sieve size	Average Flow rate ml/min	Bed volume cc	Contact Time min	# Bed volumes passed through column	Initial Hg^{2+} ppm	Final Hg^{2+} ppm
x=0.50	1.7	38 μm	5.5	10	1.82	50	50	0.15
					1.82	100	50	0.62
					1.82	200	50	1.2
x=0.50	1.7	>38 μm	2.5	10	4.0	100	50	0.022
x=0.50	1.7	>38 μm	2.5	10	4.0	100	5	0.018
x=0.50	1.7	No sieving	1.9	20	10.5	50	50	0.011
x=0.30	1.7	>45 μm	2.0	20	10.0	50	50	0.097
x=0.50	1.7	No sieving	1.5	19	12.7	50	50	0.013
x=0.50	1.7	No sieving	1.1	20	18.1	50	0.11	0.000024

Table 4.3. Comparison of mercury binding properties for functionalized mesoporous materials as well as one functionalized ceramic material.

Mesostructure[a]	Ligand Incorporation	Ligand content mmol/g	Hg^{2+} binding capacity mmol/g	Initial ppm	Final ppm	Solution to solid ratio (mL:g)
FMMS[22]	Grafting	3.2	2.5	10	0.0012	100
MP-SBA-15[23]	Grafting	-	2.3	10.2	0.00	100
MP-HMS[24]	Grafting	1.5	1.5	1.1	0.005	10,000
MP-HMS[18]	Grafting	2.39	1.17	-	-	10,000
BTP- MCM-41[21]	Grafting	1.5	5.00	-	< 0.8	200
MP-MCM-41[25]TBOS	Direct	2.29	1.26	-	-	-
MP-MCM-41[7]	Direct	4.7	2.1	-	-	-
MP-MCM-41[9]	Direct	4.03	3.8	-	-	1,000
MP-MSU-X[10]	Direct	2.3	2.3	30	~0.01	500
MP-Sol-Gel[19,26]	Direct	3.72	6.4	50	0.001	column
Tetrasulfide SBA-15[20]	Direct	4.24	13.5	10.76	0.23	100
MP-HMS[18]	Direct	0.77 2.39	0.77 1.17	-	-	10,000
MP-HMS* x=0.50	Direct	5.30	7.3	0.11	24 ppt	column

a. Ligand abbreviations used. MP-mercaptopropyl, BTP-1-benzoyl-3-thiolpropylurea, Tetrasulfide-(1,4)-bis(triethoxysilyl)propane tetrasulfide
* This work

4.4.4 Examination of the Coordination of Trapped Mercury in MP-HMS by Raman Spectroscopy

A simple stereo-coordination chemistry of S with Hg^{2+} has been offered as an explanation for the excess binding of mercury to sulfur centers immobilized in a mesostructure.[20] Raman spectroscopy along with PDF X-ray techniques, were used in the present work to examine the coordination of mercury bound to MP-HMS. The Raman spectra are shown in Figure 4.6. The mercaptan S-H stretch appears as a strong band at 2560 cm⁻¹.[27,28] A weak band at 510 cm⁻¹ assigned to a S-S stretch indicated the presence of a small amount of disulfide due to the air oxidation of adjacent thiol groups on the surface of the mesostructure.[28] The C-H stretch appears as a strong band 2900 cm⁻¹ and the bands in the 1250-1500 cm⁻¹ region correspond to C-H bending modes.[28] The decrease in intensity and the eventual disappearance of the S-H stretch with increased mercury adsorption gives evidence for the binding of the mercury to the thiol. At a Hg/S loading of 0.50 the Hg-S stretch occurs at 324 cm⁻¹. Increasing the loading of Hg/S to 1.0 or 1.3 causes the band to shift to lower energy (275 cm⁻¹). Presence of a sharp band in the Raman spectra of the mercury loaded mesostructures at 1049 cm⁻¹ is consistent with the presence of free nitrate ion (uncoordinated). Free nitrate ion is known to exhibit a strongly active Raman band at 1050 cm⁻¹.[29] Moreover, the relative intensity of the free nitrate band increases with the increasing Hg/S ratio, indicating more increased ion-pairing between nitrate and cationic mercury complexed on the surface. The assignment of this band to free nitrate is supported by the loss of this band when the samples are washed in 0.1 M NaCl (spectrum not shown).

There is no change in the intensity of the disulfide stretch upon mercury adsorption. The disappearance of the thiol at saturation loading of mercury indicates that all the mercaptans are accessible and utilized to trap mercury.

Raman active Hg-S stretching vibrations occur in the range of 180-400 cm^{-1} [30-33] for mercury (II) thiolates in both the solid state and in solution. The position of the Hg-S stretching modes strongly depends on the coordination number of mercury wherein to sulfur centers in which the Hg-S bond length is < 2.8 Å.[30] Increasing the coordination number from two to four causes a decrease in Hg-S stretching frequency.[30] For mercury in linear, two-fold coordination to methyl thiolate and ethyl thiolate ligands, the Hg – S stretch appears at 297 and 394 cm^{-1}, respectively.[34] Mercury tetrahedrally coordinated to sterically bulky thiolate ligands in Hg(SBu^t)$_2$, exhibit a Hg-S Raman stretch at 188 cm^{-1}.[34] Furthermore, the stretching frequency of the C-S bond (600-725 cm^{-1}) is sensitive to the type of alkyl group bonded to the sulfur atom.[30,33]

The shift in the Hg-S stretch frequency with increasing mercury loading is accompanied by an increase in the intensity of the uncoordinated nitrate ion band. The PDF results, together with the Raman results, leads us to propose that at low mercury loading Hg/S ≤ 0.50, the dominant surface species is an electrostatically neutral tetrahedral coordinated complex formed through bridging of the sulfur atom to two mercury centers as shown in Scheme 4.1.
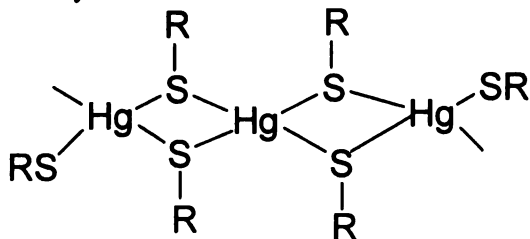
Scheme 4.1

In addition, a lesser fraction of the bound mercury is in the form of a cation mercury complex in which the mercury is linearly coordinated to bridging thiolate ligands as shown in Scheme 4.2.
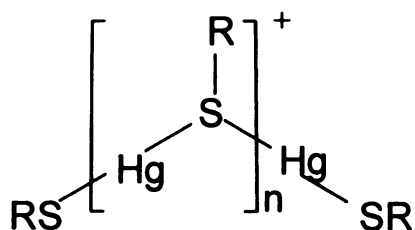
Scheme 4.2

The cation charge on the linearly coordinated mercury centers is balanced by the free nitrate ions, as evidenced by the presence of the free nitrate band at 1049 cm^{-1}. As the Hg/S ratio is increased to 1.0 and 1.3, the linearly coordinated mercury increases at the expense of the tetrahedral mercury complex. The shift from electrically neutral $Hg(SR)_2$ complex to cationic linear $Hg(SR)^+$ with increasing Hg loading is supported by the increase in the free nitrate band as well as the shift to higher frequency of the Hg-S stretch in the Raman. Both complex species are polymeric with the sulfur centers bridging at least two mercury centers. Triply bridging sulfur centers may also be present, as suggested by the fact that the Hg/S can exceed a value of 1.0 without PDF evidence of the formation of Hg-O bonds. By the time the Hg/S ratio reaches 1.30, virtually all of the thiolate centers are involved in mercury coordination, as evidenced by the absence of the S-H stretch at 2560 cm^{-1}. With increasing mercury loading, the presence of a peak at 175 cm^{-1} appears. We are unclear as to the exact identification of this peak. One possible explanation is the presence of Hg_2^{2+}. The Hg-Hg stretching vibration of Hg_2^{2+} is reported to occur at 177 cm^{-1}.[35,36] The formation of Hg_2^{2+} has been reported to occur from photochemical oxidation of Hg^{2+}.[37,38]
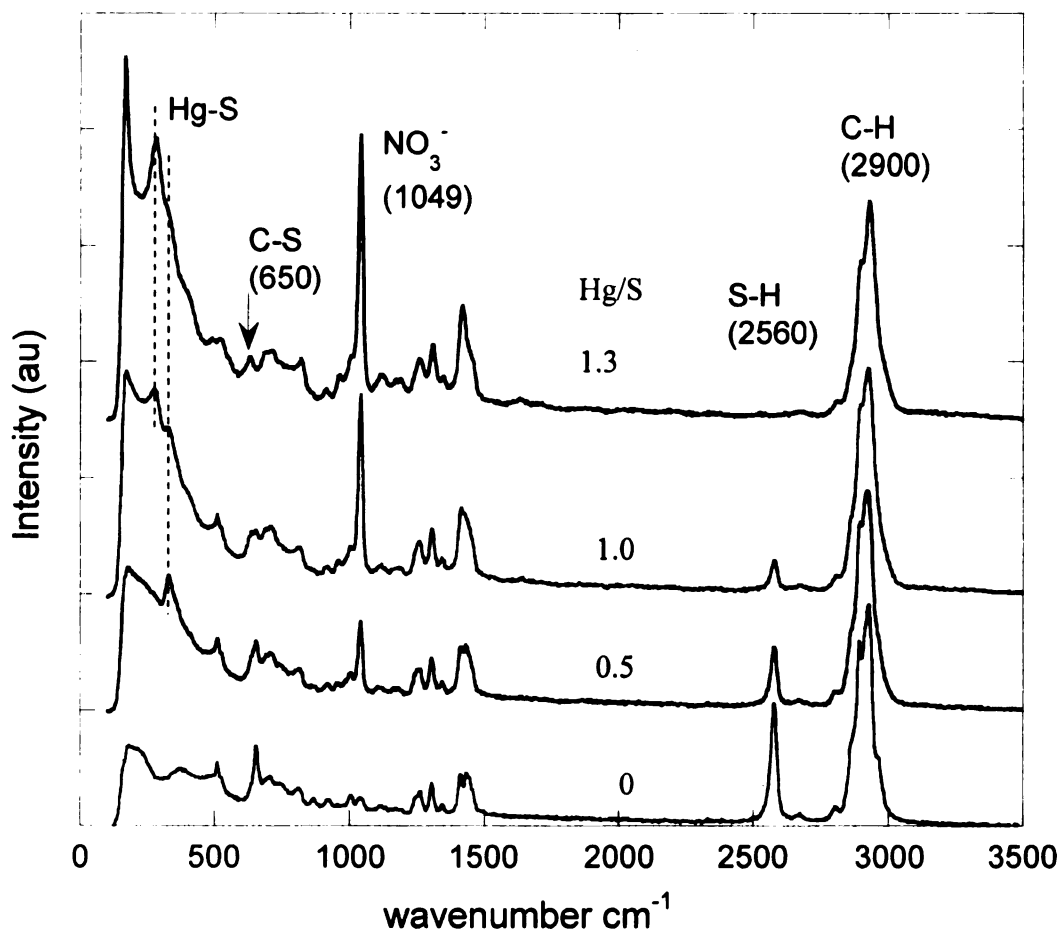
Figure 4.6. Raman spectra of thiol functionalized $(SiO_2)_{1-x}$ $(LSiO_{1.5})_x$ compositions (L=mercaptopropyl) with a wormhole framework structure, denoted MP-HMS after binding of mercury at the Hg^{2+}/SH levels shown. The spectra are offset on the y-axis for clarity.

4.4.5 Examination of the Coordination of Trapped Mercury in MP-HMS by PDF

Stoichiometric reaction of Hg^{2+} with two SH groups in MP-HMS would yield a product with a Hg: molar ratio of 1:2. However, molar ratios of 1: 1 Hg: S have been typically observed.[10,24] The 1:1 stoichiometry has been explained in terms of a bridging O between two Hg, each of which is linked to one S to form S-Hg-O-Hg-S linkages.[22] In a collaborative study with Professor Kim Hayes at the University of Michigan, we have obtained EXAFS evidence in support of S-Hg-O-Hg-OH linkages.[41]

Understanding the nature of the Hg binding in the pores of the MP-HMS is a challenge because of the disordered nature of both the pores and the pore-wall framework that support the thiol groups that trap the mercury. It is therefore not possible to use crystallographic methods to study the nature of the binding sites. From the Raman results, it is clear that the Hg binds to sulfur centers of the mercaptan ligands. However, the binding of Hg can exceed the number of mercaptan moieties. This implies that some kind of network exists inside the pores where sulfur ions can be coordinate to one Hg. Just such a situation exists in the mineral cinnabar, HgS, which has zig-zag -Hg-S-Hg-S-chains. The structure of cinnabar, HgS, is shown in Figure 4.7.

To determine if mercury binds in chains similar to that of cinnabar, the technique of atomic pair distribution function (PDF) analysis of x-ray powder diffraction data was done by our collaborators Professors Valeri Petkov and Simon Billinge. The experiments were conducted at the Advanced Photon Source (APS) at Argonne National Laboratory. The samples examined were pristine MP-HMS with =0.50 and the corresponding Hg-loaded derivatives with varying Hg: S ratios.

PDF is a diffraction technique, widely used to study amorphous materials.[42] More recently, this technique has been successfully applied to nanocrystalline and crystalline materials.[43] This technique does not presume periodicity and can be applied to any disordered material. It is capable of yielding definitive structural information on short and intermediate length scales.

The PDFs, $G(r)$, for Hg loaded MP-HMS derivatives with x=0.50 are shown in Figure 4.8. The curves are offset from each other for clarity. Also shown is the PDF of bulk silica glass and the parent trapping material MP-HMS with x=0.50 for comparison. The mesostructures are glassy in nature and this is reflected in the rapid fall-off in $G(r)$ structural features with increasing r. The curves from both the Hg loaded samples are similar to each other in shape, but are quite distinct from the bulk silica glass and parent MP-HMS with x=0.50. The presence of the strongly scattering Hg is clearly evident. In particular, strong peaks in G(r) at 2.4 Å and 3.7 Å are evident in the Hg loaded samples that are not present in the silica. The peak at 1.6 Å comes from the Si-O distance in the silica network and is present in all the samples. Intensity of the peaks at 2.4 Å and 3.7 Å grow with the higher Hg loading at higher-r. The rather sharp peak at 3.7 Å is the last sharp peak. However, there are broad bumps centered at 5.75 Å and 6.25 Å. These also originate from the coordinated mercury, but indicate that, beyond the second nearest neighbor, the Hg ions are quite disordered.
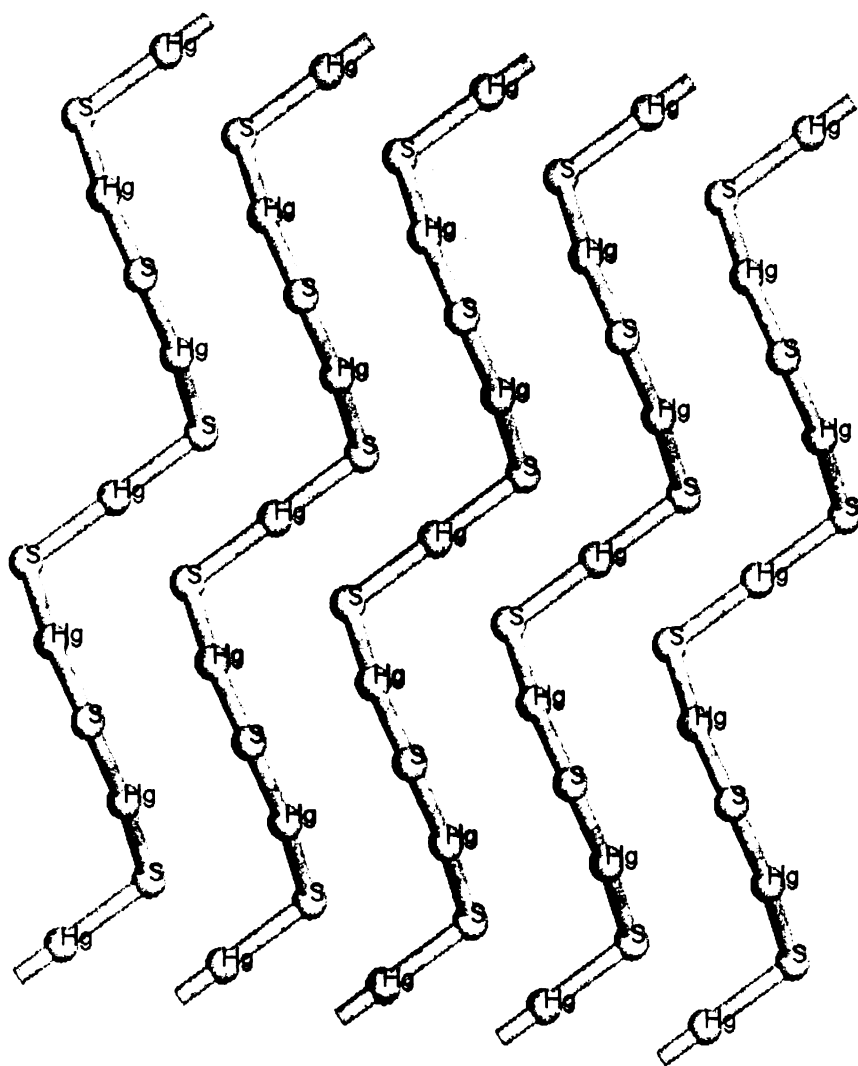
Figure 4.7. Crystallographic representation of HgS (cinnabar) structure.[44]
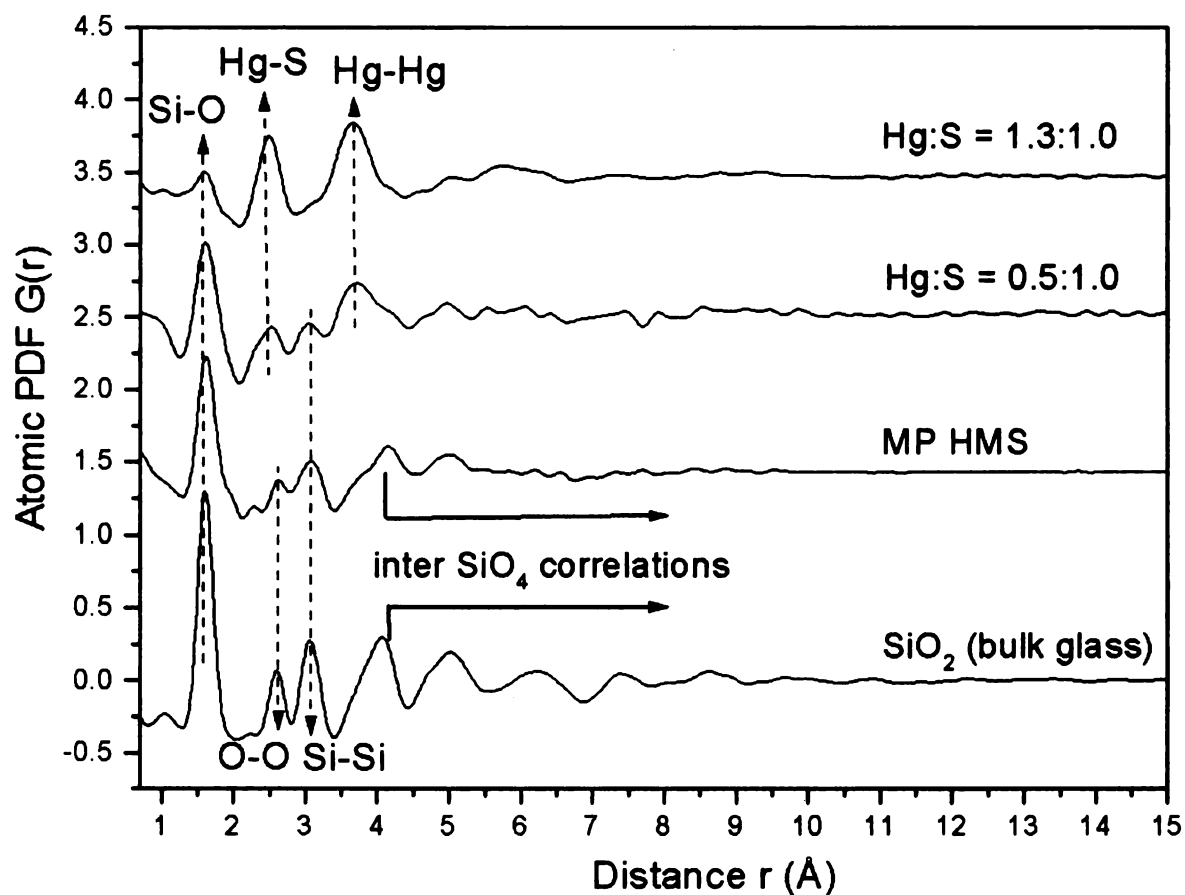
Figure 4.8. Experimental atomic PDF, G(r), for bulk silica, and thiol functionalized $(SiO_2)_{1-x}$ $(LSiO_{1.5})_x$ compositions (L=mercaptopropyl) with x=0.50 and a wormhole framework structure, denoted MP-HMS, before and after binding of mercury at the Hg^{2+}:SH levels shown.

In view of the fact that Hg^{2+} prefers two – fold linear coordination to soft ligands such as sulfur,[45] an analogous coordination environment is anticipated for mercury centers immobilized in a thiol-functionalized mesostructure. At lower mercury loadings $Hg/S \leq 0.50$ the mercury is coordinated tetrahedrally (Scheme 4.1). Whereas, the mercury changes from tetrahedral coordination to linear as the mercury loading increases (Scheme 4.2). Regardless of the level of mercaptopropyl functionalization (x), mercury is linked to sulfur as indicated by the observed Hg – S distance of 2.4 Å. This distance is in agreement with the covalent bond distance of 2.36 Å observed in HgS cinnabar.[44]

The bridging of sulfur to two mercury centers is substantiated by the observed mercury-mercury distance of 3.7 Å, which is very near the value of 3.75 Å found for the intra-chain Hg-Hg distance in solid HgS.[44] However, the chains do not appear to be uniformly spaced or ordered on the surface, because the inter-chain Hg-Hg distance of 4.15 Å found in crystalline HgS was not observed for the mesostructure. We are unable to estimate the average length of the mercury – sulfur chains from the PDF data

We find no evidence for Hg-O binding in the PDF. The loading of MP-HMS compositions with mercury(II) ions was accomplished by reaction with standardized aqueous mercuric nitrate solutions at an initial ambient pH of 2.3. At this initial pH, the predominate mercury species in solution is aquated Hg^{2+}, and the minor species is aquated $Hg(OH)^+$.[40] Thus, the presence of Hg-O bonds as well as Hg-S bonds is anticipated for the mercury saturated MP-HMS mesostructure.

Recent EXAFS results indicate that S-Hg-S complex formation contributes little to the overall Hg coordination structure in mercury loaded MP-HMS derivatives with x=0.50 and Hg/S=0.05-1.4.[41] The binding mode favored on the basis of the EXAFS data

was based on -S-Hg-OH complex formation at Hg/S < 0.5. The Hg-O path appeared to be more important at higher mercury loadings Hg/S > 0.5 with the resulting fits to the data consistent with the formation of a double layer structure of Hg attached to sulfur binding sites (-S-Hg-O-Hg-OH). However, we are not able to verify the presence of Hg-O bond formation on the basis of the PDF data. Thus, the PDF and EXAFS data do not converge to the same surface structure for Hg^{2+} ions immobilized on MP-HMS derivatives. Both methods confirm the presence of Hg-S bonds in agreement with the Raman data. Unlike EXAFS, neither the Raman data nor the PDF data provide evidence for Hg-O bond formation.

4.4.6 Regeneration of Mercury Loaded MP-HMS

The use of ion-exchange for mercury remediation would be more viable if the trapping agent was able to be regenerated. To examine the regeneration potential of MP-HMS, mercury loaded samples were washed in differing concentrations of HCl to remove the adsorbed mercury, and then the solid was washed with water to return to a near-neutral pH. The results for the regeneration experiments are given in Table 4.4. The MP-HMS was able to adsorb 99% of the mercury added initially and 99% a second time as well. These results illustrate the durability of the MP-HMS mesostructures, and its efficacious ability to trap mercury. After the regeneration cycle, MP-HMS returns to its initial binding capacity of mercury independent of the degree of functionalization. Regeneration of mercury loaded FMMS (functionalized monolayers on mesoporous supports) prepared by grafting of mercaptopropyltrimethoxysilane on MCM-41 has also been examined.[5] FMMS washed in 12 M HCl was only able to retain 41% of its binding

159

capacity upon regeneration.[5] For the first adsorption, FMMS trapped 2.51 mmol Hg/g and after regeneration was only able to adsorb 1.04 mmol Hg/g.

Regeneration of mercury-loaded mesostructures, using milder conditions than concentrated HCl has been reported.[21,46] Treatment by soaking the mercury laden mesostructure in 10% thiourea solution in aqueous 0.05 M HCl, was sufficient to remove the trapped mercury and restore more than 70% of the structures initial mercury binding capacity.[21]

Table 4.4. Regeneration performance of functionalized $(SiO_2)_{1-x}$ $(LSiO_{1.5})_x$ compositions (L=mercaptopropyl) with a wormhole framework structure denoted, MP-HMS for mercury adsorption.

MP-HMS	mmol/g SH	mmol Hg added/g MP-HMS 1X	mmol Hg/g adsorbed	% Adsorbed 1X	mmol Hg added/g MP-HMS 2X	mmol Hg/g adsorbed 2X	% Adsorbed 2X	HCl conc
x = 0.10	1.4	0.571	0.570	99.8	0.578	0.576	99.6	6 M
x = 0.10	1.4	1.19	1.17	98.3	1.188	1.17	98.4	6 M
x = 0.10	1.4	0.641	0.638	99.5	0.642	0.639	99.5	6 M
x = 0.10	1.4	0.620	0.618	99.7	0.619	0.616	99.5	12 M
x = 0.50	5.3	2.78	2.58	92.5	2.7	2.29	84.8	6 M
x = 0.50	5.3	1.24	1.24	99.8	1.243	1.24	99.4	6 M

4.4.7 Leaching of Trapped Mercury

The United Stated Environmental Protection Agency has developed the Toxicity Characteristic Leaching Procedure (TCLP). The procedure was developed under Subtitle C of the Resource Conservation and Recovery Act (RCRA) to study the mobility of hazardous substances. This test must be considered in the development of a trapping agent for remediation and de-contamination technology. The test is done in order to determine whether or not a material may be safely disposed in a landfill without further treatment. Acetic acid is used as the extraction fluid in the TCLP because it is a major component of typical municipal landfill leachates. The TCLP is widely used in the United States to determine if a waste is hazardous or if a treated waste meets the treatment standards for land disposal.[47] Thus the leaching stability of mercury laden MP-HMS under pseudo landfill conditions was evaluated in the present work.

Table 5.5 provides the results of mercury loaded MP-HMS with x=0.10 and 0.50 subjected to the TCLP. The MP-HMS was exposed to very high concentrations of mercury so as to completely saturate the mesostructure. The durability and chemical stability of the mercury-mercaptan covalent bond is evidenced by the fact that less than 0.1 percent of the trapped mercury was released to solution. Nonetheless, the EPA limit for hazardous waste is not based on percent released but rather the mercury concentration in the filtrate. To pass the TCLP test, the filtrate concentration must be less than 0.200 ppm. The lowest filtrate concentration observed for MP-HMS was 0.81 ppm. Thus the mercury laden MP-HMS would need further treatment before being disposed of in a landfill. The TCLP data reported by the Pacific Northwest National Laboratory's group for Hg^{2+} leaching from their FMMS[5] mesostructure is also given in Table 4.5. Although

they report that FMMS passes the TCLP[48] the data given indicates otherwise. However, by directly comparing the FMMS results to that of MP-HMS, the exceptional stability of MP-HMS is evident.

In addition to the chemical stability of the trapped mercury, there is also the stability toward bacterial degradation to consider. Inorganic mercury may be methylated by bacteria to give methyl mercury, the deadliest form of mercury.[49] The small pore size of the MP-HMS should prevent bacteria (at least 2000 nm in size) from solubilizing the mercury.

Table 4.5. Mercury uptake and leaching of functionalized $(SiO_2)_{1-x}(LSiO_{1.5})_x$ compositions (L=mercaptopropyl) with a wormhole framework structure denoted, MP-HMS for examination of the Toxicity Characteristic Leaching Procedure (TCLP).

MP-HMS	Initial conc Hg^{2+} in solution (ppm)	SH mmol/g	Total Hg^{2+} to trapping agent ratio (mmol/g)	Hg^{2+} mmol added/mmol SH	Hg^{2+} uptake by trapping agent (mmol/g)	Hg^{2+} desorbed to extraction fluid[a] (mmol/g)	Fraction of Hg^{2+} desorbed into extraction fluid (%)	Equilibrium conc Hg^{2+} in extraction fluid (ppm)
x=0.10	2126	1.4	1.34	0.96	1.34	0.00174	0.13	2.8
x=0.10	2126	1.4	2.01	1.43	1.93	0.00200	0.10	2.1
x=0.50	2126	5.3	2.68	0.51	2.67	0.00102	0.04	0.81
x=0.50	2126	5.3	5.35	1.00	4.89	0.00332	0.07	1.3
FMMS[37]		3.2			335 ppm		3.13	10.5

[a] EPA test fluid #1 buffer solution of acetate / acetic acid

4.5 Conclusion

The uptake of pollutant ions by an adsorbent is dependent on the product of surface area, surface density of the adsorption sites, and stoichiometry of the ion-binding site. MP-HMS has a high surface area, an ultra high surface density of thiol groups, and excellent binding capacity. MP-HMS silicas have been shown to be quite efficacious for mercury remediation. This is due in part to these structures having the highest thiol loading, 5.35 mmol SH/g of any reported mercaptan functionalized mesoporous silica. Not only does MP-HMS have the highest functional loading of mercaptan, but it is also synthesized in a simple one-pot direct-assembly manner. Furthermore, there is greater accessibility to the active sites in the interconnected three-dimensional wormhole pore networks of MP-HMS as compared to the one-dimensional hexagonal pore networks of MCM-41. This improved accessibility is evident from the high mercury binding capacity of 7.3 mmol/g and the Hg^{2+}: S ratio of 1.4 achieved with MP-HMS with x=0.50. In addition to the exceptional binding capacity, spherical MP-HMS with x=0.50 is capable of being packed into a column, and reduces mercury effluent concentration to the parts per trillion range, well below the EPA drinking water limit of 2 parts per billion. The MP-HMS mesostructure is a stable and recyclable material with a high affinity for mercury. We have also elucidated the nature of the Hg binding sites using the atomic PDF local structural probe. It was determined that the local coordination environment of Hg is rather well defined. Mercaptan moieties bind up to two Hg ions forming chains of Hg-S-Hg units on the surface.

4.6 References

(1) Keating, M. M., Kathryn; Schoeny, Rita; Rice, Gelnn; Bullock, Russell; Nichols, John "Mercury Study Report to Congress," US EPA, 1997.

(2) US EPA. "National Listing of Fish Advisories," US EPA, 2004.

(3) US EPA. "Capsule Report: Aqueous Mercury Treatment," Office of Research and Development, 1997.

(4) Mercier, L.; Pinnavaia, T. J. *Adv. Mater.* **1997**, *9*, 500-503.

(5) Feng, X.; Fryxell, G. E.; Wang, L. Q.; Kim, A. Y.; Liu, J.; Kemner, K. M. *Science* **1997**, *276*, 923-926.

(6) Liu, A. M.; Hidajat, K.; Kawi, S.; Zhao, D. Y. *Chem. Commun.* **2000**, 1145-1146.

(7) Lim, M. H.; Blanford, C. F.; Stein, A. *Chem. Mater.* **1998**, *10*, 467-+.

(8) Mercier, L.; Pinnavaia, T. J. *Environ. Sci. Technol.* **1998**, *32*, 2749-2754.

(9) Walcarius, A.; Delacote, C. *Chem. Mater.* **2003**, *15*, 4181-4192.

(10) Brown, J.; Richer, R.; Mercier, L. *Microporous Mesoporous Mat.* **2000**, *37*, 41-48.

(11) Pauly, T. R.; Liu, Y.; Pinnavaia, T. J.; Billinge, S. J. L.; Rieker, T. P. *J. Am. Chem. Soc.* **1999**, *121*, 8835-8842.

(12) Mori, Y.; Pinnavaia, T. J. *Chem. Mater.* **2001**, *13*, 2173-2178.

(13) Chupas, P. J.; Qiu, X.; Hanson, J. C.; Lee, P. L.; Grey, C. P.; Billinge, S. J. L. *J. Appl. Crystallogr.* **2003**, *36*, 1342-1347.

(14) Franson, M. A. M.; Greenberg, A. E.; Trussell, R. R.; Clesceri, L. S.; Editors *Standard Methods for the Examination of Water and Wastewater. 18th Ed*, 1992.

(15) Mercier, L.; Pinnavaia, T. J. *Chem. Mater.* **2000**, *12*, 188-196.

(16) Sing, K. S. W.; Everett, D. H.; Haul, R. A. W.; Moscou, L.; Pierotti, R. A.; Rouquerol, J.; Siemieniewska, T. *Pure Appl. Chem.* **1985**, *57*, 603-619.

(17) Liu, J.; Feng, X.; Fryxell, G. E.; Wang, L. Q.; Kim, A. Y.; Gong, M. *Chem. Eng. Technol.* **1998**, *21*, 97-100.

(18) Kim, Y.; Lee, B.; Yi, J. *Sep. Sci. Technol.* **2004**, *39*, 1427-1442.

(19) Lee, J. S.; Gomez-Salazar, S.; Tavlarides, L. L. *React. Funct. Polym.* **2001**, *49*, 159-172.

(20) Zhang, L.; Zhang, W.; Shi, J.; Hua, Z.; Li, Y.; Yan, J. *Chem. Commun.* **2003**, 210-211.

(21) Antochshuk, V.; Olkhovyk, O.; Jaroniec, M.; Park, I.-S.; Ryoo, R. *Langmuir* **2003**, *19*, 3031-3034.

(22) Feng, X.; Fryxell, G. E.; Wang, L. Q.; Kim, A. Y.; Liu, J.; Kemner, K. M. *Science* **1997**, *276*, 923-926.

(23) Liu, A. M.; Hidajat, K.; Kawi, S.; Zhao, D. Y. *Chem. Commun.* **2000**, 1145-1146.

(24) Mercier, L.; Pinnavaia, T. J. *Adv. Mater.* **1997**, *9*, 500-&.

(25) Nooney, R. I.; Kalyanaraman, M.; Kennedy, G.; Maginn, E. J. *Langmuir* **2001**, *17*, 528-533.

(26) Nam, K. H.; Gomez-Salazar, S.; Tavlarides, L. L. *Ind. Eng. Chem. Res.* **2003**, *42*, 1955-1964.

(27) Raso, S. W.; Clark, P. L.; Haase-Pettingell, C.; King, J.; Thomas, G. J., Jr. *J. Mol. Biol.* **2001**, *307*, 899-911.

(28) Kluth, G. J.; Carraro, C.; Maboudian, R. *Phys. Rev. B: Condens. Matter.* **1999**, *59*, R10449-R10452.

(29) Davis, A. R.; Irish, D. E. *Inorg. Chem.* **1968**, *7*, 1699-1704.

(30)   Hoffmann, G. G.; Brockner, W.; Steinfatt, I. *Inorg. Chem.* **2001**, *40*, 977-985.

(31)   Biscarini, P. E. F. G. P. *J. Chem. Soc. Dalton Trans.* **1984**, 953-957.

(32)   Biscarini, P.; Fusna, L.; Nivellini, G. *Spectrochim. Acta A.* **1980**, *36A*, 593-600.

(33)   Biscarini, P.; Fusina, L.; Nivellini, G. *J. Chem. Soc. Dalton Trans.* **1974**, 2140-2144.

(34)   Casals, I.; Gonzalez-Duarte, P.; Sola, J.; Miravitlles, C.; Molins, E. *Polyhedron* **1988**, *7*, 2509-2514.

(35)   Wickleder, M. S. *Z. Anorg. Chem.* **2002**, *628*, 1848-1852.

(36)   Stammerich, H. T. T. S. *J. Mol. Structure* **1967**, *1*, 55-60.

(37)   Kim, C. S.; Rytuba, J. J.; Brown, G. E. *J. Colloid Interface Sci.* **2004**, *271*, 1-15.

(38)   Kim, C. S.; Rytuba, J. J.; Brown, G. E. *J. Colloid Interface Sci.* **2004**, *270*, 9-20.

(39)   Nakamoto, K. *Infrared and Raman Spectra of Inorganic and Coordination Compounds*; Fifth ed.; John Wiley & Sons, Inc.: New York, 1997.

(40)   Baes, C. F., Jr.; Mesmer, R. E. *The Hydrolysis of Cations*; John Wiley & Sons: New York, 1976.

(41)   Chen, C.-C.; McKimmy, E. J.; Pinnavaia, T. J.; Hayes, K. F. *Environ. Sci. Technol* **2004**, *38*, 4758-4762.

(42)   Klug, H. P.; Alexander, L. E. *X-Ray Diffraction Procedures for Polycrystalline and Amorphous Materials. 2nd ed*, 1974.

(43)   Billinge, S. J. L.; Kanatzidis, M. G. *Chem. Commun.* **2004**, 749-760.

(44)   Wyckoff, R. W. G. *Crystal Structures*; Interscience Publishers: Easton PA, 1963; Vol. One.

(45)   Albert Cotton, G. W., Carlos Murillo, Manfred Bochmann *Advanced Inorganic Chemistry*; John Wiley and Sons, Incorporated: New York, 1999.

(46)   Antochshuk, V.; Jaronicc, M. *Chem. Commun.* **2002**, 258-259.

(47)   Chen, X.; Feng, X.; Liu, J.; Fryxell, G. E.; Gong, M. *Stud. Surf. Sci. Catal.* **1999**, *34*, 1121-1132.

(48)   Chen, X. B.; Feng, X. D.; Liu, J.; Fryxell, G. E.; Gong, M. L. *Sep. Sci. Technol.* **1999**, *34*, 1121-1132.

(49)   Mitra, S. *Mercury in the Ecosystem: Its Dispersion and Pollution Today*; Trans Tech Publications: New York, 1986.

Chapter 5

Arsenic trapping by functionalized mesostructures

5.1 Introduction

Arsenic, a metalloid element, is most commonly found in nature as an oxo-acid or oxyanion in solution in two different oxidation states: As(III) and As(V). As(III), termed arsenite, is present as $As(OH)_3$ up to a pH of 9, beyond which it is $[OAs(OH)_2]^-$. As(V), denoted arsenate is present as $OAs(OH)_3$ at a pH ≤ 2. From pH 2-7 it is $[O_2As(OH)_2]^-$, it then loses another proton above pH 7. The final proton is lost at pH ≥ 11.5.

Arsenic is released into the environment from both natural and anthropogenic sources. Arsenic is found naturally in rock, soil, water and air. The arsenic concentration in the earth's crust is 1.5 to 5 mg/kg. Higher concentrations are found in iron and magnesium ores, and in sulfide ores of lead, copper and zinc. Arsenic is released into the environment by dissolution from these rocks and ores. Furthermore, this dissolution is the reason so many wells are found to be contaminated by arsenic.

The anthropogenic sources of arsenic are primarily from manufacturing of metals and alloys, petroleum refining, pharmaceutical manufacturing, pesticide manufacturing, and the burning of fossil fuels. Agricultural use of arsenic includes utilization in herbicides such as monosodium methylarsonate $Na[CH_3AsO_2(OH)]$, and disodium methylarsonate $Na_2[CH_3AsO_3]$.

The concern over arsenic in drinking water has been increasing over the last two decades. Arsenic is now linked to several different cancers - skin, liver, bladder, lung, kidney and colon. The United States Environmental Protection Agency (EPA) has

170

recently lowered the limit of total arsenic in drinking water from 50 ppb to 10 ppb.[1] The EPA estimates that approximately 350,000 people in the US drink water containing over 50 ppb, and nearly 25 million drink water containing over 25 ppb arsenic. Arsenic contamination is a problem throughout the US, but the problem is not as severe as in many Asian countries. Arsenic levels in some Vietnamese groundwater wells exceed 3,000 ppb,[2] ninety per cent of the wells in some areas of Bangladesh were found to contain arsenic levels up to 14,000 times the World Health Organization (WHO) limit of 10 ppb.[3] The area most affected by 'excessive' arsenic levels in groundwater is the Bengal Basin, which has more than 40 million people drinking water containing concentrations over 10 ppb.[4,5]

The EPA and WHO limit of 10 ppb refers to total arsenic concentration. Of the two forms of inorganic arsenic found in natural waters, arsenite is the predominant form found in ground water, whereas the arsenate is the major species associated with surface waters. Arsenite adsorbs less strongly and to fewer minerals, which makes it more mobile than arsenate.[6] Moreover, arsenite is estimated to be 60-times more toxic than arsenate.[7]

The list of treatment technologies for the remediation processes of arsenic removal in water are: coagulation/precipitation, membrane/reverse osmosis, ion exchange, permeable reactive barriers, and adsorption.[8,9] Precipitation of arsenate by alum, ferric chloride, or ferric sulfate has been the most frequently used method to treat arsenic contaminated water, including groundwater, surface water, leachate, mine drainage, drinking water, and wastewater. This technology typically can reduce arsenic concentrations to the range of 50 ppb to 1,000 ppb, much higher than the EPA/WHO

limit.[8] The valence state of the arsenic and the pH of the water are important factors in the removal of the contaminants by precipitation. Arsenite typically needs to be oxidized to arsenate for the precipitation method to work or the pH has to be adjusted to a value $\geq$ 9 so that arsenite is in anionic form. Furthermore, the more soluble arsenite may reduce removal efficiency. Also, other chemicals in water might react with the arsenic and further impact the efficacy of remediation. For example, sulfate could decrease the arsenic removal in processes using ferric chloride as a coagulant, while presence of calcium or iron may increase the removal of arsenic in these processes.[8]

Membrane/reverse osmosis uses semi-permeable membranes that are selectively permeable to water and certain solutes to separate impurities from water. Membranes are usually expensive and therefore are typically considered in applications such as desalination, brackish water conversion, and the removal of specific ions that are difficult to remove by other means. This method is able to reduce the arsenic concentration to levels comparable to precipitation, but it tends to produce larger volumes of residuals and is more expensive than other arsenic treatment methods.[8]

Ion exchange is the reversible interchange of ions between the solid and liquid phase where there is no permanent change in the structure of the solid. Synthetic ion exchange resins are based on cross-linked polymer matrix, typically polystyrene cross-linked with divinyl benzene. Classically, strong-base anion exchange resins (e.g. quaternary amines) are used in arsenic removal.[8] Charged functional groups such as $HCrO_4^-$, CrO_4^{2-}, or ClO_4^- are covalently bonded to the resin and these resins have a relatively high affinity for arsenate. However, sulfate ions will compete with arsenate and reduce the removal efficiency. Additionally, since arsenite in natural water is

typically nonionic, it must be oxidized, or the pH adjusted to a value ≥ 9 for ion exchange to work. Ion exchange reduces the concentration of arsenic to less than 50 ppb.

Permeable reactive barriers (PRB) are a newer technology and used full scale at few sites. The barrier is typically zero valent iron or limestone. The mechanism of inorganic contaminants removal by the PRB is unclear; however, removal may be achieved by reductive precipitation or adsorption. One mechanism postulated is that arsenate binds tightly to the iron filling causing the zero valent iron to be oxidized to ferrous iron aerobically or anaerobically in the presence of water as shown in the following reactions:

$$\text{(anaerobic) } Fe^0 + 2\ H_2O \rightarrow Fe^{2+} + H_2 + OH^- \qquad \text{Equation 5.1}$$

$$\text{(aerobic) } Fe^0 + 2\ H_2O + O_2 \rightarrow 2\ Fe^{2+} + 4\ OH^- \qquad \text{Equation 5.2}$$
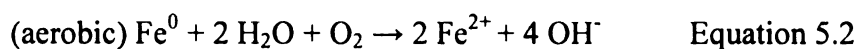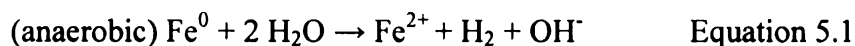
The Fe^{2+} then sorbs the arsenate through an electrostatic interaction.[8] The drawbacks of this method are chiefly due to the installation of the barrier. The contaminated plume cannot be greater than 70 feet deep, and the barrier cannot be installed in certain types of rock. In addition, the hydrolytic conductivity of the barrier must be greater than that of the aquifer to prevent preferential flow around the barrier, and there is concern with plugging the barrier.

Adsorption is the accumulation of materials at an interface, namely, the liquid/solid boundary layer. It is a mass transfer process where a substance is transferred from the liquid phase to the surface of a solid and becomes bound by chemical or physical forces.

Functionalized mesostructures have been examined as materials suitable for arsenate adsorption.[10-13] Adsorption can take place on suspended particles, as part of the

process of coagulation/co-precipitation, or on fixed media. Yet, to date, no work has been done utilizing mesostructures for arsenite adsorption. Two different methods have been used to examine arsenate adsorption by functionalized mesoporous materials. The first[10,13] involved arsenate adsorption by what the authors refer to as a "lock and key" process. The "lock" was comprised of a hexagonal MCM-41mesostrucutre grafted with ethylenediamine ligands to which copper was then adsorbed by the ethylenediamine ligands to form octahedral complexes on the surface of the mesoporous support.[14] Grafting is the process by which an organic moiety is anchored onto a silica surface through condensation of surface silanols with alkoxy groups of an organosiloxane. The copper, chelated by the amines, gave rise to positively charged hosts with 3-fold symmetry that matched the geometry of tetrahedral arsenate, the "key". The arsenate binding initially involved electrostatic ion-pairing with the immobilized octahedral copper(II) complexes in the mesostructure, followed by interactions which cause the displacement of one diamine ligand and direct binding of the arsenate with the Cu(II) center. The proposed mechanism is shown below.[14]
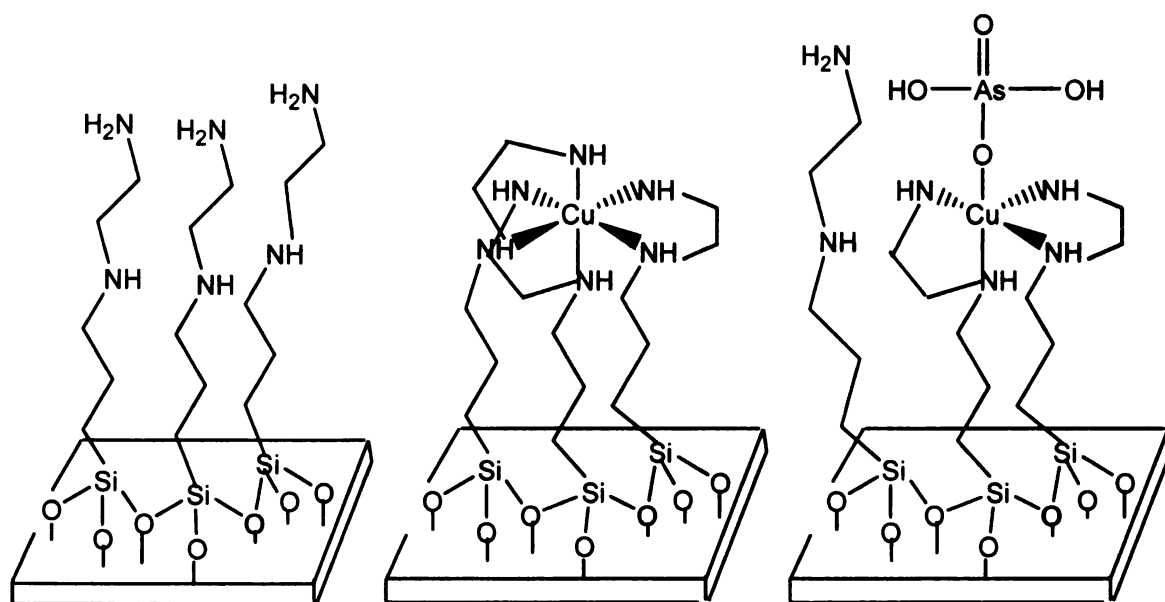
The second method used to trap arsenate is that of electrostatic interaction between a protonated amine and the anionic arsenate.[11] The amine incorporation was accomplished by the grafting method, and the amine-functionalized mesostructure was stirred in hydrochloric acid to protonate the amine.[11]

The purpose of the present work to examine the arsenite, as well as the arsenate, adsorption capacity of functionalized wormhole mesostructures which have been synthesized under near neutral conditions with the organic group incorporated by direct-assembly. In the direct-assembly of a functional mesostructure the organosilane is co-condensed with the silica precursor in the initial reaction mixture to form a product with the anhydrous composition $(SiO_2)_{1-x} (LSiO_{1.5})_x$ where L is the organic group and x is the fraction of framework silicon centers that are functionalized. One aim of the research was to devise a method of directly adsorbing arsenite; we did not want to have to either adjust the pH of the solution or to oxidize the arsenite to arsenate in order to achieve removal of arsenite. On the basis of the known ability of sulfhydryl groups in the body to bind arsenite,[15] adsorption of arsenite to the mercaptopropyl moieties in the mesostructure was examined. The mesostructures investigated included a mercaptopropyl (MP) functionalized wormhole framework HMS mesostructure, mesostructured cellular foam, and dual functionalized mercaptopropyl and aminopropyl wormhole framework HMS structure. Since earlier work successfully employed amines for arsenate trapping,[11] amines were used as the organic functionality in this work for the trapping of arsenate. The mesostructures are aminopropyl (AP) functionalized HMS and dual functionalized mercaptopropyl and aminopropyl HMS wormhole structures.

5.2 Experimental

5.2.1 Reagents

Aminopropyltrimethoxysilane, mercaptopropyltrimethoxysilane, tetraethylorthosilicate, 1,3,5-trimethylbenzene, and dodecylamine, were purchased from Aldrich and used without further purification. P-123 surfactant was donated by BASF and used without further purification. Absolute ethanol and hydrochloric acid were purchased in-house. Water was double-exchanged to remove cations and anions via a Millipore filter apparatus.

5.2.2 Material Synthesis

5.2.3 Materials for As(III) (Arsenite) Adsorption

Three different mesostructures two with the compositions $(SiO_2)_{1-x}$ $(LSiO_{1.5})_x$ and $(SiO_2)_{1-(x+y)}$ $(LSiO_{1.5})_x(L'SiO_{1.5})_y$ were examined for viability in arsenite adsorption. In these two compositions L equals mercaptopropyl (MP) and L' equals aminopropyl (AP). Wormhole framework and mesocellular foam structures functionalized with MP groups were denoted MP-HMS and MP-MCF, respectively. The dual functionalized wormhole structure is denoted MP+AP-HMS, and mercaptopropyl functionalized mesostructured cellular foam is denoted, MP-MCF. The physical properties of the dual functionalized MP+AP-HMS mesostructures were given in their entirety in Chapter 3. Only the MP-MCF physical properties will be discussed in this chapter.

5.2.4 Functionalized Wormhole Structures

MP-HMS. MP-HMS was synthesized using dodecylamine as the surfactant and (1-x) molar mixture of tetraethylorthosilicate as the silicon source and x mercaptopropyltrimethoxysilane as the organosilane. The synthesis was described in Chapter 4. The overall molar stoichiometry employed was: 1-x TEOS : x MPTMS : 0.22 DDA : 6.7 EtOH : 160 H_2O.

MP+AP-HMS. Dual functionalized MP+AP-HMS was synthesized using dodecylamine as the surfactant and a 1-(x+y) molar mixture of tetraethylorthosilicate as the silicon source and x mercaptopropyltrimethoxysilane and y aminopropyltrimethoxysilane as the organosilanes. The synthesis was described in Method II in Chapter 3. The overall molar stoichiometry employed was 1-(x+y) TEOS : x MPTMS : y APTMS : 0.22mol DDA : 5 mol EtOH : 160 mol H_2O. The equivalent values of x and y were employed for arsenite adsorption so that a theoretical loading of x=y=0.05, 0.10, 0.15, and 0.25, were synthesized. The x and y values observed will be given throughout the text.

5.2.5 Functionalized Mesocellular Foam Structures.

MP-MCF. In order to prepare MP-MCF, 2 g of P 123 ($EO_{20}PO_{70}EO_{20}$) surfactant 0.345 mmol was dissolved in 75 ml 1.6 M HCl at room temperature overnight. Next, 1.5 g of 1,3,5- trimethylbenzene was added to the surfactant solution and mixed at 40 °C for 1 h. A (1-x) : x molar mixture of tetraethylorthosilicate (TEOS) and mercaptopropyltrimethoxysilane (MPTMS) was then added dropwise, and the mixture was aged for 20 h at 40 °C to provide a reaction mixture in which the overall Si: surfactant millimolar ratio was 21.0: 0.345. To further promote framework cross-linking,

the reaction mixture was allowed to age in an oven at 100 °C for 24 h. The precipitate was filtered and let air-dry 24 h before Soxhlet extraction with ethanol. The x values tested for arsenite adsorption were x=0.10, 0.20, and 0.30.

5.2.6 Materials for As(V) (Arsenate) Adsorption

Two different functionalized wormhole mesostructures were used for arsenate trapping, one with the composition $(SiO_2)_{1-x}$ $(LSiO_{1.5})_x$ and one with the composition $(SiO_2)_{1-(x+y)}$ $(LSiO_{1.5})_x(L'SiO_{1.5})_y$, where L equals mercaptopropyltrimethoxysilane and L' equals aminopropyltrimethoxysilane. The former mesostructure is aminopropyl functionalized HMS is denoted AP-HMS and the latter is dual aminopropyl and mercaptopropyl functionalized HMS, termed MP+AP-HMS. The physical properties of the dual functionalized mesostructures were given in their entirety in Chapter 3 and only will be summarized here.

AP-HMS with x=0.10, 0.20, and 0.40 compositions were synthesized using the direct-assembly method for the organic group incorporation and an amine surfactant as the porogen. The synthesis was as described below.

5.2.7 Functionalized Wormhole Structures

AP-HMS. A 5.10 g quantity of DDA (27.5 mmol) was dissolved in 25 g of ethanol to which 75 g of water was added. A x : 1-x mixture of aminopropyltrimethoxysilane and tetraethylorthosilicate were then added dropwise to the surfactant solution, and the mixture was allowed to stir at room temperature for 24 h. Finally the precipitate was filtered and air-dried followed by Soxhlet extraction with ethanol to remove the surfactant. The overall molar stoichiometry employed was 1-x TEOS : x APTMS : 0.275 mol DDA : 6.94 mol EtOH : 41.67 mol H_2O.

MP+AP-HMS. Dual functionalized MP+AP-HMS was synthesized using dodecylamine as the surfactant and a 1-(x+y) molar mixture of tetraethylorthosilicate as the silicon source with x mercaptopropyltrimethoxysilane and y aminopropyltrimethoxysilane as the organosilanes. The synthesis was described in Method II in Chapter 3. The overall molar stoichiometry employed was 1-(x+y) TEOS : x MPTMS : y APTMS : 0.22mol DDA : 5 mol EtOH : 160 mol H_2O. The equivalent values of x and y were employed for arsenate adsorption so that x=y =0.05, 0.10, 0.15, and 0.25, for all mesostructures. Hence x=y = 0.10 indicates a total of 20% of the silicon centers are functionalized, 10% with MP and 10% with AP moieties. The observed x and y values will be used throughout the text.

5.3 Physical Measurements

The physical properties of the functionalized mesostructures were determined by nitrogen adsorption, ^{29}Si Magic Angle Spinning Nuclear Magnetic Resonance (^{29}Si MAS-NMR), and Transmission Electron Microscopy (TEM). The binding of the arsenite and arsenate to the mesostructures was examined by Raman spectroscopy. Nitrogen adsorption-desorption isotherms were measured at −196 °C on a Micrometrics ASAP 2010 sorptometer, the samples were outgassed at 80 °C and 10^{-6} Torr prior to measurement. ^{29}Si MAS-NMR spectra were collected on a Varian 400 solid state NMR spectrometer with a field strength of 400 MHz under single-pulse mode with a zirconia rotor at a spinning frequency of 4 kHz. A pulse delay of 400 s was employed so that there was sufficient time for the nuclei to relax before application of another pulse. Talc was used as a reference. TEM images were obtained on a JOEL 2200FS microscope with an accelerating voltage of 200 KV. Sample grids were prepared by sonicating samples in ethanol for 20 min, and evaporating one drop of the suspension onto a carbon coated,

holey film supported on a 3 mm, 300 mesh copper grid. For Raman spectroscopy, samples were packed into glass capillary tubes and analyzed with a Bio-Rad FT Raman Spectrometer equipped with a germanium CCD camera detector and 633 nm radiation from a HeNe laser for excitation and a resolution of 4 cm^{-1}. Laser power at the sample was estimated to be about 5mW, and the focused laser beam diameter was ~10 µm. A total of 200 scans was accumulated for each spectrum.

5.3.1 As(III) (Arsenite) Adsorption

In a typical arsenite adsorption experiment a 200-mg quantity of mesostructure was added to 20 mL of water containing different initial concentrations of H_3AsO_3. The mixture was allowed to equilibrate for a period of 20 h at room temperature. A standardized H_3AsO_3 solution was adjusted to pH = 7.0 with 0.11 N sodium hydroxide before mixing with the MP-HMS trapping agent. The equilibrated suspensions were filtered using vacuum filtration with filter paper to remove the trapping agent. The amount of arsenite in solution was determined by titration.[16] In the titration reaction, arsenite is oxidized to arsenate with I_2 under basic conditions. Once all the arsenite is oxidized to arsenate by I_2, the starch will react with the I_2 to form a blue solution. The overall equation for the titration reaction is:

$$AsO_3^{3-} + I_2 + H_2O \rightarrow AsO_4^{3-} + 2H^+ + 2I^-.$$
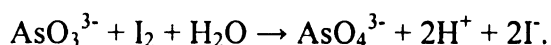
The amount of arsenite adsorbed by the trapping agent was determined by difference.

5.3.2 As(V) (Arsenate) Adsorption

Arsenate uptake by directly-assembled amine functionalized mesostructures was examined. In a typical adsorption experiment, a 200-mg quantity of mesostructure was

equilibrated in a 20 mL solution of a known concentration (ppm) arsenate, $(AsO_4)^{-3}$, solution. The suspensions were then filtered using vacuum filtration with filter paper to remove the trapping agent. The amount of arsenate was determined by difference through titration to a clear endpoint.[16] The arsenate was reduced to arsenite by I^- under acidic conditions followed by titration of the yellow iodine solution with sodium thiosulfate to a clear endpoint. The reactions are as follows:

$$AsO_4^{4-} + 2\,H^+ + 2\,I^- \rightarrow AsO_3^{3-} + I_2 + H_2O \qquad \text{Equation 5.3}$$

$$2\,Na_2S_2O_3 + I_2 \rightarrow Na_2S_4O_6 + 2\,I^- \qquad \text{Equation 5.4}$$
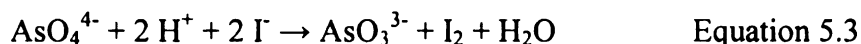
Arsenate is in the anionic form, $[O_2As(OH)_2]^-$, at the pH used for trapping (pH 7). In order to trap the arsenate anion, AP-HMS was slurried in 0.1 M HCl for 4 h to protonate the amine groups, which allowed for an electrostatic interaction between the anionic arsenate in solution and cationic amine immobilized on the mesostructure.

5.4 Results and Discussion

5.4.1 As(III) (Arsenite) Trapping

To date, no mesostructure has been used for arsenite remediation, and few methods of remediation are able to directly remove arsenite from water. Upon thorough review of the literature, the affinity of arsenite for thiols was revealed.[15,17] Consequently, three different mercaptopropyl functionalized mesostructures were prepared for use in arsenite adsorption. Wormhole MP-HMS components were chosen because of the ultra high thiol group loadings as well as the easy accessibility of the wormhole morphology as compared to a hexagonal framework morphology.[18] The dual MP + AP-HMS was selected to determine what consequence, if any, adding a hydrophilic second organic

moiety had on the arsenite adsorption by a hydrophobic mesostructure. Adsorption by a large pore foam mesostructure was also examined.

Until now, there has been no report of directly-assembled functionalized foam mesostructure. Foams are very large pore mesostructures assembled using an "oil-in-water" microemulsion templating technique. These materials were prepared under strongly acidic hydrolysis conditions from tetraethylorthosilicate (TEOS) as the silica precursor and an aqueous microemulsion of a triblock copolymer (Pluronic P123, $EO_{20}PO_{70}EO_{20}$) and 1,3,5-trimethylbenzene (TMB) as the porogen.[19]

Functionalized mesoporous materials have been extensively used for heavy metal remediation. However, most metals are not present as oxyanions. Therefore, cations are much smaller and more able to easily fit into the pores of mesostructures. The organic groups in functionalized mesostructures can be embedded in the framework walls. Therefore, a larger pore might allow for greater accessibility. Accordingly, directly-assembled mercaptopropyl functionalized mesoporous foam denoted MP-MCF, was synthesized.

The ^{29}Si MAS-NMR, nitrogen isotherms, and TEM images for MP-MCF compositions are shown in Figures 5.1, 5.2-5.5, and 5.6, respectively. From the relative intensities of the T^3 resonance of $RSi(OSi)_3$ units at -69 ppm and the Q^3 and Q^4 resonances in the region of -100 to -110 ppm, respectively (Figure 5.1). It can be seen that functional group incorporation into the foam framework was quantative. For MP-MCF compositions with x=0.20 and 0.30, the x-value observed was essentially equal to the x-value expected indicating 95 to 100% incorporation of the organic moiety into the framework. However, for the MP-MCF with x=0.10 the organic group incorporation is

only 60% of the expected value. This is attributed to the larger systematic error with determining the functional group concentration by NMR at low organic loadings.

The nitrogen isotherms for the MP-MCF with x=0.00, 0.10, and 0.20 (shown in Figures 5.2-5.4) are typical for large pore foam structures. They have well-expressed adsorption steps at partial pressures between 0.2 and 0.5, indicating the presence of uniform mesopores for each mesostructure. In addition, these three mesostructures exhibit H2 type hysteresis loops that occur above partial pressure of 0.5, which is typical of large pore foam structures.[20] Furthermore, the hysteresis loop systematically becomes broader as the amount of added organosilane increases, indicating these compositions have large cells that are connected by small windows. The above functionalized mesocellular foams desorb much of their nitrogen at relative pressures of 0.40-0.45. The desorption of nitrogen at this pressure at 77 K is not due to capillary evaporation but rather to the instability of the meniscus of the condensed nitrogen in the pores.[20-22] Thus the window size as calculated from the BJH model is not expected to be accurate. In Figure 5.5, the nitrogen isotherm for MP-MCF with x=0.30, does not show the mesopore filling step; rather it shows a linear uptake indicating the structure is non-porous.

The TEM images shown in Figure 5.6 illustrates the large pore foam structure for MP-MCF with x=0.00, 0.10, and 0.20. However, the compositions were no longer mesostructured, or even structured for that matter, beyond x=0.20. This loss of structure is further evident in the TEM images of Figure 5.3. The TEM images for x =0.0 and 0.10 are typical of foam structures, whereas the product with x = 0.30 is non-structured. An attempt was made to synthesize MP-MCF with x=0.40 and 0.50. These structures had a surface area less than 5 m^2/g, and the nitrogen isotherms were typical of non-porous

materials.   Table 5.1 summarizes the physical properties of the mercaptopropyl functionalized mesostructured cellular foam derived from the above characterization techniques. The surface areas and pore volume of the organo-functional MCF derivatives decrease as the amount of added organosilane increases. Additionally, a decrease in window size and cell size with an increase in functionalization was observed. The decrease in size suggests that the organosilane was incorporated into the pore walls of the mesostructure. The amount of mercaptopropyl loading for mesostructured MP-MCF compositions x=0.20 was not as large as has been achieved with MP-HMS mesostructures x=0.50.
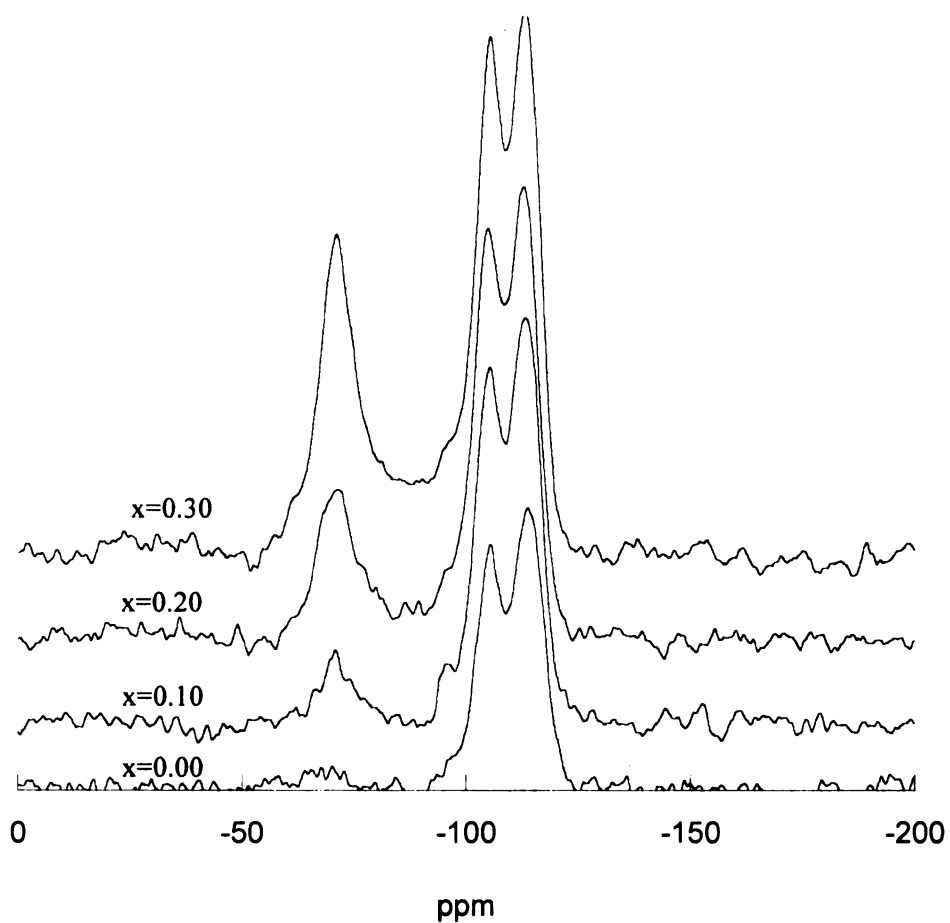
Figure 5.1. ^{29}Si MAS NMR spectra for functionalized $(SiO_2)_{1-x}(LSiO_{1.5})_x$ compositions (L=mercaptopropyl) with intended mesocellular foam framework structures, denoted MP-MCF. The Q^3 and Q^4 resonances of the SiO_4 centers appear in the chemical shift region of -100 to -110 ppm, respectively. The T^3 resonance of the $LSiO_3$ centers appear near -69 ppm.

185
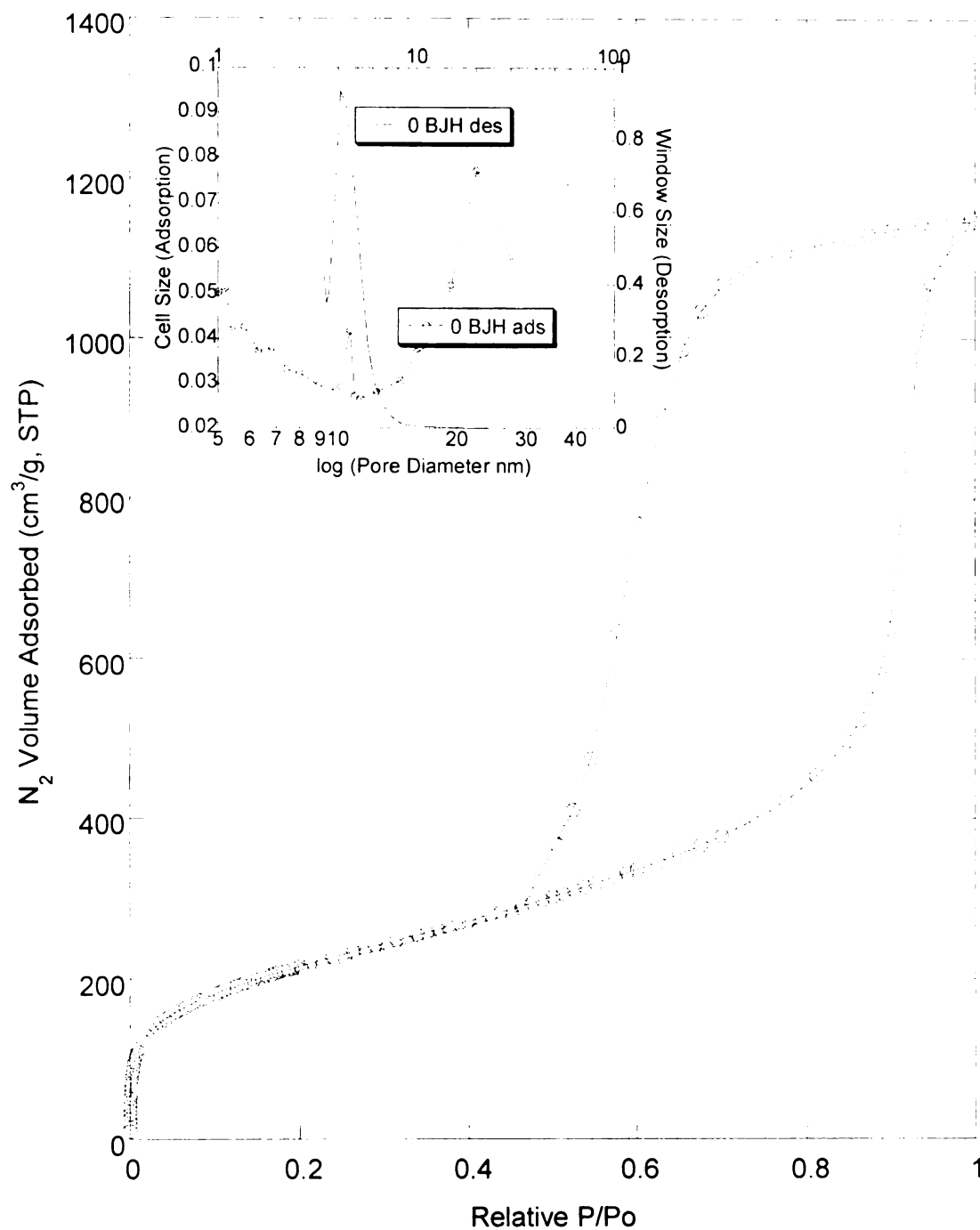
Figure 5.2. Nitrogen adsorption-desorption isotherm for silica with a mesocellular foam structure (x=0.00). The insets provide the BJH distribution for the cell size and the window size obtained from the adsorption and desorption isotherm, respectively.
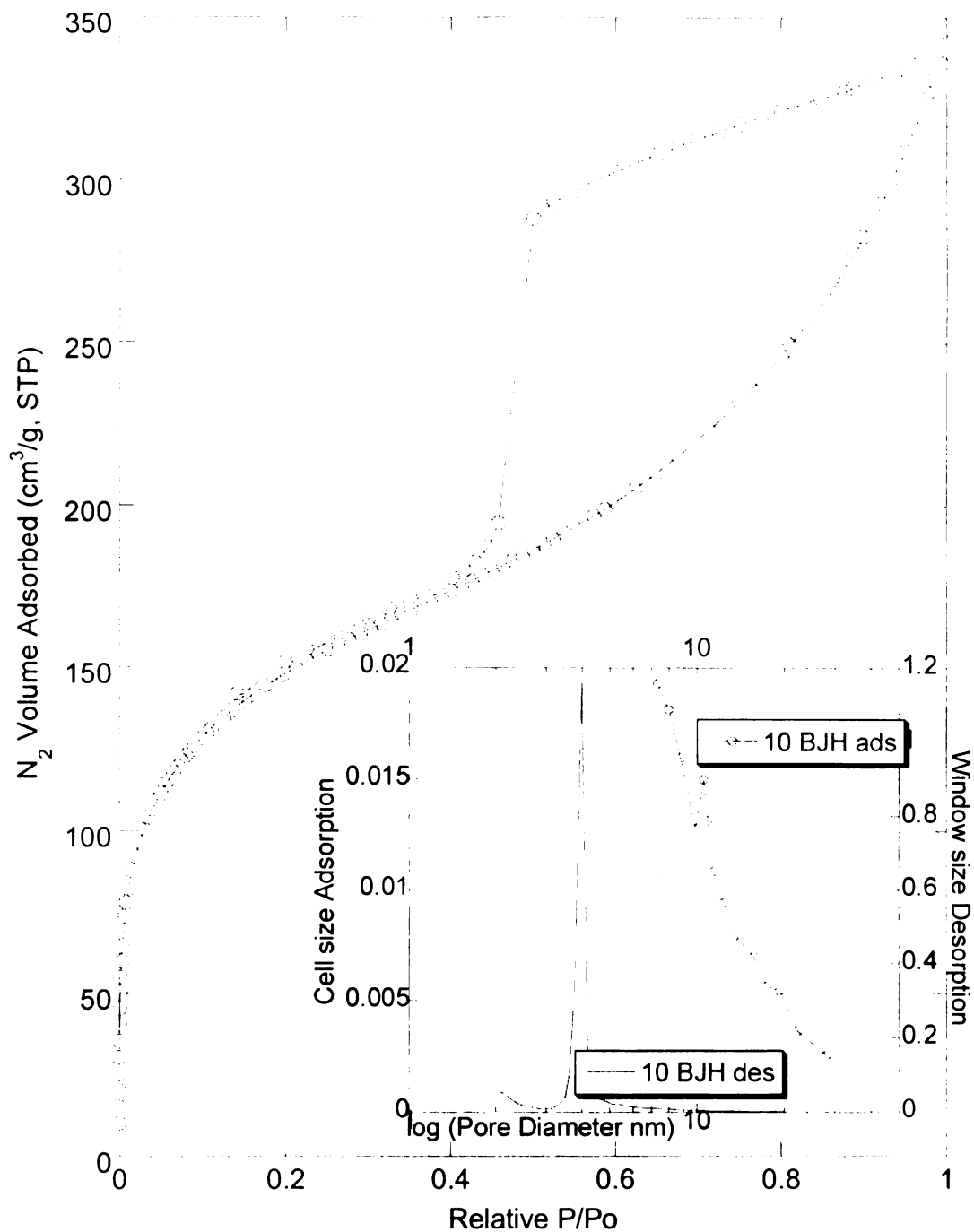
Figure 5.3. Nitrogen adsorption-desorption isotherm for functionalized $(SiO_2)_{1-x}$ $(LSiO_{1.5})_x$ compositions (L=mercaptopropyl); x=0.10 with a mesocellular foam framework structure, denoted MP-MCF. The insets provide the BJH distribution for the cell size and the window size obtained from the adsorption and desorption isotherm, respectively.
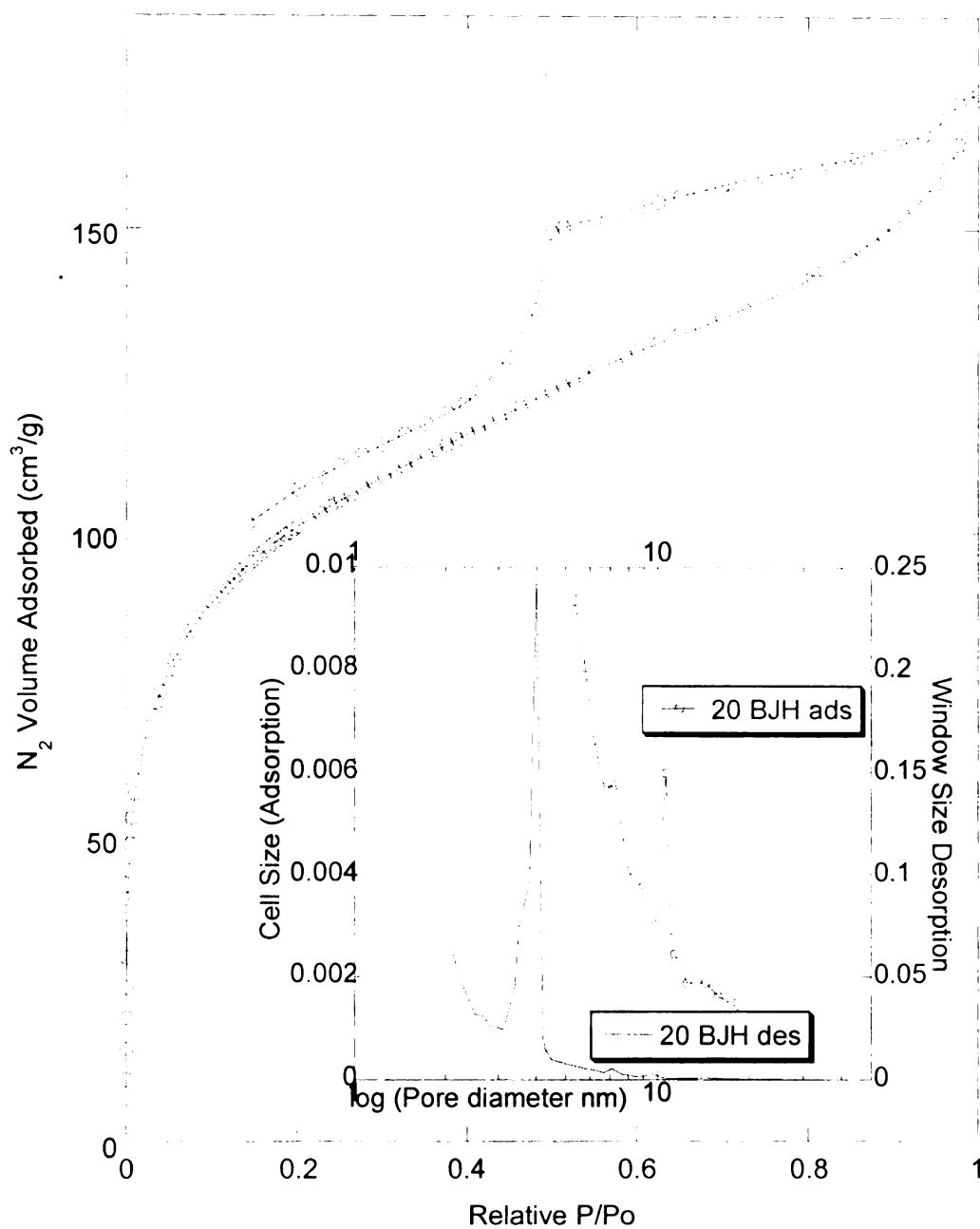
Figure 5.4. Nitrogen adsorption-desorption isotherm for functionalized $(SiO_2)_{1-x}$ $(LSiO_{1.5})_x$ compositions (L=mercaptopropyl); x=0.20 with a mesocellular foam framework structure, denoted MP-MCF. The insets provide the BJH distribution for the cell size and the window size obtained from the adsorption and desorption isotherm, respectively.
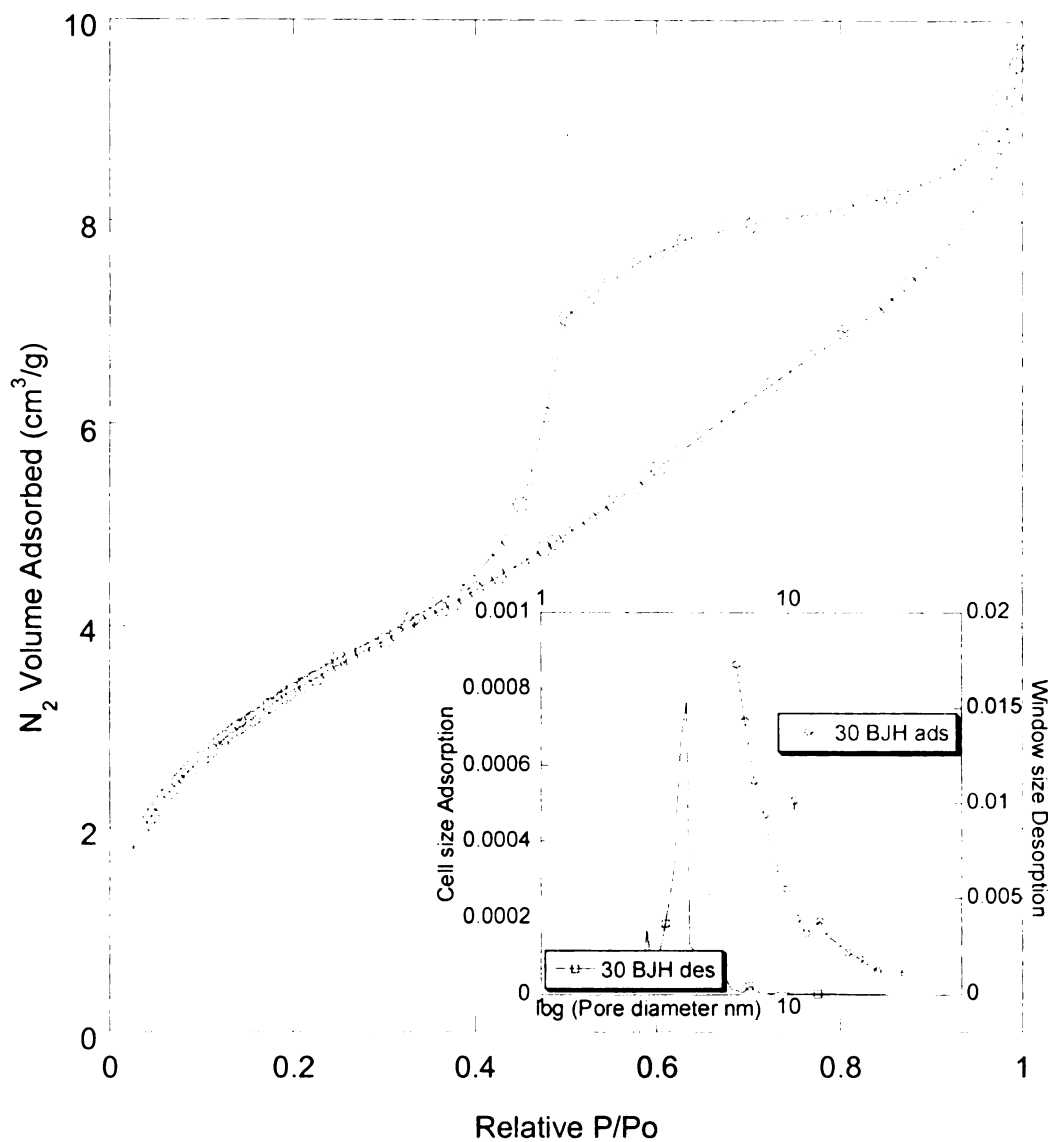
Figure 5.5. Nitrogen adsorption-desorption isotherm for functionalized $(SiO_2)_{1-x}$ $(LSiO_{1.5})_x$ composition (L=mercaptopropyl); x=0.30. The insets provide the BJH distribution for the cell size and the window size obtained from the adsorption and desorption isotherm, respectively.
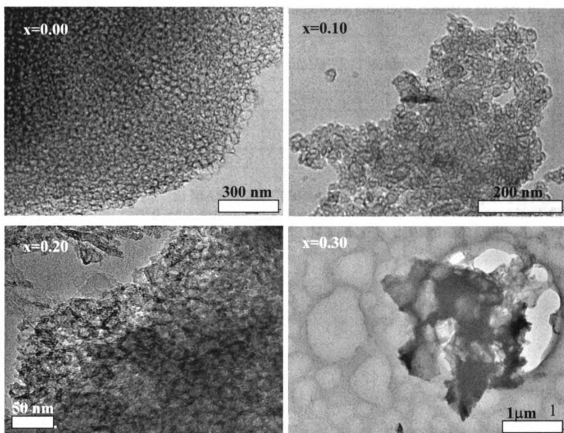
Figure 5.6. TEM image for functionalized $(SiO_2)_{1-x}(LSiO_{1.5})_x$ compositions (L= mercaptopropyl) with a mesocellular foam framework structure, denoted MP-MCF.

Table 5.1. Textural properties of functionalized $(SiO_2)_{1-x}$ $(LSiO_{1.5})_x$ compositions (L= mercaptopropyl) with a mesocellular foam framework structure, denoted MP-MCF.

MP-MCF	x_{theo}	x_{obs}[a]	mmol SH/g	SA[b] m^2/g	Pore volume[c] cm^3/g	Widow size[d] nm	Cell size[e] nm
x=0.0	0.00	0.00	0.0	791	1.7	4.5	21.5
x=0.1	0.10	0.06	0.84	537	0.5	4.0	11.0
x=0.2	0.20	0.19	2.5	364	0.25	4.0	11.0
x=0.3	0.30	0.30	3.6	13	0.01	-	-

[a]x-value determined by ^{29}Si MAS NMR. [b]Calculated from nitrogen adsorption isotherms by BET method [c]Total pore volume at P/P_0=0.98 [d]BJH window size determined from desorption branch of nitrogen isotherm. [e]BJH cell size determined from adsorption branch of nitrogen isotherm.

191

As previously stated, three different mesostructures were used of for arsenite trapping, namely MP-HMS and MP-MCF derivatives with wormhole and mesocellular foam framework structures, respectively, and the dual functionalized MP+AP-HMS with a wormhole framework structure. MP-HMS with $x=0.50$ has the highest mercaptan content of any of the aforementioned mesostructures. Therefore, it would be expected to have the highest arsenite adsorption capacity. To examine the effect of increased organo-functionality on arsenite adsorption, uptake curves were determined. Differing concentrations of arsenite were equilibrated with MP-HMS derivatives with $x=0.10$-0.50 for 24 h at ambient temperature, and the arsenite uptake was determined by difference. The uptake curves for MP-HMS with $x=0.10$-0.50 are shown in Figure 5.7. As expected, the mesostructure with the highest organic loading does indeed adsorb the greatest amount of arsenite. But each of the mercaptan functionalized compositions, regardless of level of organic moiety incorporation, are capable of adsorbing arsenite. The MP-HMS with $x=0.10$ and 0.20 quantatively adsorb arsenite essentially quantitatively only at arsenite loadings, which correspond to the binding of arsenite up to 10% of the mercaptans or to a SH/As ratio ≥ 10. For MP-HMS with $x=0.30$, quantative uptake of arsenite is observed up to SH/As ≥ 6.7 or up to 15% of the mercaptans are bound by arsenite. MP-HMS with $x=0.40$ and 0.50 quantative uptake is observed up to SH/As ≥ 5 or up to 20% of the mercaptans have been accessed. Therefore, the higher the ligand loading, i.e. the larger the x value, the greater the uptake of arsenite. The maximum arsenite binding capacity of 150 mg arsenite/g of trapping agent was obtained for MP-HMS with $x=0.50$. Thus, arsenite adsorption by MP-HMS mesostructures of the type $(SiO_2)_{1-x}(SiO_{1.5}L)_x$ is quantitative up to overall SH/As ratios $\geq 5 \geq 10$ depending on the

level of MP functionality of the mesostructure. The above dependence of As(III) binding on the level of MP functionalization suggests that only 10-20% of the SH sites are accessible for reaction with arsenite. The remaining SH groups appear to be blocked or buried in the walls of the mesostructure.

MP-HMS with x=0.30 and 0.50 compositions were also tested for arsenate adsorption. The trapping of arsenate by MP-HMS was found to be negligible, less than 2%, illustrating the selectivity of the mercaptan functionality for arsenite adsorption. The selectivity of arsenite binding in the presence of anions found in nature was also examined. Arsenite trapping in the presence of nitrate, a common ion present in water, was conducted. The uptake of a 161 ppm solution of arsenite by MP-HMS with x=0.50 in the presence 855 ppm nitrate was examined. The overall SH/As(III) molar ratio was 5:1 SH:As. More than 96% of the As(III) was removed from solution whether NO_3^- was present or not.

Table 5.3 and Table 5.4 provide the results for arsenite adsorption by the MP-MCF composition and dual functional MP+AP-HMS derivative, respectively. The uptake of arsenite by these components parallel the behavior observed for MP-HMS derivatives. An excess of thiol to total As(III) was necessary for 95% uptake of arsenite. Furthermore, the degree of functionalization of the mesostructures influenced the efficiency of arsenite loading.
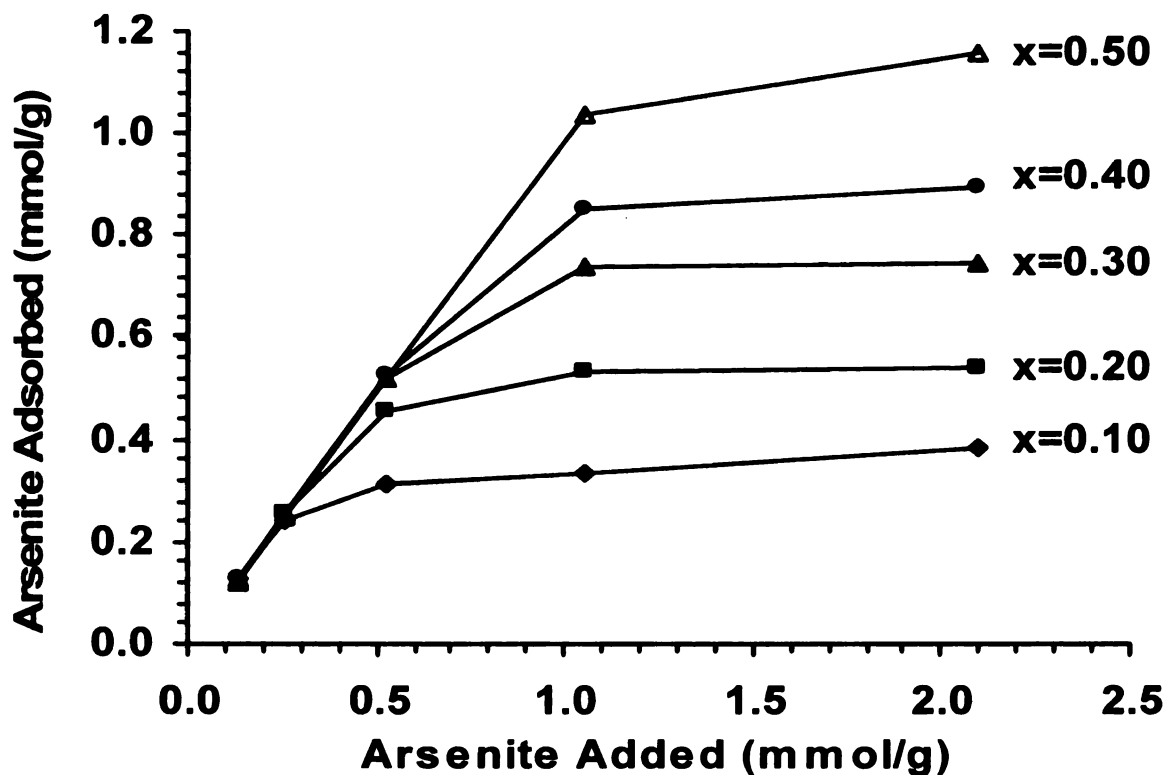
Figure 5.7. Arsenite uptake curve for functionalized $(SiO_2)_{1-x}$ $(LSiO_{1.5})_x$ compositions (L=mercaptopropyl) with a wormhole framework structure, denoted MP-HMS. Total volume of arsenite solution, with varying concentrations, was 20 mL; mass of MP-HMS was 200 mg. The loading of SH/g for each mesostructure is given in Table 5.2.

Table 5.2. Arsenite adsorption by functionalized $(SiO_2)_{1-x}$ $(LSiO_{1.5})_x$ compositions (L=mercaptopropyl) with a wormhole framework structure, denoted MP-HMS.

MP-HMS	Initial ppm (H_3AsO_3)	Final ppm (H_3AsO_3)	mmol SH/g theoretical	mmol H_3AsO_3 added /g	mmol SH / mmol H_3AsO_3 added	mmol H_3AsO_3 adsorbed /g	mmol SH/ mmol H_3AsO_3 adsorbed	% Removal
x=0.00	323	317	0	0.525	∞	$4.88*10^{-4}$	∞	1.83
x=0.10	645	258	1.50	0.525	2.86	0.315	4.76	60.0
x=0.10	323	22.3	1.50	0.263	5.70	0.244	6.15	93.1
x=0.10	161	3.32	1.50	0.131	11.5	0.129	11.6	97.9
x=0.20	645	85.7	2.72	0.525	20.8	0.455	5.97	86.7
x=0.20	323	4.69	2.72	0.263	10.3	0.259	10.5	98.6
x=0.20	161	9.47	2.72	0.131	20.8	0.124	21.9	94.1
x=0.30	645	3.29	3.75	0.525	7.14	0.522	7.18	99.4
x=0.30	323	6.30	3.75	0.263	14.3	0.257	14.6	98.1
x=0.30	161	4.78	3.75	0.131	28.6	0.127	29.5	97.0
x=0.40	1291	32.2	4.61	1.05	4.39	1.02	4.50	97.5
x=0.40	562	6.30	4.61	0.457	10.1	0.452	10.2	98.9
x=0.40	323	8.03	4.61	0.263	17.5	0.252	18.3	97.5
x=0.40	161	9.39	4.61	0.131	35.2	0.121	38.1	94.2
x=0.50	1291	6.63	5.35	1.05	5.10	1.04	5.10	99.5
x=0.50	645	4.79	5.35	0.525	10.2	0.521	10.3	99.3
x=0.50	161	6.21	5.35	0.131	40.8	0.126	42.5	96.2

Table 5.3. Arsenite adsorption by functionalized $(SiO_2)_{1-x}$ $(LSiO_{1.5})_x$ compositions (L=mercaptopropyl) with a mesocellular framework structure, denoted MP-MCF.

MP-MCF	Initial ppm (H_3AsO_3)	Final ppm (H_3AsO_3)	mmol SH/g	mmol H_3AsO_3 added/g	mmol SH/ mmol H_3AsO_3 added	mmol H_3AsO_3 adsorbed /g	mmol SH/ mmol H_3AsO_3 adsorbed	% Removal
x=0.10	323	228	0.84	0.263	3.19	0.077	10.9	29.2
x=0.20	2580	2014	2.48	2.10	1.18	0.460	5.39	21.9
x=0.20	323	10	2.48	0.263	9.4	0.255	9.73	97.0
x=0.30	2580	1936	3.60	2.10	1.71	0.524	6.87	25.0
x=0.30	323	16	3.60	0.263	13.7	0.250	14.4	95.0

Table 5.4. Arsenite adsorption by dual-functionalized $(SiO_2)_{1-(x+y)}$ $(LSiO_{1.5})_x$ $(L'SiO_{1.5})_y$ compositions (L=mercaptopropyl, L'=aminopropyl) with a wormhole framework structure, denoted MP+AP-HMS.

MP+AP-HMS	Initial ppm (H_3AsO_3)	Final ppm (H_3AsO_3)	mmol SH/g calculated	mmol H_3AsO_3 added /g	mmol SH/ mmol H_3AsO_3 added	mmol H_3AsO_3 adsorbed /g	mmol SH/ mmol H_3AsO_3 adsorbed	% Removal
x=0.05 y=0.03	323	214	0.70	0.263	2.66	0.088	7.95	33.6
x=0.10 y=0.05	323	24.8	1.37	0.263	5.21	0.242	5.66	92.3
x=0.10 y=0.05	129	14.4	1.37	0.105	13.1	0.093	14.7	88.8
x=0.15 y=0.12	1291	840	1.77	1.05	1.69	0.367	4.82	34.9
x=0.15 y=0.12	323	56.3	1.77	0.263	6.73	0.217	8.15	82.5
x=0.25 y=0.19	1291	978	2.82	1.05	2.69	0.254	11.1	24.2
x=0.25 y=0.19	645	378	2.82	0.525	5.37	0.217	13.0	41.3
x=0.25 y=0.19	323	3.00	2.82	0.263	10.7	0.260	10.8	99.0
x=0.25 y=0.19	161	3.13	2.82	0.131	21.5	0.129	21.9	98.1

Irrespective of the level of thiol functionalization of the mesostructure and synthesis method used to form the mesostructure, each composition was able to reduce the arsenite concentration by 95% or more, provided that the overall SH/As(III) ratio was $\geq$ 5, or more preferably $\geq$ 10. For > 95% As(III) removal by MP-HMS with x=0.10, 0.20, and 0.30, a thiol: As ratio of at least 10:1 is needed. For MP-HMS with x=0.40 and 0.50, quantative arsenite trapping is observed at a 5:1 mercaptan to arsenite ratio. The MP-HMS silicas with x=0.10 and 0.20 were efficient at adsorbing arsenite at initial concentrations of 322 ppm and below. MP-HMS with x=0.30 was able to reduce initial concentrations of 645 ppm by 95%. MP-HMS with x=0.40 and 0.50 were efficient for trapping arsenite at initial concentrations of 1290 ppm. Hypothetically, a 1:1 mercaptan to arsenite adsorption should be possible. It would seem however that not all the thiol groups are accessible or there is not a one-to-one binding of arsenic(III).

The larger pore foams did not outperform the smaller pore mesostructures as might have been expected. The same 10:1 excess of thiol to arsenite ratio was needed for efficient trapping of arsenite by MP-MCF as MP-HMS. Higher levels of arsenite uptake might have been achieved if a higher degree of functionalization beyond x values of 0.30 could have been accomplished for the foam structures.

For arsenite uptake by dual functionalized MP+AP-HMS, the mercaptopropyl ligands also need to be in excess of the arsenite. Specifically 10:1 excess of mercaptan to As(III) is needed to attain 99% removal. For MP + AP-HMS with x=0.10 or 0.15 the uptake of As(III) is comparable to MP-HMS derivatives with x=0.10 or 0.20 (98% removal of arsenite at 161 ppm). The similarities between the mercaptopropyl functionalized HMS silica and the dual functional HMS indicated that the

mercaptopropyl organic content is the main factor determining arsenite uptake. The amine moiety plays no role in facilitating arsenite uptake. However, the dual functionalized silica does reduce the arsenite levels to the lowest final concentration observed, namely 3 ppm.

Increases in framework thiol functionalization result in comparatively small increases in arsenite binding. This suggests that only a fraction of the framework sites are active for arsenite binding. Special mercaptan sites are involved in trapping the arsenite or the arsenic(III) binding mechanism involves multiple thiol-arsenite interactions. Raman spectroscopy was utilized in an attempt to elucidate the mechanism for binding arsenite to mercaptan. The spectra are shown in Figure 5.8. The mercaptan S-H stretch appears as a strong band at 2560 cm^{-1}.[23,24] A weak band at 510 cm^{-1} assigned to a S-S stretch indicated the presence of a small amount of disulfide due to the air oxidation of adjacent thiol groups on the surface of the mesostructure.[24] The C-H stretch appears as a strong band 2900 cm^{-1}.[24] The S-H stretch at 2560 cm^{-1} decreased as the arsenite loading increased, indicating that the trapping of arsenite is due to the formation of an As-S bond. No change in the intensity of the S-S stretch at 510 cm^{-1} was observed with any arsenite binding, ruling out the interaction of the disulfide moiety with arsenite. The disulfide is present in the initial mesostructure due to oxidation of neighboring thiols during the synthesis of MP-HMS. The As-S stretch is present in the range of 212-450 cm^{-1}.[25,26] The As-O has a strong symmetric stretch around 850 cm^{-1} and a strong anti-symmetric stretch around 415 cm^{-1}.[27] A stretch at 375 cm^{-1} is present in the mesostructures with adsorbed arsenite; however, it is present in the parent material

MP-HMS with x=0.50 as well. Nonetheless, this stretch does grow significantly with arsenite adsorption, indicating the presence of an As-S bond.

The possibility that arsenite was oxidized to arsenate by exposure to the air was investigated. The MP-HMS mesostructure was loaded with 322 ppm As(III) and a titration for determination of As(V) was done by adding I⁻ to the filtrate and titrating the mixture to a clear end point with sodium thiosulfate.[16] The titration results showed there was no As(V) present. By ruling out reaction of arsenite with disulfide and oxidation of arsenite to arsenate, it is possible to propose a binding mechanism involving an arsenite-mercaptan reaction. The proposed binding mechanism involving the formation of thioarsenite is shown in Scheme 5.1.

Scheme 5.1.
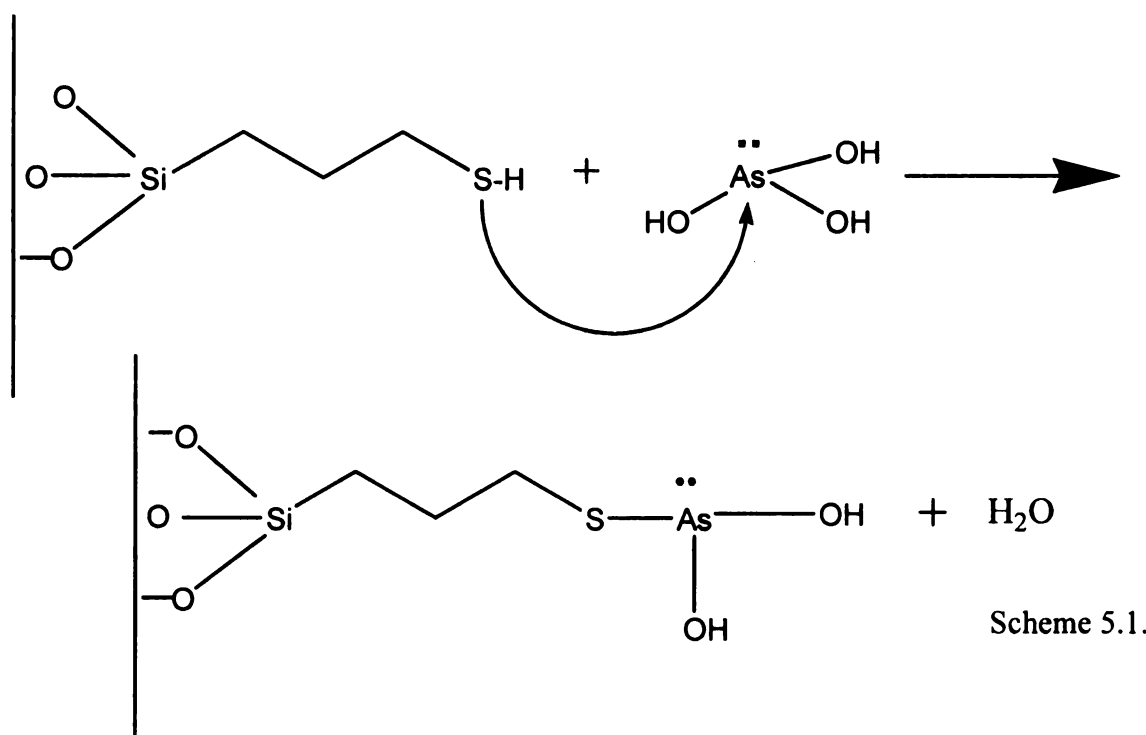
At least one As-S bond is proposed, but two or even three bonds are more likely based on the excess of mercaptan needed for quantative arsenic adsorption. The MP-HMS with x=0.40 and 0.50 are able to quantatively adsorb arsenite at an overall SH: As (III) ratio of 5:1, half that of the other mesostructures. MP-HMS derivatives with x=0.40 and 0.50 have high loadings of mercaptans (twice that of x=0.20), and thus, there is a greater chance for binding of arsenite to two or three adjacent SH centers.

The nucleophilic displacement of the As-OH bonds by mercaptan groups results in thioarsenite formation and the release of water in the process. The displacement of As-OH bonds by thiol is a known mechanism for arsenate reductase, which catalyzes the reduction of arsenate to arsenite in order to detoxify prokaryotes and eukaryotes systems.[28]

In addition to the possible coordination of arsenite by multiple mercaptan ligands, another possible explanation for the inability of all the mercaptan ligands to bind in a one-to-one manner with the arsenite is related to the accessibility of the thiol groups. The Raman spectra do not rule out the possibility that arsenite might be coordinating to special thiol sites. Limited presence of these "special" sites might be a reason that binding of one ligand to one arsenite is not observed. Most of the thiol moieties may be pulled back onto the wall of the mesostructure by van der Waals interactions, and are not dangling from the surface like pendent groups. But with increased functionalization, steric effects might cause some of the mercaptan moieties to protrude out into the pore and those protruding organic groups are more accessible for arsenite binding.

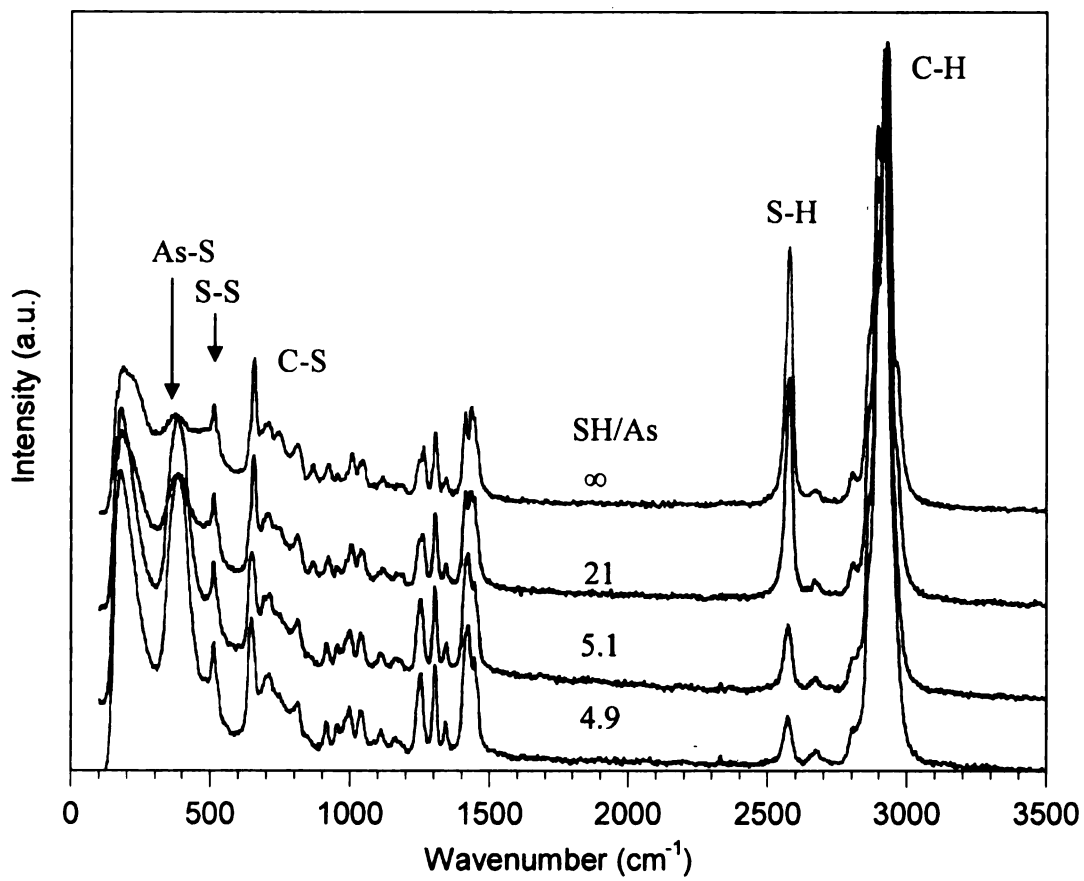Figure 5.8. Raman spectra of functionalized $(SiO_2)_{1-x}(LSiO_{1.5})_x$ compositions (L=mercaptopropyl) with a wormhole framework structure (denoted MP-HMS) after binding of arsenite at the SH/As levels shown. The spectra are offset on the y-axis for clarity.

5.4.2 Arsenate Trapping

As previously discussed in Chapter 1, the functionalization of silica mesostructures with amines is quite difficult to achieve via the direct-assembly method. One possible reason for this is mesostructure collapse due to the basic character of the amine which can contribute to the local hydrolysis of the organosilane reagent in the presence of water.[29] An aminopropyl functionalized mesostructure was prepared by direct assembly, under near neutral pH conditions using an alkylamine as the porogen. This structure is denoted AP-HMS. The physical properties are given in Table 5.5. An attempt was made to synthesized AP-HMS with x=0.10, 0.20, and 0.40. However, AP-HMS compositions with x=0.40 formed no precipitate. The surface areas for AP-HMS with x=0.10 and 0.20 are around 70% lower than MP-HMS mesostructures. Yet these AP-HMS silicas have high pore volumes (1.00 and 1.22 cm^3/g respectively) which is advantageous for trapping materials. Not only was it not possible to prepare higher functionalized structures, but only 60% of the added organosilane added was actually incorporated into the framework as determined by ^{29}Si MAS NMR and elemental analysis. For AP-HMS with x=0.10 aminopropyl added, the actual aminopropyl incorporation was x=0.05. For AP-HMS with x=0.20 aminopropyl added the actual x value was x=0.10. The x value given throughout this work will refer to the actual amount incorporated.

AP-HMS was characterized by nitrogen adsorption desorption. The isotherms are shown in Figure 5.9. Both mesostructures have typical type IV isotherms with a well-defined mesopore step at partial pressure between 0.4 and 0.6 signaling the presence of

uniform mesopores. The products do show high textural porosity, which is taken to be the void space between particles.

The TEM images of AP-HMS with x=0.05 and 0.10 are shown in Figure 5.10. Both images illustrate a wormhole framework, which is the expected morphology for mesostructures prepared via hydrogen bonding pathway, not an electrostatic assembly pathway. The loading of the amine functional groups was not as high as that of the mercaptan functionalized materials used for arsenite adsorption. In turn, with a lower organic loading, lower arsenate adsorption is expected.

Table 5.5. Physical properties of functionalized $(SiO_2)_{1-x}(SiO_{1.5}L)_x$ compositions where L=aminopropyl with a wormhole framework, denoted AP-HMS.

x_{theo}	x_{obs}[a]	NH_2 mmol/g	Pore volume[b] cm^3/g	Pore diameter[c] nm	SA[d] m^2/g
x=0.10	0.05	0.75	1.00	2.4	707
x=0.20	0.10	1.43	1.22	3.1	426

[a]x-value determined by ^{29}Si MAS NMR. [b]Total pore volume at P/P_0=0.98 [c]BJH pore diameter size determined from adsorption branch of nitrogen isotherm. [d]Surface area determined by BET model.
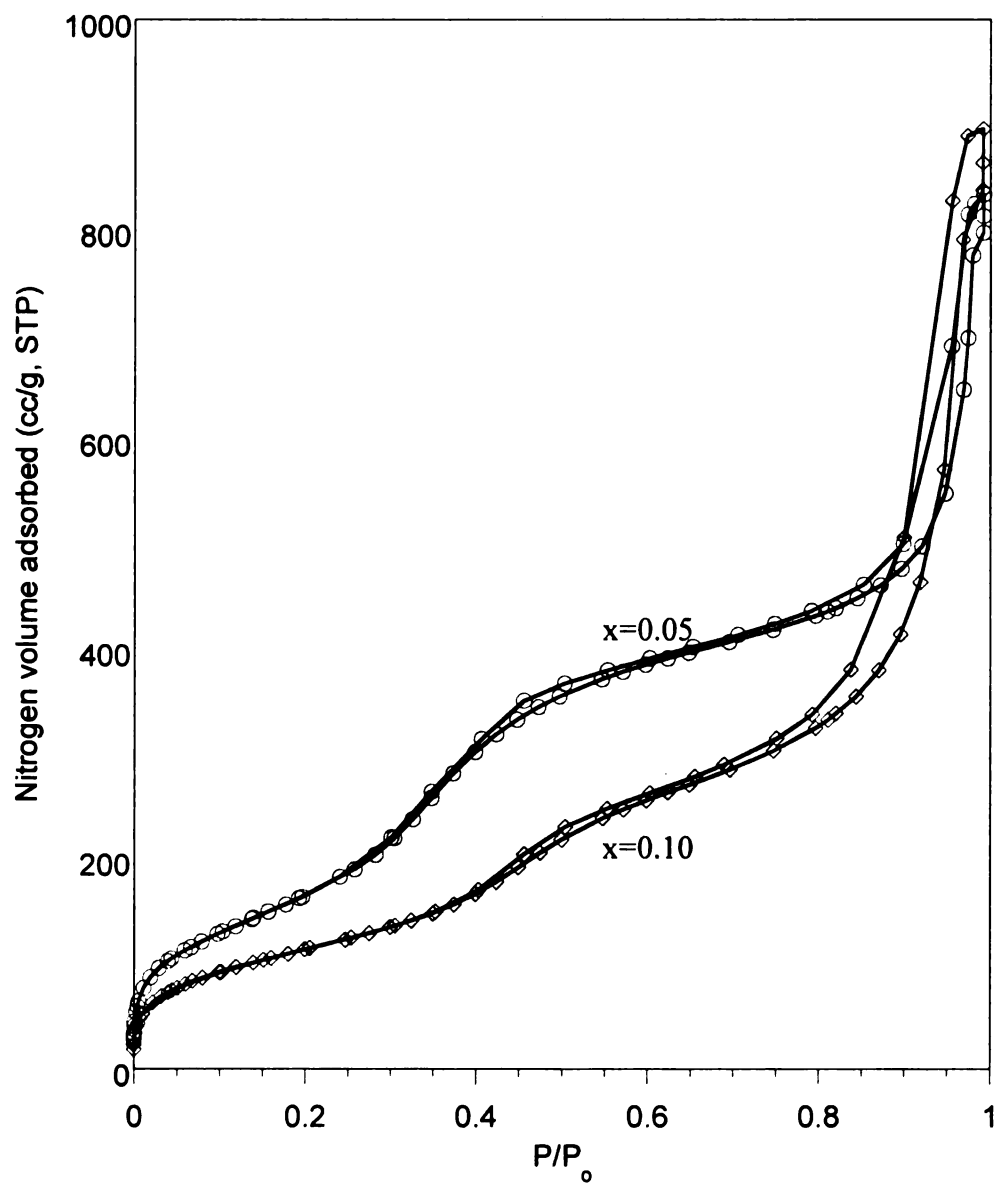
Figure 5.9. Nitrogen adsorption-desorption isotherm for functionalized $(SiO_2)_{1-x}$ $(LSiO_{1.5})_x$ compositions (L=aminopropyl) with a wormhole framework structure, denoted AP-HMS.
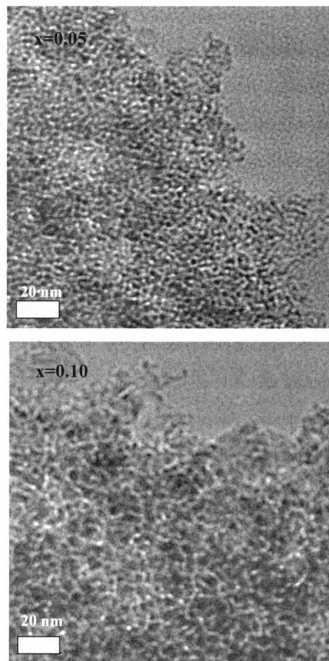
Figure 5.10. TEM images for functionalized $(SiO_2)_{1-x}(LSiO_{1.5})_x$ compositions (L=aminopropyl) with wormhole framework structure, denoted AP-HMS.

Table 5.6 is a comparison of arsenate adsorption by AP-HMS with x=0.10,

MP+AP-HMS with varying x and y loadings. Included for comparison are amine

functionalized hexagonal MCM-41 with x=0.10, 0.20, and 0.30 and cubic SBA-1 with

x=0.20, 0.30, and 0.40[11] mesostructures that have been used for arsenate adsorption. The

functionalization of MCM-41 and SBA-1 was accomplished by grafting. Grafting is the

process by which an organic moiety is anchored onto a silica surface through

condensation of surface silanols with alkoxy groups of an organosiloxane. MCM-41 and

SBA-1 were grafted with an aminopropyl, 1-(2-aminoethyl)-3-aminopropyl, or

propyldiethylenetriamine[11] ligands denoted AP, NN, and NNN, respectively. All AP-

HMS, MCM-41, and SBA-1 mesostructures for arsenite adsorption were protonated

before adsorption by stirring in 0.1 M HCl for 4 h. An attempt was made to adsorb

arsenate on non-protonated AP-HMS, but the resulting arsenate uptake was less than 2%.

Protonation of the mesostructure is necessary because the binding mechanism of arsenate

involves electrostatic interaction between the anionic arsenate and the cationic amine.

For the amine to be cationic it must be protonated; in all cases protonation was

effectively accomplished by acidification of the mesostructure after synthesis, but before

arsenate adsorption.

Protonated AP-HMS with x=0.10 adsorbs an amount of arsenate equivalent to the

hexagonal NN MCM-41 and the cubic AP-SBA-1, provided that the overall $NH_2/As(V)$

ratio is ≥ 6. The small difference in uptake can be in part attributed to MCM-41 having

hexagonal pore morphology thus there is a greater chance for pore blockage when

grafting the functional group as well as possible pore blockage by the arsenate. SBA-1 is

a cubic structure with thick walls and a cage-type pores as opposed to the wormhole pore

morphology of MP-HMS. The cage-type pores might allow for greater accessibility of larger molecules such as arsenate. Furthermore, the reduction of concentration of arsenate is comparable for all three materials. Protonated AP-HMS is able to trap 91% of the arsenate present in a 321 ppm solution, provided that the overall NH_2/As(V) ratio is ~6. An equivalent uptake was found for NNN MCM-41, indicating the wormhole morphology of the HMS definitely improves accessibility to the functional sites. It takes three times as many amines to reduce the arsenate concentration to the same value as with a monoamine on HMS. Under the same conditions, NNN-SBA-1 reduces the arsenate concentration by 99%. This suggests that large pores and high amine loading provide for an effective trapping agent. Arsenate uptake, like arsenite uptake requires a large excess of amine groups in the mesostructure. At the pH used, arsenate should have a -1 charge, and the protonated amine has a +1 charge. Thus, a 1:1 electrostatic binding would be expected. However, the ratio of ligand to arsenate necessary for quantative uptake of arsenate was around 10:1 for each mesostructure (MCM-41, SBA-1, and AP-HMS) and was never 1:1 even when the trapping agent was exposed to a large excess of arsenate.

A dual functionalized mesostructure was prepared and utilized with the idea that mercaptopropyl moieties are selective for arsenite binding and aminopropyl moieties are selective for arsenate trapping. This approach might provide an effective remediation media that would adsorb both forms of arsenic. The protonated MP+AP-HMS is effective for arsenate (and arsenite) trapping. The organic loadings of AP-HMS and MP+AP-HMS are very similar with 1.43 and 1.7 mmol NH_2/g, respectively. The arsenate trapping is slightly better for the dual functional material than the aminopropyl

alone, 98% versus 90%, respectively, under comparable conditions. For all mesostructures there does need to be substantial excess of total amine ligand to total As(V) in the reaction system. The ratio of aminopropyl:arsenate $\geq$ 6.0 was needed for quantative uptake of arsenate by MP+AP-HMS or AP-HMS. However, the dual functional MP+AP-HMS is able to reduce the concentration of arsenate to one of the lowest reported of any mesostructure namely, 5 ppm. One explanation for the improved arsenate trapping by the dual functional mesostructure is the thiols might play a role in arsenate reduction.

The occurrence of some very interesting chemistry for arsenate adsorption to MP+AP-HMS was observed by Raman spectroscopy (Figure 5.11).

Table 5.6. Performance of functionalized $(SiO_2)_{1-(x+y)}$ $(LSiO_{1.5})_x$ $(L'SiO_{1.5})_y$ compositions (L=mercaptopropyl, L'=aminopropyl), denoted MP+AP-HMS and functionalized $(SiO_2)_{1-x}$ $(LSiO_{1.5})_x$ compositions (L=aminopropyl), denoted AP-HMS with a wormhole framework structure for arsenate adsorption and grafted AP, NN, NNN SBA-1 and AP, NN, NNN MCM-41, where NN is 1-(2-aminoethyl)-3-aminopropyl and NNN is propyldiethylenetriamine.

Adsorbent[a]	mmol NH2/g	Initial ppm $(H_2AsO_4)^-$	Final ppm $(H_2AsO_4)^-$	mmol $(H_2AsO_4)^-$ added /g	mmol NH2/ mmol $(H_2AsO_4)^-$ added	mmol $(H_2AsO_4)^-$ adsorbed /g	mmol NH2/ mmol $(H_2AsO_4)^-$ adsorbed	% Removal
AP-MCM-41[II]	1.46	115	25.1	0.17	8.59	0.13	11.2	78.2
NN-MCM-41[II]	2.76	164	21.4	0.24	11.5	0.21	13.1	87.0
NNN-MCM-41[II]	3.53	316	30.3	0.46	7.67	0.41	8.61	90.4
AP-SBA-1[II]	1.90	204	28.4	0.30	6.33	0.26	7.30	86.1
NN-SBA-1[II]	3.33	214	14.6	0.31	10.7	0.29	11.5	93.2
NNN-SBA-1[II]	4.39	255	0.65	0.37	11.9	0.37	11.9	99.7
MP-HMS x=0.50	0.00	643	624	0.468	-	0.014	-	3.0
AP-HMS x=0.10 not protonated	1.43	321	316	0.233	6.14	0.0041	348	1.70
AP-HMS x=0.10	1.43	321	29.7	0.233	6.14	0.211	6.78	90.8
x=0.10 y=0.05 MP+AP-HMS	0.81	331	162	0.240	3.38	0.123	6.59	51.2
x=0.15 y=0.12 MP+AP-HMS	1.35	336	91.1	0.243	5.56	0.177	7.63	72.9
x=0.25 y=0.19 MP+AP-HMS	1.7	646	240	0.468	3.63	0.294	5.78	63.0
x=0.25 y=0.19 MP+AP-HMS	1.7	327	5.48	0.237	7.17	0.230	7.39	98.0
x=0.25 y=0.19 MP+AP-HMS	1.7	161	4.85	0.167	10.18	0.113	15.0	97.0

[a]All amine-functionalized mesostructures were protonated before arsenate adsorption unless otherwise specified. The MCM-41 and SBA-1 derivatives were prepared by grafting.
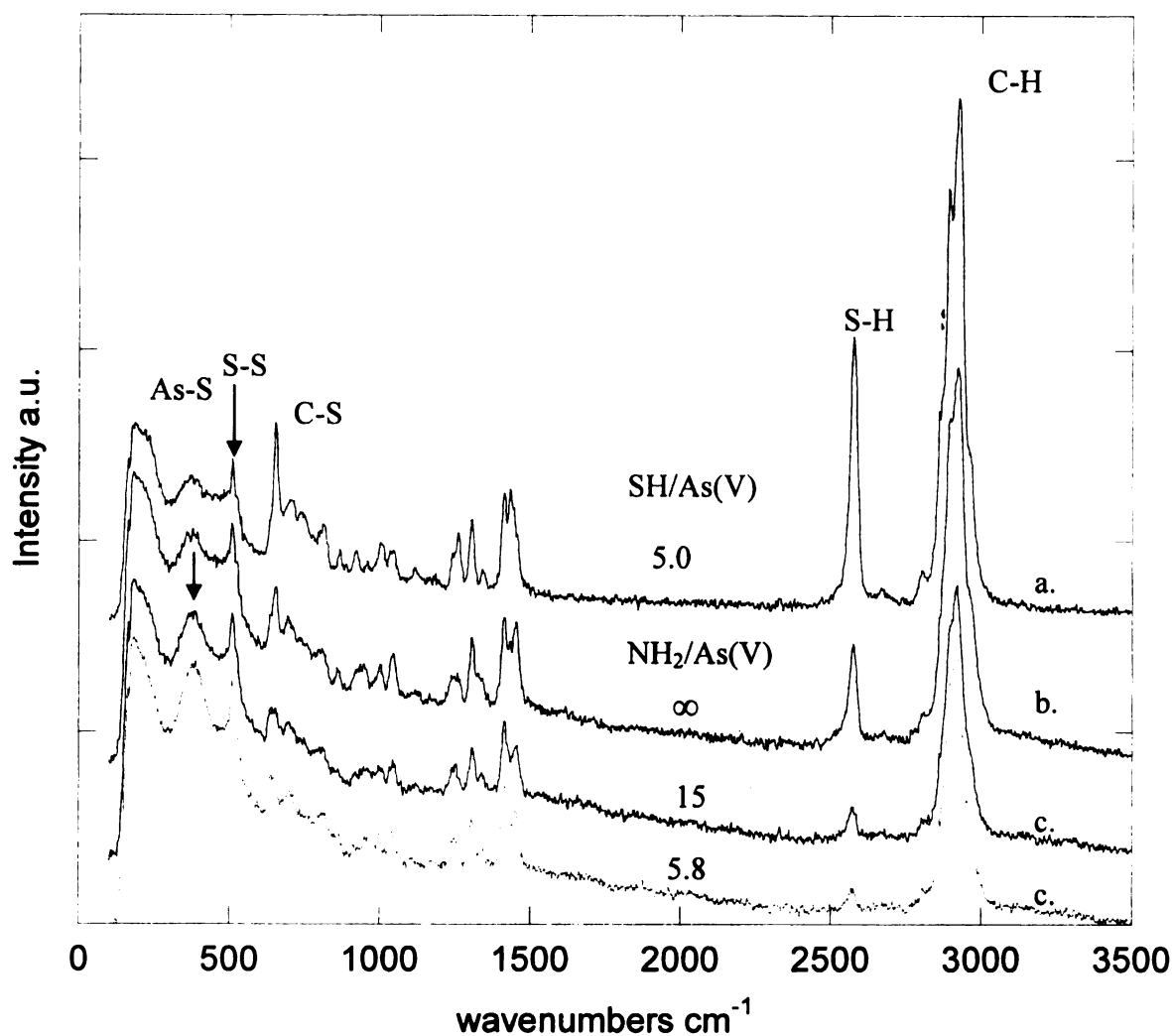
Figure 5.11. a. Raman spectrum of functionalized $(SiO_2)_{1-x}$ $(LSiO_{1.5})_x$ with x=0.50 composition (L=mercaptopropyl), denoted MP-HMS after arsenate adsorption SH/As (V)=5.0. b. Raman spectrum of functionalized $(SiO_2)_{1-(x+y)}$ $(LSiO_{1.5})_x$ $(L'SiO_{1.5})_y$ compositions (L=mercaptopropyl, L'=aminopropyl) with a wormhole framework structure, denoted MP+AP-HMS. c. and d. Raman spectra of functionalized $(SiO_2)_{1-(x+y)}$ $(LSiO_{1.5})_x$ $(L'SiO_{1.5})_y$ compositions (L=mercaptopropyl, L'=aminopropyl) with a wormhole framework structure, denoted MP+AP-HMS for arsenate adsorption; after binding of arsenate at the NH_2/As (V) levels shown. The spectra are offset on the y-axis for clarity.

211

The thiol Raman band is retained for the protonated mesostructure as evidenced by the S-H stretch at 2560 cm^{-1}.[23,24] However, a decrease in the S-H stretch was observed with arsenate trapping. No change in intensity of this stretch was expected upon exposure to arsenate because the arsenate showed no affinity for MP-HMS. Furthermore, a change in the intensity of the S-S stretch at 510 cm^{-1} was observed with arsenate binding, signaling an increase in the amount of disulfide present with arsenate loading. The disulfide is initially formed through the oxidation of neighboring thiols during the synthesis of MP+AP-HMS. The increase in the intensity of the disulfide band with exposure to arsenate loading indicates that arsenate is being reduced to arsenite by the thiol, which is acting as a reducing agent. In turn, the thiol is being oxidized to disulfide. Moreover, the As-S stretch,[25] in the region of 375-450 cm^{-1} grows in intensity with arsenate adsorption. This indicates the trapping of arsenite through reaction with the remaining thiol. The reactions are shown below:

$$2 \text{ [H}_2\text{AsO}_4]^- + 6 \text{ RSH} \rightarrow 2 \text{ [H}_3\text{AsO}_3] + 3 \text{ RS-SR} + 2 \text{ H}_2\text{O} \qquad \text{Equation 5.5}$$

$$\text{RSH} + [\text{H}_3\text{AsO}_3] \rightarrow \text{RS-As(OH)}_2 + \text{H}_2\text{O} \qquad \text{Equation 5.6}$$
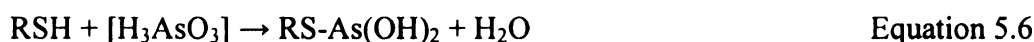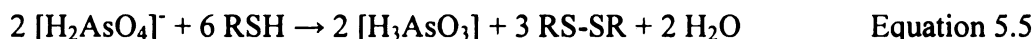
The Raman spectrum of MP-HMS with x=0.50 after trapping of arsenate is shown in Figure 5.11. No arsenate adsorption occurred on the MP-HMS with x=0.50 and no increase in Raman intensity was observed at the frequency expected for an As-S stretch. There is no doubt that the change in the intensity of the As-S band for the MP+AP-HMS samples is due to the adsorption of arsenite. To further determine if the arsenite was indeed being trapped by the thiol, the arsenate filtrate after exposure to the MP+AP-HMS trapping agent was examined for the presence of arsenite. The titration for arsenite was done under basic conditions, so that any arsenite in solution was oxidized to arsenate by

I₂. It was verified that no arsenite was in the MP+AP-HMS filtrate exposed to arsenate and therefore must have been trapped by the remaining thiol. Although this reduction reaction of arsenate by thiol was unexpected, it is not unprecedented.

In the biologically important arsenate reductase mechanism, the system by which arsenate is reduced to arsenite in the body in order to rid itself of the pollutant, a deprotonated thiol (from a cysteine) binds arsenate.[28] Thiol is then oxidized to disulfide, and the arsenate is reduced to arsenite with a concomitant release of water. The reaction for the arsenate reductase mechanism is illustrated below:

$$2RS^- + [AsO_2(OH)_2]^- \rightarrow [AsO_2(OH)]^{2-} + RS\text{-}SR + OH^-$$

This thiol-and amine-rich environment involved in the arsenate reductase mechanism is mimicked in the dual functionalized HMS system. So although arsenate has no affinity for the mercaptan functionalized HMS, in a system like a biological one, which is rich in amines and thiols, a more suitable trapping environment is created. The arsenate is trapped by the protonated amines and then is reduced by the thiol to arsenite. The thiol is oxidized to disulfide, but the arsenite is then trapped by the remaining unoxidized thiol.

It is prudent to examine the "lock-and-key" process proposed by Fryxell,[30] where the coordination of the arsenate is like the insertion of a key, while the displacement of the ethylenediamine ligand corresponds to the opening for trapping arsenate. The Cu(en)₃ complex is approximately octahedral, the first two en ligands being strongly bound and the third being still labile.[10] In the computer modeling, the cationic octahedral complex contains an electrophilic basket with C_3 symmetry that forms an ideal host for a tetrahedral anion.[10] The coordination of arsenate (hypothesized to be through an

213

oxygen) to immobilized Cu(II) is an effective method to trap arsenate; up to 99% removal is possible.[14] Expanding upon this method, Yoshitake et al. examined use of other transition metals, Fe^{3+}, Co^{2+}, Ni^{2+}, and Cu^{2+} immobilized by ethylenediamine ligands grafted on MCM-41 and MCM-48.[13] The iron and cobalt were the central cations that were superior to the other metals in terms of arsenate adsorption capacities and selectivity. As opposed to Fryxell's work, Yoshitake protonated the ethylenediamine functionalized material before adsorption of the metal centers. EXAFS was done on the transition metal loaded mesostructure as well as the arsenate loaded mesostructure, and it was determined that the coordination of the immobilized metal centers were $M(en)_2Cl_n$ and $M(en)Cl_n$, not $M(en)_3$ as hypothesized by the other reported work.[11] Based on the EXAFS results, the model of adsorption proposed is two arsenate ions are directly coordinated to Fe^{3+} center, and the another is bound in the outer sphere to compensate the positive charge of the ferric cation. No explanation was given by either work as to the discrepancy between the coordination of the arsenic. One work reports the arsenate is coordinated through an arsenic-transition metal bond.[11] As opposed to the other work, in which coordination of the arsenate is between the transition metal and an oxygen of the arsenate.[14]

Although a transition metal coordinated by ethylenediamine functional groups does trap arsenate, the method is not one of choice. The metal center might possibly leach out, and adding metals to an already polluted area is never the goal. Furthermore, the method is complex and involves a many step-synthesis for the mesostructure, grafting of the ligand, adsorption of the transition metal, and finally, adsorption of the arsenate.

Efficient arsenate removal can be accomplished by electrostatic interaction of a protonated amine and anionic arsenate.

5.5 Conclusion

5.5.1 Arsenite Adsorption

Three mesostructures have been demonstrated to be selective and proficient adsorbents for toxic arsenite. This is the first time the remediation of arsenite by a mesoporous material has been reported. It is also the first time a dual functionalized mesostructure has been utilized in arsenic trapping. Arsenite concentration was reduced by up to 99%. Moreover, this adsorption method of arsenite by mercaptopropyl functionalized mesostructures requires no additional steps of oxidation of arsenite to arsenate, protonation of the material, or immobilization of other metals before the trapping of arsenite may be accomplished. In addition to the ease of trapping demonstrated, the material itself is prepared in a simple one-pot synthesis with the template being removed by Soxhlet extraction, which allows for recovery and ability to recycle the surfactant.

Experimental evidence illustrates that the arsenite coordinates directly to the mercaptan for formation of thioarsenite and release of water. Although the arsenite adsorbed increases as the loading the functional group increases, as would be expected, further information on the binding mechanism of the arsenite to mercaptan needs to be examined further. At low loadings of mercaptans, x=0.10-0.30, arsenite uptake is quantative up to a 10:1 mercaptan:arsenite ratio. For the higher functionalized MP-HMS structures with x=0.40 and 0.50, quantative uptake of arsenite is observed until a ratio of 5:1 mercaptan:arsenite. The increased uptake of arsenite with increasing

functionalization can be attributed to either a greater number of ligands present for greater uptake of arsenite or that coordination of arsenite by mercaptans is not in a 1:1 ratio. In the higher functionalized mesostructures there is a greater probability of mercaptans being adjacent to each other. As a result, they may be able to coordinate two or three mercaptans to the arsenite, or both mechanisms could be correct. The MP-HMS with x=0.40 and 0.50 are more likely to have a greater number of mercaptan moieties in close proximity to each other. This closeness might allow for multiple As-S bonds to be formed. The presence of disulfide, from the oxidation by air of two adjacent mercaptans, is observed in all loadings of MP-HMS. This indicates that some of the ligands are in very close proximity to each other regardless of organo loading. Investigation of regeneration and the ability of MP-HMS to reduce arsenite levels to those accepted by the EPA for drinking water are the next steps for this study.

5.5.2 Arsenate Adsorption

Aminopropyl functionalized mesostructures have been shown to be successful for trapping arsenate, provided the amine is protonated to allow for an electrostatic interaction between the cationic amine and anionic arsenate. The directly-assembled AP-HMS was able to reduce arsenate concentration by 90% with a six-fold excess of amine with respect to arsenate. Nonetheless, NN and NNN-SBA-1,[11] which had a greater amount of amines incorporated by the grafting method of functionalization (3.33 and 4.39 mmol NH_2/g respectively), were able to reduce concentrations of arsenate by 98%, again with an excess of amine ligand. An AP-HMS with comparable organic loadings was not successfully prepared. All mesostructures quantatively adsorbed arsenate up to around a 10:1 ligand to arsenate ratio, a 1:1 binding was not observed for any

216

mesostructure even with excess ligand. For comparable levels of aminofunctionalization, the wormhole structure of HMS mesostructures or cubic pore structure of SBA-1 materials allow for greater accessibility to the active sites than the hexagonal morphology of MCM-41 mesostructures.

Dual mercaptopropyl and aminopropyl functionalized HMS can be synthesized in a simple one-step process with high levels of organic loadings possible. The MP+AP-HMS mesostructure is very utilitarian. Not only is it effective for arsenate trapping, but it is also successful for arsenite remediation. The AP moieties need to be protonated for arsenate adsorption; yet, this acidification does not affect the effectiveness of arsenite adsorption. Furthermore, the MP+AP-HMS appears to mimic the biologically important arsenate reductase mechanism. The protonated amine moieties coordinate to the arsenate which in turn acts as an oxidizing agent to oxidize neighboring thiols to disulfide. The arsenite formed as part of the oxidation/reduction mechanism, is in turn trapped by the remaining thiols. Organically functionalized mesostructures are potentially valuable arsenic remediation materials.

5.6 References

(1)   US EPA,. http://www.epa.gov/safewater/arsenic.html. **2002.**

(2)   Berg, M.; Tran, H. C.; Nguyen, T. C.; Pham, H. V.; Schertenleib, R.; Giger, W. *Environ. Sci. Technol.* **2001**, *35*, 2621-2626.

(3)   World Health Organization, www.who.int/inffs/en/fact210.html **2001.**

(4)   Tanabe, K.; Yokota, H.; Hironaka, H.; Tsushima, S.; Kubota, Y. *Appl. Organomet. Chem.* **2001**, *15*, 241-251.

(5)   Smedley, P. L.; Kinniburgh, D. G. *Appl. Geochem.* **2002**, *17*, 517-568.

(6)   Oremland, R. S.; Stolz, J. F. *Science* **2003**, *300*, 939-944.

(7)   Jain, C. K.; Ali, I. *Water Res.* **2000**, *34*, 4304-4312.

(8)   US EPA, www.epa.gov/tio/download/remed/542r02004/arsenic_report.pdf. **2002.**

(9)   Fryxell, G. E.; Liu, J.; Hauser, T. A.; Nie, Z.; Ferris, K. F.; Mattigod, S.; Gong, M.; Hallen, R. T. *Chem. Mater.* **1999**, *11*, 2148-2154.

(10)   Yoshitake, H.; Yokoi, T.; Tatsumi, T. *Chem. Mater.* **2002**, *14*, 4603-4610.

(11)   Yoshitake, H.; Yokoi, T.; Tatsumi, T. *Chem. Lett.* **2002**, 586-587.

(12)   Yoshitake, H.; Yokoi, T.; Tatsumi, T. *Chem. Mater.* **2003**, *15*, 1713-1721.

(13)   Fryxell, G. E.; Liu, J.; Hauser, T. A.; Nie, Z. M.; Ferris, K. F.; Mattigod, S.; Gong, M. L.; Hallen, R. T. *Chem. Mater.* **1999**, *11*, 2148-2154.

(14)   Torchinskii, Y. M. *Sulfur in Proteins*; Pregamon Press: New York, **1981**.

(15)   Fritz, J. S.; Schenk, G. H. *Quantitative Analytical Chemistry. 4th Ed*; Allyn and Bacon: Boston, **1979**.

(16)   Howard, A. G.; Volkan, M.; Ataman, D. Y. *Analyst* **1987**, *112*, 159-162.

(17)   Mori, Y.; Pinnavaia, T. J. *Chem. Mater.* **2001**, *13*, 2173-2178.

(18)   Schmidt-Winkel, P.; Lukens, W. W.; Zhao, D. Y.; Yang, P. D.; Chmelka, B. F.; Stucky, G. D. *J. Am. Chem. Soc.* **1999**, *121*, 254-255.

(19)   Sing, K. S. W.; Everett, D. H.; Haul, R. A. W.; Moscou, L.; Pierotti, R. A.; Rouquerol, J.; Siemieniewska, T. *Pure Appl. Chem.* **1985**, *57*, 603-619.

(20)   Galarneau, A.; Desplantier, D.; Dutartre, R.; Di Renzo, F. *Microporous Mesoporous Mater.* **1999**, *27*, 297-308.

(21)   Inoue, S.; Hanzawa, Y.; Kaneko, K. *Langmuir* **1998**, *14*, 3079-3081.

(22)   Raso, S. W.; Clark, P. L.; Haase-Pettingell, C.; King, J.; Thomas, G. J., Jr. *J. Mol. Biol.* **2001**, *307*, 899-911.

(23)   Kluth, G. J.; Carraro, C.; Maboudian, R. *Phys. Rev. B: Condens. Matter* **1999**, *59*, R10449-R10452.

(24)   Iyer, R. G.; Kanatzidis, M. G. *Inorg. Chem.* **2004**, *43*, 3656-3662.

(25)   Helz, G. R.; Tossell, J. A.; Charnock, J. M.; Pattrick, R. A. D.; Vaughan, D. J.; Garner, C. D. *Geochim. Cosmochim. Acta* **1995**, *59*, 4591-4604.

(26)   Baran, E. T., Mormann; and Wolfgang, Jeitschko *J. Raman Spectrosc.* **1999**, *30*, 1049-1051.

(27)   Messens, J.; Martins, J. C.; Van Belle, K.; Brosens, E.; Desmyter, A.; De Gieter, M.; Wieruszeski, J.-M.; Willem, R.; Wyns, L.; Zegers, I. *Proc. Natl. Acad. Sci. U. S. A* **2002**, *99*, 8506-8511.

(28)   Walcarius, A.; Etienne, M.; Lebeau, B. *Chem. Mater.* **2003**, *15*, 2161-2173.

(29)   Fryxell, G. E.; Lin, Y.; Wu, H.; Kemner, K. M. *Stud. Surf. Sci. Catal.* **2002**, *141*, 583-590.